Chance favors only the prepared mind.

– Louis Pasteur

University of Alberta

EFFECTS OF INTERFERENCE ON CARRIER TRACKING IN FADING AND SYMBOL SYNCHRONIZATION

by

Amin Emad

A thesis submitted to the Faculty of Graduate Studies and Research
in partial fulfillment of the requirements for the degree of

Master of Science

Department of Electrical and Computer Engineering

Fall 2009
Edmonton, Alberta

Examining Committee

Norman C. Beaulieu, Electrical and Computer Engineering

Michael A. Kouritzin, Mathematical and Statistical Sciences

Sergiy Vorobyov, Electrical and Computer Engineering

To my Family

Abstract

Synchronization is a very important part of every digital communication receiver. While in bandpass coherent transmission, frequency and phase synchronization play a very important role in reliable transmission, symbol timing recovery is a necessary part of every baseband and bandpass coherent receiver. This dissertation deals with the problem of synchronization in the presence of fading and interference.

First, the performance of an automatic frequency control loop is investigated using two parameters of average switching rate and mean time to loss of lock. These parameters are derived in closed-form or as integral-form formulas for different scenarios of modulated and unmodulated signals in different fading channels when there is one interference signal present at the input of the AFC. Then, the results are generalized to the noisy fading scenario and it is shown that in Rayleigh fading case, the performance of AFC becomes better when the desired signal is noisier.

In the second part, the problem of symbol timing recovery is investigated in systems that are subject to intersymbol interference and non-data-aided maximum likelihood synchronizer is derived in these channels. Then, a new simple bound on the performance of synchronizers is derived and compared to the previously known lower bounds. It is shown that while this lower bound solves the shortcomings of the well known modified Cramer-Rao bound at small values of signal-to-noise-ratio, it is much easier to compute compared to another well known bound, the detection theory bound.

Acknowledgements

First and foremost I would like to express my sincere gratitude to my supervisor Dr. Norman C. Beaulieu who has supported me throughout my thesis with his knowledge and patience. Undoubtedly, the fulfilment of this project would not have been possible without his insightful comments and suggestions. His profound expertise and academic achievements have always inspired me for my future carrier.

I would like to offer my deepest appreciation to my evaluation committee members Dr. Michael A. Kouritzin and Dr. Sergiy Voroboyov for their useful comments and suggestions.

My heartfelt thanks go to the talented and enthusiastic colleagues and friends Amir Masoud Rabiei, Golnaz Farhadi, Payam Dehghani, Reza Nikjah, Mahdi Ramezani, and Xin Wang for their helpful discussions throughout the completion of this project. I would also like to thank Iraj Hosseini, Ali Sharifkhani, Ramin Babaei, Pedram Paysarvi, Sijing Jiang, and my other colleagues for providing a friendly and professional environment.

I gratefully thank my best friend Nima Lashkari for his tremendous support during the many years of friendship. I also want to thank my other good friends in Edmonton for the unforgettable memories we shared together. To name a few out of many, Arash Talebi, Moslem Noori, Sahar Movaghati, Omid Taheri, Raman Yazdani, and Saeid Kaviani.

I would like to cordially thank my beloved parents, Mehrnoosh and Kamran, whose continuous encouragement and support I have relied throughout my studies. The last but not the least, I would like to thank my grandparents Badri and Abdollah for their dedication and love.

Table of Contents

List of Tables

List of Figures

List of Abbreviations

Abbrv.	Definition	First Use
PLL	Phase-Locked Loop	1
AFC	Automatic Frequency Control	1
CCI	Cochannel Interference	2
ACI	Adjacent Channel Interference	2
ISI	Intersymbol Interference	2
ASR	Average Switching Rate	3
MTLL	Mean Time to Loss of Lock	3
LOS	Line-of-Sight	4
ML	Maximum Likelihood	4
ZC	Zero Crossing	5
CRB	Cramer-Rao Bound	5
SNR	Signal-to-Noise Ratio	5
DTB	Detection Theory Bound	5
LDTB	Lower Bound on Detection Theory Bound	5
i.n.d	Independent Non-Identically Distributed	6
i.i.d	Independent Identically Distributed	6
VCO	Voltage Controlled Oscillator	8
FDD	Frequency Difference Detector	8
PDF	Probability Density Function	12
ELD	Early-Late Detector	15
ZCD	Zero-Crossing Detector	15
MMD	Mueller and Mueller Detector	15
GAD	Gardner Detector	15

List of Symbols

Symbol	Definition	First Use
Re	The real value operator	10
f_c	The carrier frequency	10
$f_A(\alpha)$	Probability density function of α	12
τ	The timing offset	13
$\hat{\tau}$	The estimate of τ	13
$\{\hat{c}_i\}$	Sequence of transmitted data	13
$E[\cdot]$	The expectation operator	15
$P(\mathbf{r}'\|\tau)$	JPDF of vector $\mathbf{r}'$ given τ	16
$E_{\mathbf{r}}$	Expectation operator over the vector $\mathbf{r}$	19
$f_{A,\dot{A}}(\alpha,\dot{\alpha})$	The JPDF of A and $\dot{A}$	21
$N_Y(\lambda)$	The level crossing rate of Y through λ	22
$Pr[A]$	The probability of event A	40
$G_w(f(\theta))$	The transform that fills the valleys of $f(\theta)$ with respect to θ	64
$\mathcal{F}[\cdot]$	The Fourier transform operator	65

Chapter 1

Introduction

In a digital link, data is transmitted using a sequence of pulses sent from the transmitter and received at the receiver. The ultimate task of a receiver is to find a replica of the data that is conveyed by the received pulses. In order to extract data from the received signal, the receiver needs to know the time base of the signal also referred to as reference parameters [1]. Synchronization is the process of finding the reference parameters of the received signal. In the process of detection, three reference parameters play a very important role. These parameters are frequency, timing, and phase.

In coherent bandpass digital communications, the first step of detecting the transmitted data is to extract the baseband data signal using a local reference [2]. This local reference should regenerate the frequency and phase of the received signal. The circuits that perform this task are called carrier synchronizers. One of the most important circuits that is used to recover the phase of the received signals in coherent receivers is the phase-locked loop (PLL). A PLL is a control system that automatically adjusts the phase of a locally generated signal to track the phase of the received signal. This circuit has two modes of operation [3, Ch. 4]. In the tracking mode, the state variables of the PLL have values close to the steady state values. However, the initial values of these state variables might be very different from their steady state values. In the acquisition mode, the initial values of the loop are brought to the tracking mode. Although a PLL is a near optimum tracking device [3], it has a poor performance in the acquisition mode. In order to overcome this problem, in many coherent receivers, an automatic frequency control (AFC) loop is used as an acquisition aid to the PLL. An AFC loop is used to control the frequency of a received signal. The usage of the AFC is not limited to coherent detection. Since an AFC is more robust to link disturbances than a PLL [4], in noncoherent receivers, it is used as a necessary part of the digital link to control the frequency of the received signals.

In addition to carrier synchronization, every baseband or bandpass receiver should also perform

timing synchronization. In the receiver, the output of the demodulator should be sampled periodically, once in every symbol interval, in order to recover the transmitted data. The optimum sampling times correspond to the widest opening of the eye diagram [2]. Since the propagation delay from the transmitter to the receiver is generally unknown, symbol timing recovery is needed in every receiver in order to determine the optimum sampling location to achieve reliable detection.

Symbol timing recovery can be accomplished in several ways. One way is to synchronize the transmitter and receiver clocks to a precise master clock. In this scenario, the receiver should consider the time delay between the transmitter and receiver and compensate for this relative time delay. This method can be used in radio transmission systems that work in the very low frequency band (below 30 kHz) [2].

Another method is to transmit the clock frequency along with the data. The receiver can use a narrowband filter to extract the clock frequency and thus the clock signal for sampling. Although this method is very simple, it consumes some of the transmitter power to transmit the clock signal and also a fraction of the frequency bandwidth should be allocated for transmitting the clock signal. This method is used in telephone transmission systems which use large bandwidths to transmit signals from different users [2].

Another method is to extract the clock signal from the received signal. This is the method that is used in many wireless communication systems to achieve synchronization.

In wireless communications, synchronization is a challenging task as a result of many factors such as multipath fading, interference, and noise. Multipath fading occurs as a result of constructive and destructive addition of multipath signal components and not only affects the power of the received signal, but also adds a random delay to the signal. One of the most important types of interference is cochannel interference (CCI). CCI occurs as a result of interrupting signals from other users operating in the same frequency channel. Interference can also occurs as a result of signals in adjacent channels interfering with the desired signal. This type of interference is called the adjacent channel interference (ACI). Another important type of interference is intersymbol interference (ISI). The ISI occurs when symbols of a signal interfere with other symbols of the same signal. Moreover, the presence of additive white Gaussian noise in the system is inevitable. Consequently, in addressing the problem of synchronization, it is very important to know the effect of these factors on the performance of the synchronizers in order to design an appropriate and realistic synchronizer.

1.1 Motivations and Contributions

In a wireless channel, usually there is more than one user and therefore the presence of more than one signal at the input of a receiver is highly expected. Most of these signals are filtered at the input of the receiver, however, some of these signals might pass through the filter as a result of inadequate filtering. The signals that have passed through the filter can be signals sent with the same carrier frequency as the desired signal (CCI), or they can be signals sent in adjacent channels (ACI). One should note that the carrier frequency of the interference signals that are sent through the same channel as the desired signal changes from its original value before reaching the receiver. This change in the carrier frequency of the signals can be as a result of the effects of the wireless channel such as Doppler frequency shift [5] or it can be as a result of the frequency drift of the local carrier oscillators in the transmitters. Note that the local oscillators of the transmitters of the interference signals and the desired signal are different and also the paths they take to reach to receiver are different. As a result, either the CCI signals or the ACI signals that have passed through the bandpass filter of the receiver and the desired signal, would have different frequencies.

It is known that if there are two signals at the input of an AFC, the AFC locks on the signal with larger amplitude [6, Ch. 19]. The amplitude of the received signals depend on several factors such as the modulation, fading, and noise. Since these factors change with time, the relative amplitudes of the interference signal and the desired signal also change with time. This change in the relative amplitudes of the received signals causes AFC jumps at the receiver. Every jump from the received signal to the interference signal and vice versa, generates a transient in the filters of the receiver which corrupts the performance of the filters and produces an internally generated outage in the receiver. In addition, these jumps consume energy in the circuits of the receiver and therefore the power consumption of the receiver increases. One measure that can quantify this effect is the average switching rate (ASR). The ASR shows how often a jump occurs in an AFC from the desired signal to the interferer and vice versa. By having this measure and the filter characteristics of a specific receiver, one can find the average time that the receiver is in outage as a result of these transients. Another way that an outage may occur in a receiver is if the AFC locks on the interferer instead of the desired signal. Therefore, for this period of time, the output of the AFC is not reliable. One parameter that can be used to characterize this behaviour of an AFC is the mean time to loss of lock (MTLL). This parameter gives the average time that an AFC remains locked on the desired signal and can be considered as a measure of the reliability time of the AFC's output.

Although the outage generated by the channel is well investigated in the literature, there is a

lack of reported results on the internally generated outage of the receiver. In reference [7], the ASR and the MTLL of an AFC loop have been derived when the desired signal and the interferer are unmodulated and are subject to Rayleigh fading. Meanwhile, wireless systems often operate in fading that is not Rayleigh distributed. For instance, many real world fading channels are better modeled by the Rician and Nakagami-*m* distributions. Furthermore, in many scenarios, the desired signal and the interferer pass through different transmission environments and therefore they can have different fading statistics [8]–[11]. For instance, if there is a line-of-sight (LOS) path between the transmitter of the desired signal and the receiver, the channel of the desired signal is better modeled by Rician fading. Meanwhile, there may not be a dominant multipath reflection in the interferer's channel. In this case, the fading affecting the interferer is better modeled by a Rayleigh (pure scattering) or a Nakagami distribution. Other dissimilar channel scenarios may appear as well when there is not a LOS path between the transmitter of the desired signal and the receiver. Furthermore, practical signals are modulated and the time behaviour of the modulating signals can affect the AFC performance significantly.

In this thesis, the result in [7] for the ASR of an AFC in Rayleigh/Rayeligh scenario is generalized to include the case of modulated carriers. Moreover, using a different method from that employed in [7], the ASR and the MTLL of an AFC in Rician/Rician and Nakagami/Nakagami fading are derived and several cases regarding the modulation of transmitted signals are considered. Moreover, the performance of an AFC in dissimilar fading channels, Rician/Rayleigh, Rayleigh/Rician, Rician/Nakagami, Nakagami/Rician, Nakagami/Rayleigh, and Rayleigh/Nakagami are investigated. And finally, the performance of an AFC in the presence of noise in Rayleigh/Rayleigh and Rician/Rician channels are considered and closed-form expressions and integral form formulas are derived for the ASR and the MTLL of an AFC.

Symbol timing recovery has been widely investigated during the last decades and different bit-synchronizers have been introduced in the literature (for a review see [12] and [1]). One of the well known methods that is widely used to estimate the timing offset of a received signal is the maximum likelihood (ML) method [13]. The application of this method in most scenarios leads to a rather complicated solution; however, its optimality makes this method an appropriate benchmark to which other synchronizers can be compared. The ML bit-synchronizers are derived for an inter-symbol interference (ISI)-free channel in [14]–[16]; however, the application of this method in the practical scenario in which symbols are subject to ISI, needs more clarification. In several papers, the ML synchronizers derived in [14]–[16] for an ISI-free channel, have been applied to ISI channels without any modifications, because of their simplicity, which has lead to some misunderstandings.

For example in [17], the authors investigated the performance of some zero-crossing (ZC)-based synchronizers in ISI channels and instead of comparing the results with the ISI ML synchronizer, they compared the results to the ISI-free ML synchronizer; consequently, they concluded that the ZC-based methods perform better than the ML synchronizer in many practical cases. In order to clarify this matter, the true ISI ML synchronizer is derived in the last chapter of this thesis and its performance is compared to the performance of an ML synchronizer derived for an ISI-free channel and the ZC-based synchronizer introduced in [17].

Finding bounds on the performance of a synchronizer has always been an interesting subject, since these bounds can be used as benchmarks to which the performance of practical synchronizers can be compared. A fundamental lower bound is the Cramer-Rao bound (CRB) [13], [18]; however,the computation of a true CRB is a challenging task in many practical cases. An alternative lower bound that is widely used in the literature is the modified Cramer-Rao bound [1], [19]. Although the CRB and MCRB provide useful bounds for moderate to high values of signal-to-noise ratio (SNR), they are known to have some shortcomings particularly at small values of SNR [13], [20], [21]. Another lower bound on the MSE of parameter estimators which has its origins in detection theory was introduced in [22]–[24]. This bound has been used to estimate the random delay of a single deterministic signal [22]–[24]. Moreover, in [21] it was used in the symbol timing recovery problem for a received signal consisting of a random sequence of pulses in an ISI-free channel. It was shown that this lower bound does not suffer from the shortcoming of the MCRB at small values of SNR. While the detection theory bound (DTB)[1] in the ISI-free scenario can in some instances be solved in closed-form [25], its application to the symbol timing recovery problem in an ISI channel requires computing a double integral numerically plus an expectation over all the possible sequences of the received signals [21], which can sometimes only be done using the Monte Carlo method. In this thesis, a lower bound on the DTB is derived for an ISI channel which only requires computing a single definite numerical integral on the interval $[0, 1]$. This lower bound on the DTB (LDTB) is compared to both the DTB and the MCRB and it is shown that not only does this bound preserve the appropriate behaviour of the DTB at small values of SNR, but it is also almost as tight as the MCRB for moderate values of SNR.

In the last chapter of this thesis, the true ISI ML synchronizer is derived and its performance is compared to the ISI-free ML synchronizer. It is shown that the use of the ISI-free ML synchronizer as a lower bound in an ISI channel, as has been done in [17], is not correct. Moreover, the DTB is

[1] The term detection theory bound (DTB) was introduced in [21] to concisely denotate this bound. We use this nomenclature here.

applied to timing estimation in ISI-channels and it is shown that it is a very tight lower bound to the ML synchronizer. In addition, a lower bound is derived for the DTB, which is much simpler than the DTB, does not suffer from the shortcomings of the MCRB at small values of SNR, and is almost as tight as the MCRB at moderate values of SNR.

1.2 Thesis Outline

This thesis is organized as follows. Chapter 2 reviews the background of this study. In the first part of this chapter, the automatic frequency control loops are described and previous works on the performance of these devices are reviewed. Then, the channel models are reviewed and different channels that are used in this thesis are introduced. In the second part, the problem of symbol timing recovery is presented and maximum likelihood synchronizers are explained in detail. Then, the bounds on the performance of symbol timing synchronizers are reviewed.

In Chapter 3, the mean time to loss of lock and the average switching rate of an automatic frequency control loop operating in fading in the presence of a single interferer are derived. Closed-form expressions and integral form formulas are derived for the ASR of an AFC for the general case of modulated carriers as well as important special cases of similar modulations and unmodulated carriers. The MTLL is also derived in closed-from for the case of unmodulated carriers. The general results include, as special cases, some previous more restricted results. Fading channels are assumed to be independent non-identically distributed (i.n.d.) with Rayleigh, Rician and Nakagami-*m* distributions while the special case of independent identically distributed (i.i.d.) channels is also considered. Corresponding numerical examples are provided and discussed to illustrate the results.

In Chapter 5, the mean time to loss of lock and the average switching rate of an automatic frequency control (AFC) loop are derived for the case of two received signals in dissimilar fading channels. The channels are assumed to have Rayleigh, Rician and Nakagami-*m* distributions. Numerical examples are provided to illustrate the effect of these fading scenarios on the performance of an AFC in the presence of cochannel interference.

In Chapter 6, the performance of an automatic frequency control (AFC) loop in a noisy fading channel when an interference signal is present at the input of the AFC is studied. Independent non-identically distributed (i.n.d.) channels with Rayleigh and Rician fading are considered. The received signals are assumed to be narrowband and linearly modulated while the analysis is applicable to the unmodulated scenario as well. Closed-form expressions and integral form formulas are derived for the mean time to loss of lock (MTLL) and the average switching rate (ASR) of an AFC.

Numerical examples are provided to illustrate the effects of noise and slow fading on the performance of an AFC in the presence of an interferer. It is shown that in some scenarios, an AFC has a better performance if the desired signal is corrupted by more noise.

In Chapter 7, the maximum likelihood (ML) criterion for symbol timing estimation is derived for a sequence of pulse amplitude modulated pulses in the presence of intersymbol interference (ISI) and Gaussian noise. The performance of this synchronizer is used as a benchmark to evaluate the performance of other synchronizers in a practical scenario. It is shown that a previous lower bound based on the ISI-free ML synchronizer cannot be used to lower bound the mean square error (MSE) of bit-synchronizers. A detection theory bound (DTB) is applied to the symbol timing recovery problem in an ISI channel and it is shown that this bound is a tight lower bound on the MSE of the ML synchronizer. A simple lower bound on this DTB is derived and it is shown that the simple bound is almost as tight as the well known modified Cramer-Rao bound (MCRB) at moderate values of SNR while it does not suffer from the shortcomings of the MCRB at small values of SNR.

Chapter 2

Background

2.1 Automatic Frequency Control

Automatic frequency control loops are used in digital receivers to control the frequency of the modulated received signals. In its simplest form, the block diagram of an AFC loop is shown in Fig. 2.1. As can be seen in this block diagram, the basic components of an AFC consist of a frequency difference detector (FDD), a loop filter, and a voltage controlled oscillator (VCO). When the input signal enters the AFC, the frequency difference detector generates an error voltage which is proportional to the difference between the carrier frequency of the received signal and the local frequency which is provided by the VCO. Then, the output of the FDD is filtered by the loop filter and then is applied to the VCO to drive the local frequency of the VCO towards the carrier frequency of the received signal. When the local frequency of the VCO equals the carrier frequency of the received signal, the error voltage is equal to zero and the system remains in steady state. In practice, these steps may be implemented digitally, since digital implementation of AFC is often more stable and reliable; however, one should note that if the sampling rate is sufficiently high to avoid aliasing, the analog and digital models will be similar [26].

In [27], two FDDs are introduced that can work in small loop bandwidths and large initial frequency offsets. Reference [28] deals with application of FDDs in the systems that the carrier fre-

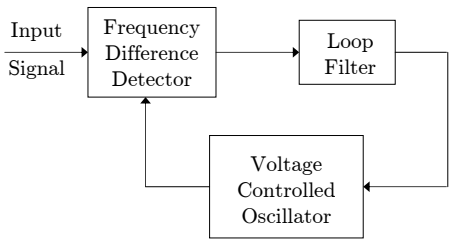

Figure 2.1. The block diagram of an automatic frequency control loop.

quency offsets are limited to a fraction of the data rate. In [4], [29]–[32] quadricorrelator FDDs are described that can work with frequency offsets as large as the data rate and digital implementations of these FDDs are presented in [33]. In [34] a FDD based on dual-filter detectors is described. In references [3], [26] FDDs derived from maximum likelihood (ML) principles are discussed.

The performance of an AFC in an interference-free noisy environment has been previously investigated in the literature. In references [4], [26], [35], [36], the variance of the frequency error has been used to evaluate the tracking performance of an AFC in the presence of additive noise. In [26] and [36], the effect of additive noise on the S-curve of some class of FDDs in automatic frequency control loops is discussed. Moreover, some formulas are derived for the variance of the frequency error in these AFCs to evaluate their performance in the presence of additive Gaussian noise. In [4] and [35], the AFC loop tracking performance is studied for several AFC loops and the variance of the frequency error is derived for these loops. In [37] and [38], the probability of loss of lock caused as a result of noise has been used to investigate the performance of an AFC. Moreover, in [39], a probability density function is derived for the frequency control loops.

However, noise is not the only disturbance that can affect the performance of an AFC. Since there are several users in a wireless channel, the presence of more than one signal at the input of a receiver is commonplace. In many cases, the signals that use same frequency channels, reach the receiver with different carrier frequencies as a result of channel effects such as Doppler frequency shift or local oscillator drift at the transmitter. If the difference between the carrier frequencies of these signals is small enough such that they cannot be filtered at the input of the receiver, they can produce some difficulties for the process of frequency recovery. This issue has been addressed and investigated in [6] for a single interference signal. It has been shown that if the difference between the carrier frequencies of the desired signal and interference signal is much smaller than the carrier frequencies and also the modulation is slow, the AFC will lock on the signal with larger amplitude. In this thesis, this problem is addressed in different fading and noise scenarios to evaluate the performance of an AFC in the presence of interference, multipath fading, and additive Gaussian noise.

2.1.1 Channel Model

When a signal is transmitted through a wireless channel, the channel affect the signal characteristics and therefore the signal received at the receiver is different from the transmitted signal. Several models are introduced in the literature to describe the different effects of wireless channels. One of the most important models that is widely used to characterize the wireless channels is the multipath

fading. Multipath fading is a result of the constructive and destructive addition of different multipath components of the signal. Multipath fading is a frequency-flat fading [40], i.e., all the spectral components of the signal are affected similarly by the channel. Since a deterministic model for multipath fading channels is not available most of the time, these channels are characterized statistically.

In multipath fading channels, if a single pulse is transmitted, the received signal will appear as a pulse train [5]. The pulses in this train correspond to the line-of-sight (LOS) component or scatter components associated with an individual scatterer or a cluster of scatterers. Fig. (2.2) shows a multipath fading channel when there is not an LOS component. The transmitted signal can be modeled as

$$x(t) = \text{Re}\{u(t)\exp(j2\pi f_c t)\} \tag{2.1}$$

where $u(t)$ is the equivalent lowpass signal for $x(t)$ and f_c is the carrier frequency. In the absence of noise, the received signal has a model equal to

$$r(t) = \text{Re}\left\{\sum_{n=0}^{N(t)} \alpha_n(t)u(t-\tau_n(t))\exp\left[j(2\pi f_c(t-\tau_n(t))+\phi_{D_n})\right]\right\} \tag{2.2}$$

where $N(t)$ is the number of multipath components, $\tau_n(t)$ is the delay of each component, $\alpha_n(t)$ is the path gain, and ϕ_{D_n} is the Doppler phase shift associated with the nth component.

One should note that this channel has a time-varying nature. This arises as a result of a moving transmitter or receiver. This movement causes the location of the reflectors to change in the transmission path and therefore changes the characteristics of the channel. However, these changes are very slow compared to the constructive and destructive addition of multipath components. Considering these two classes of changes caused by the channel, the characteristics of the multipath channels are described using random processes.

The detailed derivation of these characteristics are presented in [2], [5], [41]. If the spread of the time delay associated with the LOS component and multipath components is small compared to the inverse signal bandwidth, then these components are non resolvable and cause narrowband fading. In this scenario, (2.2) can be rewritten as

$$r(t) = \text{Re}\left\{u(t)\exp(j2\pi f_c t)\left(\sum_n \alpha_n(t)\exp(-j\phi_n(t))\right)\right\}. \tag{2.3}$$

In order to characterize the channel, we assume the transmitted signal $x(t)$ to be unmodulated with a random phase offset ϕ_0. Therefore,

$$r(t) = \text{Re}\left\{\left[\sum_{n=0}^{N(t)} \alpha_n(t)e^{-j\phi_n(t)}\right]e^{j2\pi f_c t}\right\} = r_I(t)\cos 2\pi f_c t - r_Q(t)\sin 2\pi f_c t \tag{2.4a}$$

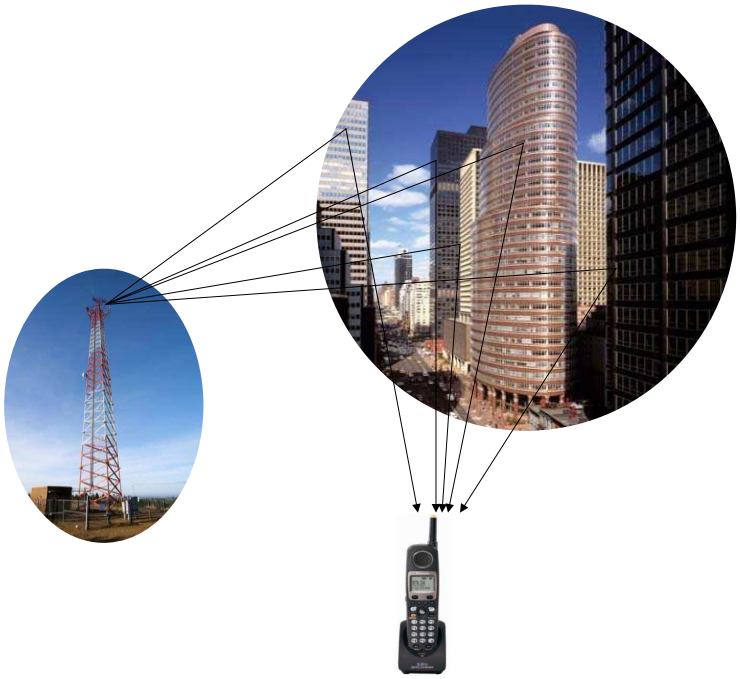

Figure 2.2. A multipath fading channel model.

where the in-phase and quadrature components of $r(t)$ are given by

$$r_I(t) = \sum_{n=1}^{N} \alpha_n(t) \cos \phi_n(t), \tag{2.4b}$$

$$r_Q(t) = \sum_{n=1}^{N} \alpha_n(t) \sin \phi_n(t) \tag{2.4c}$$

and

$$\phi_n(t) = 2\pi f_c \tau_n(t) - \phi_{D_n} - \phi_0. \tag{2.4d}$$

It has been shown that if $N(t)$ is large, then $r_I(t)$ and $r_Q(t)$ can be approximated as jointly Gaussian random processes[1] [5]. If we assume that the channel parameters change slowly with respect to time, there is not a dominant LOS component in the received signal, and for each component, the term $2\pi f_c \tau_n$ changes rapidly relative to all other phase terms in the expression of $\phi_n(t)$, then $\phi_n(t)$ is uniformly distributed in $[-\pi, \pi]$ and also $\mathrm{E}[r_I(t)] = \mathrm{E}[r_Q(t)] = 0$. Consequently, $r_I(t)$ and $r_Q(t)$ are zero-mean Gaussian random processes. Moreover, it can be shown that $\mathrm{E}[r_I(t) r_Q(t)] = 0$ and therefore $r_I(t)$ and $r_Q(t)$ are uncorrelated and since Gaussian, they are also independent. If

[1] A rigorous derivation might use normalized quantities here. We recall the derivation in [5] where normalization is not used.

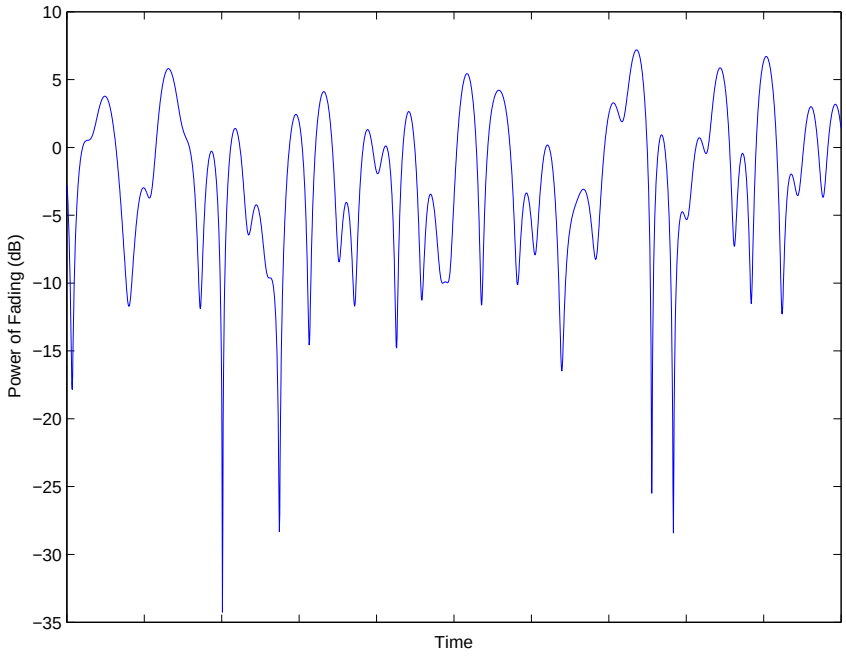

Figure 2.3. The power of fading in a Rayleigh fading channel in dB.

we assume a variance of σ^2 for both in-phase and quadrature components, the signal envelope $A(t) = |r(t)| = \sqrt{r_I(t)^2 + r_Q(t)^2}$ is Rayleigh distributed [42],

$$f_A(\alpha) = \frac{\alpha}{\sigma^2} \exp\left(-\frac{\alpha^2}{2\sigma^2}\right) \qquad \alpha \geqslant 0. \tag{2.5}$$

This multipath fading model is called Rayleigh fading. The amplitude of a Rayleigh fading channel modeled using Jakes model [41] is shown in Fig. (2.3).

If the channel has a fixed LOS component, then the received signal is the superposition of a complex Gaussian random component and a LOS component. The signal envelope can be shown to be Rician distributed [43]

$$f_A(\alpha) = \frac{\alpha}{\sigma^2} \exp\left(-\frac{\alpha^2 + \mu^2}{2\sigma^2}\right) I_0\left(\frac{\alpha\mu}{\sigma^2}\right) \qquad \alpha \geqslant 0 \tag{2.6}$$

where μ^2 is the power in the LOS component, $2\sigma^2$ is the power in the non-LOS component, and the function $I_0(\cdot)$ is the modified Bessel function of the first kind and zeroth order [44]. Fig. (2.4) shows the probability density function (PDF) of Rician fading for different Rice factors defined as, $K = \frac{\mu^2}{2\sigma^2}$, and $\sigma^2 = 1$.

Another model that is widely used in the literature is the Nakagami-*m* fading [40]. The PDF of the envelope of fading in this model is

$$f_A(\alpha) = \frac{2m^m \alpha^{2m-1}}{\Gamma(m)(2\sigma^2)^m} \exp\left(-\frac{m\alpha^2}{2\sigma^2}\right) \qquad \alpha \geqslant 0 \tag{2.7}$$

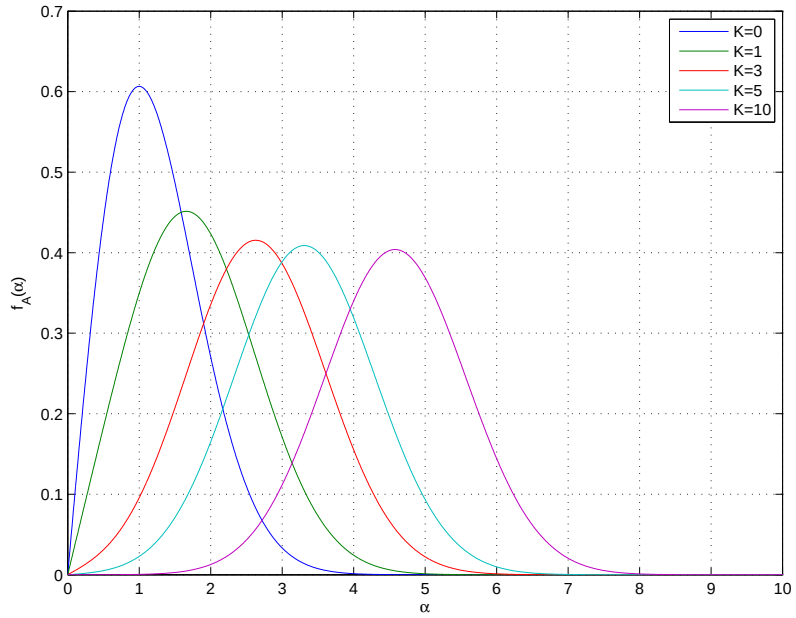

Figure 2.4. Probability density function of Rician fading for different Rice factors.

where m is the Nakagami-*m* fading parameter which ranges from $\frac{1}{2}$ to ∞. Fig. (2.5) shows the probability density function (PDF) of Nakagami-*m* fading for different values of m and $\sigma^2 = 1$.

2.2 Symbol Timing Recovery

The problem of symbol synchronization is to find the optimum sampling instances in order to extract the data from the received signal. For a pulse sequence with a pulse rate of $1/T$, the sampling rate would be $1/T$. However, the problem of symbol timing recovery includes finding the timing offset of the received signal in order to sample at the maximum opening of the eye diagram. The model of the received signal for a sequence of PAM modulated pulses can be expressed as

$$x(t,\tau) = \sum_i c_i g(t - iT - \tau) \tag{2.8}$$

where $g(t)$ is the received pulse shape, T is the inverse of the sampling rate, τ is the timing offset which can be modeled as an uniformly distributed random variable in $[0, T)$, and c_i is the ith transmitted data symbol. We can define $g(t)$ such that the best sampling instances would be at $t = kT+\tau$ for $k = 0, \pm1, \pm2, \cdots$. The objective is to estimate the timing offset of the received signal, $\hat{\tau}$. Then this estimate is used to sample the received signal at $t = kT + \hat{\tau}$ to obtain a sequence of samples $\{\hat{c}_i\}$. Fig. 2.6 shows the block diagram for a baseband receiver.

If we consider a normalized pulse shape, i.e., $g(t = 0) = 1$, then the difference between $\{\hat{c}_i\}$ and $\{c_i\}$ is only due to the intersymbol interference (ISI). If we have perfect timing recovery, $\hat{\tau} = \tau$,

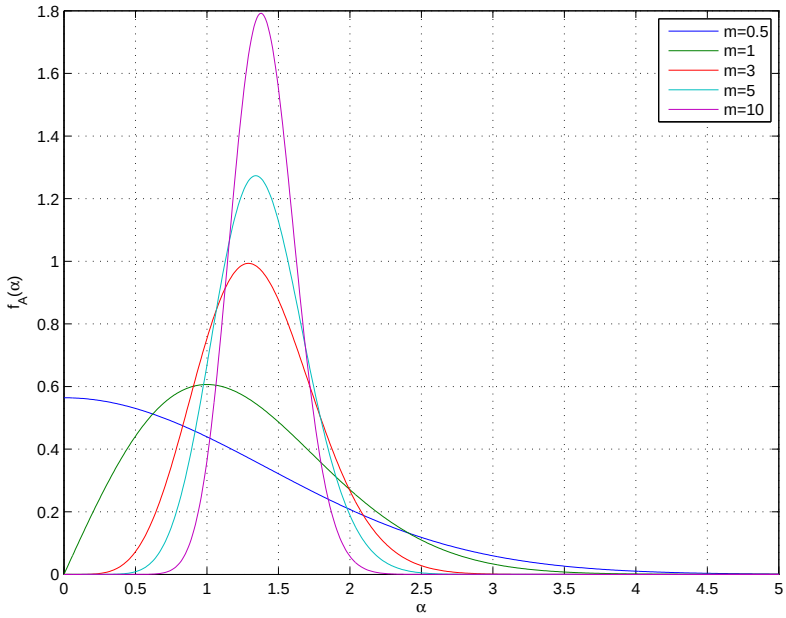

Figure 2.5. Probability density function of Nakagami-*m* fading for different Nakagami parameters.

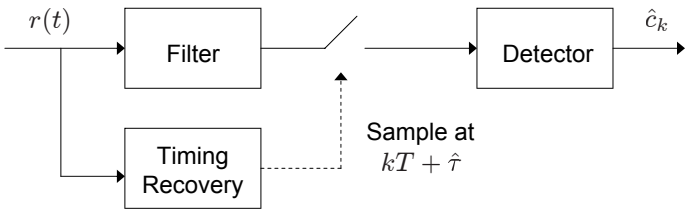

Figure 2.6. The block diagram of a baseband receiver (after [1, Fig. 2.1]).

then

$$\hat{c}_i - c_i = \sum_{i \neq k} c_i g(kT - iT). \tag{2.9}$$

If the pulses satisfy the Nyquist criterion for zero intersymbol interference [2], $g(iT) = 0$ for $i \neq 0$, then this term vanishes and $\hat{c}_i = c_i$. For bandlimited Nyquist pulses even for very small values of timing error, the ISI term could be significant. In order to achieve better performance in recovering the data samples, we should first find an accurate estimate of the timing offset.

Most of the existing algorithms for symbol timing synchronization are derived either through heuristic arguments or by using maximum likelihood (ML) estimations [1]. Examples for the former are early-late detectors (ELD) [45], zero-crossing detectors (ZCD) proposed by Gardner [1], Mueller and Mueller detectors (MMD) [46], the Gardner detector (GAD) [47], and etc.. For a review on the heuristically derived algorithms one can see [12] and [1]. Since the focus of this thesis is on ML-derived synchronizers, we review the previous works done to derive ML synchronizers.

2.2.1 Maximum Likelihood Timing Recovery in ISI-free Systems

One of the well known methods that is widely used to estimate the timing offset of a received signal is the maximum likelihood (ML) method [13]. In [14]–[16] the ML estimator of the timing offset for one symbol interval observation has been derived for binary pulse amplitude modulation (PAM) in the case that the symbol duration is equal to the inverse of sampling rate. The model considered for the received signal in this case is

$$r(t) = x(t, \tau) + n(t) \tag{2.10a}$$

$$x(t, \tau) = \sum_i c_i g(t - iT - \tau) \tag{2.10b}$$

where $n(t)$ is the additive white Gaussian noise (AWGN) with two-sided spectral density equal to $N_0/2$, $g(t)$ is the received pulse shape (a pulse that has a length equal to T), T is the inverse of the sampling rate and τ is the timing offset which can be modeled as an uniformly distributed random variable in $[0, T)$; in this equation, c_i is the ith transmitted data symbol.

In order to derive an ML estimation for τ, one can consider two classes of methods, decision-directed (DD) or data-aided (DA) timing estimators and non-data-aided (NDA) estimators. In the former, the data symbols $\{c_i\}$ are known and can be used to find the timing phase of the received signal. In the latter, the data symbols are not known, however c_i can be modeled as a zero-mean random variable such that for any two transmitted data symbols, $E[c_i c_j] = C\delta(i - j)$, where $E[\cdot]$ denotes the expectation operation, $\delta(\cdot)$ is the Kronecker delta function and C is the energy of each bit.

When the the binary modulated process is characterized over an exact bit interval, T, $x(t,\tau)$ is either equal to $g_1(t,\tau)=g(t)$ or $g_2(t,\tau)=-g(t)$. Using the Karhunen-Loéve (KL) expansion [13], and considering a complete orthonormal basis $\{\psi_i(t)\}$, one has

$$g_k(t,\tau)=\sum_{i=1}^{\infty} g_{ki}(\tau)\psi_i(t) \tag{2.11a}$$

$$g_{ki}(\tau)=\int_{\tau+jT}^{\tau+(j+1)T} g_k(t,\tau)\psi_i(t)dt. \tag{2.11b}$$

Similarly, $r(t)$ and $n(t)$ can be represented using the KL expansion during the interval $[\tau+jT,\tau+(j+1)T)$, conditioned on τ. If the kth signal waveform is received during the one observation period, by denoting the truncated vector representation of these signals by a prime, one has

$$\mathbf{r}'=\mathbf{g}'_k+\mathbf{n}'. \tag{2.12}$$

The maximum likelihood synchronizer criterion is

$$\hat{\tau}=\arg\max_{\tau} P(\mathbf{r}'|\tau) \tag{2.13}$$

where $P(\mathbf{r}'|\tau)$ is the JPDF of vector $\mathbf{r}'$ given τ and can be found by finding the expectation of $P(\mathbf{r}'|\tau,\mathbf{g}'_k)$ over all possible values of $\mathbf{g}'_k$.

Non-Data-Aided Maximum Likelihood Synchronization

In this case, the data symbols are unknown and are modeled as equiprobable random variables. Since the elements of $\mathbf{n}'$ are independent Gaussian random variables, one has

$$P(\mathbf{r}'|\tau,\mathbf{g}'_k)=\prod_{i=1}^{N}\frac{1}{\sqrt{\pi N_0}}\exp\left(-\frac{|r_i-g_{ki}|^2}{N_0}\right)=\frac{1}{(\pi N_0)^{N/2}}\exp\left(-\frac{1}{N_0}\sum_{i=1}^{N}|r_i-g_{ki}|^2\right)$$

where N is the length of the truncated vectors. Having this conditional probability density function (PDF) and considering the fact that the two possible signal waveforms are equiprobable, one can find

$$P(\mathbf{r}'|\tau)=A\sum_{k=1}^{2}\exp\left(-\frac{1}{N_0}\sum_{i=1}^{N}|r_i-g_{ki}|^2\right) \tag{2.14}$$

where A is a constant and therefore has no impact on the location of the maximum of $P(\mathbf{r}'|\tau)$. After some manipulations, one can find the likelihood function $\Lambda(\mathbf{r}'|\tau)$ to be

$$\Lambda(\mathbf{r}'|\tau)=\sum_{k=1}^{2}\exp\left(-\frac{1}{N_0}\sum_{i=1}^{N}|g_{ki}|^2+\frac{2}{N_0}\sum_{i=1}^{N}r_i g_{ki}\right). \tag{2.15}$$

After tending N to infinity, one has

$$\hat{\tau}=\arg\max_{\tau}\sum_{k=1}^{2}\exp\left(-\frac{1}{N_0}\int_{\tau+jT}^{\tau+(j+1)T}|g_k(t,\tau)|^2dt+\frac{2}{N_0}\int_{\tau+jT}^{\tau+(j+1)T}r(t)g_k(t,\tau)dt\right).$$

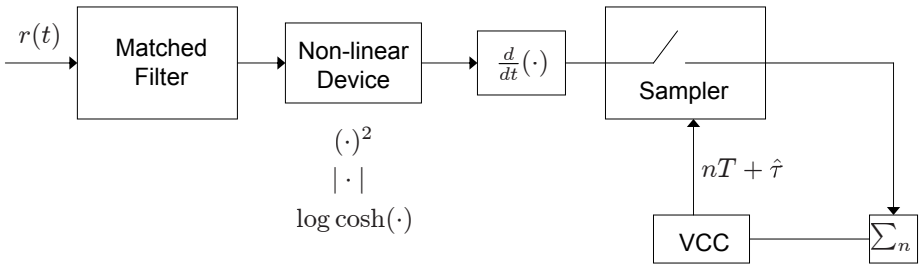

Figure 2.7. The block diagram of NDA ML synchronizer (after [2, Fig. 5.3-2]).

Since $|g_1(t,\tau)|^2 = |g_2(t,\tau)|^2$, $g_1(t,\tau) = g(t)$, $g_2(t,\tau) = -g(t)$, and also for any value of τ the term $\exp\left(-\frac{1}{N_0}\int_{\tau+jT}^{\tau+(j+1)T}|g(t)|^2dt\right)$ is a constant,

$$\hat{\tau} = \arg\max_{\tau}\left[\exp\left(\frac{2}{N_0}\int_{\tau+jT}^{\tau+(j+1)T} r(t)g(t)dt\right) + \exp\left(-\frac{2}{N_0}\int_{\tau+jT}^{\tau+(j+1)T} r(t)g(t)dt\right)\right].$$

Consequently, the NDA ML synchronizer in ISI-free channels for one symbol observation time is equal to

$$\hat{\tau} = \arg\max_{\tau}\cosh\left(\frac{2}{N_0}\int_{\tau+jT}^{\tau+(j+1)T} r(t)g(t)dt\right). \tag{2.16}$$

If we consider an observation time equal to LT, the NDA ML synchronizer can be found directly from (2.16) to be

$$\hat{\tau} = \arg\max_{\tau}\sum_{j=1}^{L}\log\cosh\left(\frac{2}{N_0}\int_{\tau+jT}^{\tau+(j+1)T} r(t)g(t)dt\right). \tag{2.17}$$

Using some approximations, one can simplify the NDA ML synchronizer. Since $\log(\cosh x) \approx \frac{1}{2}x^2$ for small values of x, after some manipulations one can approximate the ML synchronizer with [2]

$$\hat{\tau} = \arg\max_{\tau}\sum_{n} y_n^2(\tau) \tag{2.18a}$$

where

$$y_n(\tau) = \int_T r(t)g(t-nT-\tau)dt. \tag{2.18b}$$

This approximation can be used for small values of signal-to-noise ratio (SNR).

Finding the maximum in 2.18 can be done using the derivation. Since for $\tau = \hat{\tau}$, we have

$$\frac{d}{d\tau}\sum_{n} y_n^2(\tau) = 2\sum_{n} y_n(\tau)\frac{dy_n(\tau)}{d\tau} = 0. \tag{2.19}$$

An implementation of a tracking loop based on the NDA ML synchronizer is shown in Fig. 2.7.

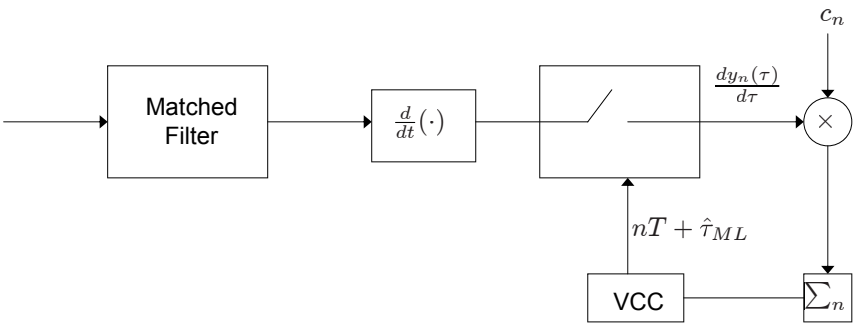

Figure 2.8. The block diagram of DA ML synchronizer (after [2, Fig. 5.3-1]).

Data-Aided Maximum Likelihood Synchronization

In this case, the transmitted data is known at the transmitter. For instance, a training might be transmitted to achieve DA ML synchronization. As a result when $\{\hat{c}_i\}$ is transmitted,

$$P(\mathbf{r}'|\tau) = \frac{1}{(\pi N_0)^{N/2}} \exp\left(-\frac{1}{N_0}\sum_{i=1}^{N}|r_i - \hat{g}_i|^2\right).$$

Consequently, after some manipulations the DA ML synchronizer is

$$\hat{\tau} = \arg\max_{\tau} \Lambda_{DA}(\tau) \tag{2.20a}$$

where

$$\Lambda_{DA}(\tau) = \sum_i c_i \int_T r(t)g(t - iT - \tau)dt. \tag{2.20b}$$

A necessary condition for $\hat{\tau}$ is

$$\frac{d\Lambda_{DA}(\tau)}{d\tau}\ |_{\hat{\tau}} = \sum_n c_n \frac{d}{d\tau}[y_n(\tau)] = 0. \tag{2.21}$$

This result suggests an implementation as shown in Fig. 2.8.

2.2.2 Performance Limits in Symbol Timing Synchronization

A very important question that arises in every estimation problem is, what is the ultimate accuracy that is achievable in the estimation problem. To answer this question, it is needed to establish bounds to the achievable accuracy to provide benchmarks against which the performance of practical synchronizers can be compared. Several bounds have been introduced in the literature. A fundamental lower bound is the Cramer-Rao bound (CRB) [13], [18] which provides a lower bound on the minimum mean square error (MSE) in estimating a random parameter using an unbiased estimator and is widely used in problems of symbol timing synchronization (for some examples see [48] and [49, Ch. 8]).

If λ is the random variable for which we want to find an estimate and $\mathbf{r}$ is the vector representation of the observed waveform, then if $\hat{\lambda}$, be an unbiased estimate for λ, $E[\hat{\lambda} - \lambda] = 0$,

$$E\left[(\hat{\lambda} - \lambda)^2\right] \geqslant \left\{ E_{\mathbf{r}}\left[\left(\frac{\partial \log P(\mathbf{r}|\lambda)}{\partial \lambda} \right)^2 \right] \right\}^{-1} = \left\{ -E_{\mathbf{r}}\left[\frac{\partial^2 \log P(\mathbf{r}|\lambda)}{\partial \lambda^2} \right] \right\}^{-1} \tag{2.22}$$

where $P(\mathbf{r}|\lambda)$ is the probability density function of $\mathbf{r}$ for a given λ and $E[\cdot]$ is the expectation operation. The conditional probability $P(\mathbf{r}|\lambda)$ can be found using

$$P(\mathbf{r}|\lambda) = \int_{-\infty}^{\infty} P(\mathbf{r}|\mathbf{w}, \lambda) P(\mathbf{w}) d\mathbf{w} \tag{2.23}$$

where $\mathbf{w}$ is a vector that contains all the unwanted parameters such as the data, the phase, and the frequency of the received signal. However, the computation of a true CRB is a challenging task in many practical cases. An alternative lower bound that is widely used in the literature is the modified Cramer-Rao bound (MCRB) [1], [19]. The MCRB is defined as

$$\mathrm{MCRB}(\lambda) = \frac{1}{E_{\mathbf{r},\mathbf{w}}\left\{ \left[\frac{\partial \log P(\mathbf{r}|\mathbf{w},\lambda)}{\partial \lambda} \right]^2 \right\}}. \tag{2.24}$$

Although the CRB and MCRB provide useful bounds for moderate to high values of signal-to-noise ratio (SNR), they are known to have some shortcomings particularly at small values of SNR [13], [20], [21]. When the SNR of the received signal decreases, the performance of the synchronizer deteriorates and its MSE increases. However, the minimum MSE cannot become larger than the variance of a uniform distribution, since this is the MSE of a synchronizer that simply picks random values for the timing offset. Therefore, the variance of a uniform distribution is an upper bound on the minimum MSE. However, the MCRB increases without limit as the SNR of the received signal decreases and therefore is not a lower bound of the MSE at small values of SNR. Another lower bound on the MSE of parameter estimators is the detection theory bound (sometimes called Ziv-Zakai bound) was introduced in [22]–[24]. This bound has been used to estimate the random delay of a single deterministic signal [22], [24]. Moreover, in [21] it was used in the symbol timing recovery problem for a received signal consisted of random sequence of pulses in an ISI-free channel. It was shown that this lower bound does not suffer from the shortcoming of the MCRB at small values of SNR, tending to the variance of a uniform distribution.

Chapter 3

Performance of an AFC Loop in the Presence of a Single Interferer in Similar Fading Channels

In a wireless link, multipath fading channels can be modeled in different ways. For instance, if there is not a line-of-sight (LOS) between the transmitter and receiver, the channel is better modeled by a Rayleigh or a Nakagami-*m* distribution. On the other hand, in the case that a LOS exists between the transmitter and receiver, the channel is better modeled by a Rician distribution. In this chapter, the performance of an AFC is investigated in independent non-identically distributed similar channels, i.e., the desired channel and the interference channel are considered to be either Rayleigh/Rayleigh, Rician/Rician, or Nakagami/Nakagami distributed.

3.1 System and Channel Models

The system considered in this chapter consists of two bandpass received signals at the input of an AFC. These signals are modeled as

$$x_i(t) = s_i(t)A_i(t)\cos\left(\omega_i t + \theta_i(t) + \Phi_i(t)\right) \qquad i = 1, 2 \tag{3.1}$$

where $x_1(t)$ is the desired received signal, $x_2(t)$ is the interferer; $s_i(t) \geq 0$ and $\theta_i(t)$ are the base-band transmitted signal and its phase, respectively, which depend on the pulse shape, modulation scheme, and transmitted data; in this model, $A_i(t)$ is a random amplitude process which depends on the channel statistics and represents the effect of multipath fading while $\Phi_i(t)$ is the random phase of the channel modeled in each time instant as an uniformly distributed random variable in $[0, 2\pi)$. Note that ω_i denotes the carrier angular frequency.

The branches are assumed to be independent at each time instant such that A_1 and A_2 are independent as well as their time derivatives, $\dot{A}_1$ and $\dot{A}_2$. The joint statistics of A_i and $\dot{A}_i$ depend on

the power spectral density (PSD) and the moments of the received signals [41]. These moments are defined as

$$c_{in} = (2\pi)^n \int_{f_i - f_{m_i}}^{f_i + f_{m_i}} (f - f_i)^n W_i(f) df, \qquad i = 1, 2 \tag{3.2}$$

where f_i is the carrier frequency, f_{m_i} is the maximum Doppler frequency and $W_i(f)$ is the PSD of the ith unmodulated received signal. If $W_i(f)$ is symmetric around the carrier frequency, A_i and $\dot{A}_i$ are independent at each time instant [41], [50], [51]. In a Rayleigh fading channel, the joint probability density function (JPDF) of A_i and $\dot{A}_i$ is

$$f_{A_i,\dot{A}_i}(\alpha_i, \dot{\alpha}_i) = \frac{\alpha_i}{\sigma_i^2} \exp\left(-\frac{\alpha_i^2}{2\sigma_i^2}\right) \frac{1}{\sqrt{2\pi\dot{\sigma}_i^2}} \exp\left(-\frac{\dot{\alpha}_i^2}{2\dot{\sigma}_i^2}\right) \tag{3.3}$$

where $\sigma_i^2 = c_{i0}$ and $\dot{\sigma}_i^2 = c_{i2}$. In the case that A_i is corrupted by Rician fading,

$$f_{A_i,\dot{A}_i}(\alpha_i, \dot{\alpha}_i) = \frac{\alpha_i}{\sigma_i^2} \exp\left(-\frac{\alpha_i^2 + \mu_i^2}{2\sigma_i^2}\right) I_0\left(\frac{\alpha_i \mu_i}{\sigma_i^2}\right) \frac{1}{\sqrt{2\pi\dot{\sigma}_i^2}} \exp\left(-\frac{\dot{\alpha}_i^2}{2\dot{\sigma}_i^2}\right) \tag{3.4}$$

where $I_0(\cdot)$ is the zero-order modified Bessel function of the first kind [44], μ_i^2 is the power in the line-of-sight (LOS) component and $\sigma_i^2 = c_{i0}$ and $\dot{\sigma}_i^2 = c_{i2}$ for $i = 1, 2$. In the case that A_i is Nakagami distributed with Nakagami fading parameter, m_i, where m_i is an integer or half integer, one has [52]

$$f_{A_i,\dot{A}_i}(\alpha_i, \dot{\alpha}_i) = \frac{2 m_i^{m_i} \alpha_i^{2m_i - 1}}{\Gamma(m_i)(2\sigma_i^2)^{m_i}} \exp\left(-\frac{m_i \alpha_i^2}{2\sigma_i^2}\right) \frac{1}{\sqrt{2\pi\dot{\sigma}_i^2}} \exp\left(-\frac{\dot{\alpha}_i^2}{2\dot{\sigma}_i^2}\right) \tag{3.5}$$

where $\sigma_i^2 = c_{i0}$ and $\dot{\sigma}_i^2 = \frac{c_{i2}}{m_i}$.

3.2 Average Switching Rate

In reference [6, Ch. 19], it has been shown that if the difference between the carrier frequencies of the desired signal and the interferer, $|f_1 - f_2|$, is much smaller than the carrier frequencies and also, the modulations of the received signals are slow compared to $|f_1 - f_2|$, the AFC will lock on the signal with the larger amplitude. These conditions are fulfilled in the case of adjacent-channel interference (ACI), most of the time in the case of abutting-channel interference[1], and sometimes in the case of cochannel interference [6, Ch. 19]. Considering these conditions, one can find the ASR and the MTLL of an AFC using the relative statistics of the received signals.

3.2.1 Method of Analysis

In [7], the average switching rate of an AFC has been found for unmodulated received signals in Rayleigh fading by evaluating the level crossing rate of the ratio of the signals' envelopes, Y. This

[1] In [6], the signals sent in the immediate neighbour channel of the desired signal are called the abutting-channel interference while the signals sent in other adjacent channels of the desired signal are called the adjacent-channel interference

method can also be used for Rayleigh fading with modulated carriers, however, our investigations indicate that this method does not yield tractable solutions for many cases of Rician and Nakagami fading. This method can be described as follows. If the amplitude of the desired signal, s_1A_1, is larger than the amplitude of the interferer, s_2A_2, a jump occurs if s_2A_2 becomes larger than s_1A_1 which is equivalent to $Y = \frac{s_1A_1}{s_2A_2}$ becomes smaller than 1. On the other hand, if $s_1A_1 < s_2A_2$, a jump occurs if s_1A_1 becomes larger than s_2A_2 or equivalently Y becomes larger than 1. Therefore, the ASR is equal to the level crossing rate (positive going plus negative going) of Y through 1, $N_Y(1)$. One has [43]

$$N = N_Y(1) = \int_{-\infty}^{\infty} |\dot{y}| \, f_{Y,\dot{Y}}(1, \dot{y}) d\dot{y} \tag{3.6}$$

where $f_{Y,\dot{Y}}(y, \dot{y})$ is the JPDF of Y and its time derivative, $\dot{Y}$.

The average switching rate can also be found using the random process $Z = s_1A_1 - s_2A_2$. If the AFC is locked on the desired signal, $x_1(t)$, a jump occurs if the amplitude of the interferer, becomes larger than the amplitude of $x_1(t)$, i.e., Z becomes smaller than zero. Similarly, if the AFC is locked on $x_2(t)$, a jump occurs if s_1A_1 becomes larger than s_2A_2, i.e., Z becomes larger than zero. Therefore, the ASR, N, is equivalent to the zero level crossing rate of Z, $N_Z(0)$. One has [43]

$$N = N_Z(0) = \int_{-\infty}^{\infty} |\dot{z}| \, f_{Z,\dot{Z}}(0, \dot{z}) d\dot{z} \tag{3.7}$$

where $f_{Z,\dot{Z}}(z, \dot{z})$ is the JPDF of Z and its time derivative, $\dot{Z}$.

Application to modulated carriers

In the first method, we need to find $f_{Y,\dot{Y}}(y, \dot{y})$. To do that, we first find the JPDF of B_i and $\dot{B}_i$ which are the amplitude of the ith received signal and its time derivative, respectively,

$$B_i = s_i A_i$$
$$\dot{B}_i = s_i \dot{A}_i + \dot{s}_i A_i$$

where $i = 1, 2$. The Jacobian of this transformation is equal to s_i^2. Thus, $f_{B_i,\dot{B}_i}(\beta_i, \dot{\beta}_i)$ can be found with respect to $f_{A_i,\dot{A}_i}(\alpha_i, \dot{\alpha}_i)$ as shown in the following equation,

$$f_{B_i,\dot{B}_i}(\beta_i, \dot{\beta}_i) = \frac{1}{s_i^2} f_{A_i,\dot{A}_i}\left(\frac{\beta_i}{s_i}, \frac{s_i\dot{\beta}_i - \dot{s}_i\beta_i}{s_i^2}\right) \tag{3.8}$$

where $f_{A_i,\dot{A}_i}(\alpha_i, \dot{\alpha}_i)$ is expressed in (3.3-3.5) for different fading scenarios. Note that B_i and $\dot{B}_i$ are not independent in general, however, since the branches are independent,

$$f_{B_1,\dot{B}_1,B_2,\dot{B}_2}(\beta_1, \dot{\beta}_1, \beta_2, \dot{\beta}_2) = f_{B_1,\dot{B}_1}(\beta_1, \dot{\beta}_1) f_{B_2,\dot{B}_2}(\beta_2, \dot{\beta}_2).$$

Now, we can use the transformation

$$B_1 = B_2 Y$$
$$\dot{B}_1 = B_2 \dot{Y} + \dot{B}_2 Y$$
$$B_2 = B_2$$
$$\dot{B}_2 = \dot{B}_2$$

to find

$$f_{B_2,\dot{B}_2,Y,\dot{Y}}(\beta_2, \dot{\beta}_2, y, \dot{y}) = \beta_2^2 f_{B_2,\dot{B}_2,B_1,\dot{B}_1}(\beta_2, \dot{\beta}_2, \beta_2 y, \beta_2 \dot{y} + \dot{\beta}_2 y). \tag{3.9}$$

Then,

$$f_{Y,\dot{Y}}(y, \dot{y}) = \int_0^\infty \int_{-\infty}^\infty f_{B_2,\dot{B}_2,Y,\dot{Y}}(\beta_2, \dot{\beta}_2, y, \dot{y}) d\beta_2 d\dot{\beta}_2. \tag{3.10}$$

Having this JPDF, one can use (3.6) to obtain the average switching rate. This method is used to obtain the ASR of an AFC in Rayleigh/Rayleigh scenario.

In the second method, we first need to find $f_{Z,\dot{Z}}(z, \dot{z})$. Since in the modulated carriers scenario

$$\dot{Z} = s_1 \dot{A}_1 - s_2 \dot{A}_2 + \dot{s}_1 A_1 - \dot{s}_2 A_2, \tag{3.11}$$

$\dot{Z}$ not only depends on the time-derivatives of the fading in the channels, but also depends on the fadings through $\dot{s}_1$ and $\dot{s}_2$. In order to further simplify (3.7), one can use the definition of conditional probability,

$$f_{Z,\dot{Z}}(z, \dot{z}) = f_{\dot{Z}|Z}(\dot{z}|z) f_Z(z),$$

to obtain

$$N = f_Z(0) \int_{-\infty}^\infty |\dot{z}| f_{\dot{Z}|Z}(\dot{z}|0) d\dot{z}. \tag{3.12}$$

The conditional probability density function $f_{\dot{Z}|Z}(\dot{z}|0)$ in (3.12) can be found using the theorem of total probability [42],

$$f_{\dot{Z}|Z}(\dot{z}|0) = \int_0^\infty f_{\dot{Z}|A_2,Z}(\dot{z}|\alpha_2, 0) f_{A_2|Z}(\alpha_2|0) d\alpha_2. \tag{3.13}$$

The conditional PDFs in (3.13) can be found using the definitions of Z and $\dot{Z}$. By substituting A_1 from the definition of Z into (3.11), one has

$$\dot{Z} = s_1 \dot{A}_1 - s_2 \dot{A}_2 + A_2 \left(\frac{\dot{s}_1 s_2}{s_1} - \dot{s}_2 \right) + Z \frac{\dot{s}_1}{s_1} \tag{3.14}$$

where $\dot{s}_i$ is the derivative of s_i with respect to time. It can be seen in Eqs. (3.3)-(3.5) that $\dot{A}_i$ has a Gaussian distribution and is independent of A_i. Therefore if Z and A_2 are given in (3.14), $\dot{Z}$

is equal to the summation of two scaled independent Gaussian random processes and a constant. Consequently,

$$f_{\dot{Z}|A_2,Z}(\dot{z}|\alpha_2,0)=\frac{1}{\sqrt{2\pi\Omega}}\exp\left[\frac{-\left(\dot{z}-\alpha_2\left(\frac{\dot{s}_1 s_2}{s_1}-\dot{s}_2\right)\right)^2}{2\Omega}\right] \tag{3.15}$$

where $\Omega = s_1^2\dot{\sigma}_1^2+s_2^2\dot{\sigma}_2^2$. Using $A_2 = \frac{s_1}{s_2}A_1-\frac{1}{s_2}Z$ and the fundamental transformation theorem [42], one can derive

$$f_{A_2|Z}(\alpha_2|0) = \frac{s_2}{s_1}f_{A_1}\left(\frac{s_2}{s_1}\alpha_2\right). \tag{3.16}$$

In order to find the average switching rate, one still needs to find $f_Z(0)$. $f_Z(z)$ can be found using the transformation

$$Z = s_1A_1 - s_2A_2$$

$$\Delta = s_1A_1.$$

The Jacobian of this transformation is equal to s_1s_2; hence

$$f_{\Delta,Z}(\delta,z) = \frac{1}{s_1s_2}f_{A_1}\left(\frac{\delta}{s_1}\right)f_{A_2}\left(\frac{\delta-z}{s_2}\right)$$

and consequently

$$f_Z(0) = \int_{\delta=0}^{\infty}\frac{1}{s_1s_2}f_{A_1}\left(\frac{\delta}{s_1}\right)f_{A_2}\left(\frac{\delta}{s_2}\right)dy. \tag{3.17}$$

Then, the ASR can be found using (3.12)-(3.17). This method is used to find the ASR in Rician/Rician and Nakagami/Nakagami scenarios in this chapter.

Previous work has considered exclusively unmodulated carriers. An interesting result that obtains for modulated carriers is the following. Considering Eq. (3.15), it can be seen that in general, $f_{\dot{Z}|A_2,Z}(\dot{z}|\alpha_2,0)$ and consequently $f_{\dot{Z},Z}(\dot{z},0)$ are not even functions of $\dot{z}$. As a result, the short-term positive-going zero-crossing rate (PZCR) and negative-going zero-crossing rate (NZCR) of Z are not equal, i.e.,

$$\int_0^{\infty}\dot{z}f_{Z,\dot{Z}}(0,\dot{z})d\dot{z} \neq \int_{-\infty}^{0}|\dot{z}|\,f_{Z,\dot{Z}}(0,\dot{z})d\dot{z} \tag{3.18}$$

in contrast to the case of unmodulated carriers. However, since we deal with practical scenarios in which the sign of $\dot{s}_1s_2-\dot{s}_2s_1$ changes with respect to time, in some time periods NZCR$>$PZCR and in others NZCR$\leq$PZCR and therefore this behaviour does not cause any problem in the long term. In the special case that the baseband transmitted signals are replicas of each other, $s_1(t) = ks_2(t)$ where k is a constant, one has

$$N=f_Z(0)\int_{-\infty}^{\infty}|\dot{z}|\frac{1}{\sqrt{2\pi\Omega}}\exp\left(-\frac{\dot{z}^2}{2\Omega}\right)d\dot{z}=\sqrt{\frac{2\Omega}{\pi}}f_Z(0) \tag{3.19}$$

where $f_Z(0)$ can be obtained using (3.17). Note that Eq. (3.19) is also applicable to the scenario of unmodulated received signals, i.e., $s_1 = s_2 = 1$.

3.3 Mean Time to Loss of Lock

The MTLL is a measure that shows the average time that an AFC locks on the desired signal before jumping to the interferer. The MTLL for unmodulated signals in fading channels can be found using [53]

$$T = \frac{2F}{N} \tag{3.20}$$

where N is the ASR of the AFC and F is the probability that the amplitude of the desired signal is larger than the amplitude of the interferer, i.e., $F = Pr[s_1A_1 > s_2A_2]$. In order to find this probability, we can use the transformation

$$Y = \frac{s_1A_1}{s_2A_2}$$
$$T = s_2A_2.$$

The Jacobian of this transformation is equal to $\frac{s_1s_2}{t}$, consequently

$$f_{Y,T}(y,t) = \frac{t}{s_1s_2} f_{A_1,A_2}\left(\frac{yt}{s_1}, \frac{t}{s_2}\right). \tag{3.21}$$

Since A_1 and A_2 are independent (for a fixed time), integrating (3.21) over t yields

$$f_Y(y) = \int_0^\infty \frac{t}{s_1s_2} f_{A_1}\left(\frac{yt}{s_1}\right) f_{A_2}\left(\frac{t}{s_2}\right) dt \tag{3.22}$$

and therefore $F = Pr[s_1A_1 > s_2A_2] = Pr[Y > 1]$ can be obtained using

$$F = \int_{y=1}^\infty \int_{t=0}^\infty \frac{t}{s_1s_2} f_{A_1}\left(\frac{ty}{s_1}\right) f_{A_2}\left(\frac{t}{s_2}\right) dtdy. \tag{3.23}$$

3.4 Derivation of the Results

In this part we apply the methods described in the previous sections to different channels to derive the ASR and MTLL of an AFC.

3.4.1 ASR and MTLL in Rayleigh/Rayleigh scenario

Rayleigh/Rayleigh scenario represents the case in which there is not a line-of-sight (LOS) between the transmitter and receiver in both channels, i.e., interference channel and desired channel, and the fading in these channels can be modeled using a Rayleigh distribution. In this scenario, we use (3.6)

to find the ASR. By integrating (3.9) over $\dot{\beta}_2$ from $-\infty$ to ∞,

$$f_{B_2,Y,\dot{Y}}(\beta_2,y,\dot{y}) = \frac{1}{\sqrt{2\pi}s_1^2s_2^2\sigma_1^2\sigma_2^2}\frac{y}{\sqrt{y^2s_2^2\dot{\sigma}_2^2+s_1^2\dot{\sigma}_1^2}}\beta_2^4\exp\left(-\frac{\beta_2^2C(y,\dot{y})}{2}\right) \tag{3.24a}$$

where

$$C(y,\dot{y}) = y^2\left(\frac{1}{s_1^2\sigma_1^2}+\frac{\dot{s}_1^2}{s_1^4\dot{\sigma}_1^2}\right)+\frac{1}{s_2^2\sigma_2^2}+\frac{\dot{s}_2^2}{s_2^4\dot{\sigma}_2^2}+\frac{\dot{y}^2}{s_1^2\dot{\sigma}_1^2}-\frac{2\dot{s}_1y\dot{y}}{s_1^3\dot{\sigma}_1^2} \\ -\frac{(s_1s_2^3y\dot{y}\dot{\sigma}_2^2-\dot{s}_1s_2^3y^2\dot{\sigma}_2^2-\dot{s}_2s_1^3\dot{\sigma}_1^2)^2}{s_1^4\dot{\sigma}_1^2s_2^4\dot{\sigma}_2^2(y^2s_2^2\dot{\sigma}_2^2+s_1^2\dot{\sigma}_1^2)}. \tag{3.24b}$$

By integrating (3.24) over β_2 using [54, (3.381.11)],

$$\int_0^\infty x^4e^{-cx^2}dx = \frac{\Gamma(\frac{5}{2})}{c^{\frac{5}{2}}} \tag{3.25a}$$

where c is a constant, one can find the JPDF of Y and $\dot{Y}$,

$$f_{Y,\dot{Y}}(y,\dot{y}) = \frac{3}{2s_1^2s_2^2\sigma_1^2\sigma_2^2}\frac{y}{\sqrt{y^2s_2^2\dot{\sigma}_2^2+s_1^2\dot{\sigma}_1^2}}C(y,\dot{y})^{-5/2}. \tag{3.26}$$

Since we only need $f_{Y,\dot{Y}}(1,\dot{y})$ to find the ASR,

$$f_{Y,\dot{Y}}(1,\dot{y}) = \frac{3}{2s_1^2s_2^2\sigma_1^2\sigma_2^2}\frac{\sqrt{d_3}}{(d_3\dot{y}^2+2d_2\dot{y}+d_1)^{5/2}} \tag{3.27a}$$

where

$$d_1 = \left(\frac{1}{\sigma_1^2s_1^2}+\frac{1}{\sigma_2^2s_2^2}+\frac{(\dot{s}_2s_1-\dot{s}_1s_2)^2}{s_1^2s_2^2(s_2^2\dot{\sigma}_2^2+s_1^2\dot{\sigma}_1^2)}\right) \tag{3.27b}$$

$$d_2 = \frac{\dot{s}_2s_1-\dot{s}_1s_2}{s_1s_2(s_2^2\dot{\sigma}_2^2+s_1^2\dot{\sigma}_1^2)} \tag{3.27c}$$

$$d_3 = \frac{1}{s_2^2\dot{\sigma}_2^2+s_1^2\dot{\sigma}_1^2}. \tag{3.27d}$$

Note that in these equations, s_1 and s_2 are time-dependent. Now, we can use (3.6) to find the ASR. The result is

$$N = N_Y(1) = M\frac{\sqrt{d_3}(d_1d_3+d_2^2)}{\sqrt{d_1}(d_1d_3-d_2^2)^2} \tag{3.28a}$$

if

$$|d_2| < \sqrt{d_1d_3} \tag{3.28b}$$

where

$$M = \frac{1}{s_1^2s_2^2\sigma_1^2\sigma_2^2}. \tag{3.28c}$$

In order to find this result, [54, (3.252.7)] has been used,

$$\int_0^\infty \frac{x^ndx}{(ax^2+2bx+c)^{n+\frac{3}{2}}} = \frac{n!}{(2n+1)!!\sqrt{c}(\sqrt{ac}+b)^{n+1}}, \tag{3.29}$$

Table 3.1. The average switching rate of an AFC in Rayleigh/Rayleigh fading channels.

Fading	System Model	Average Switching Rate
Rayleigh	i.i.d. $s_1 = s_2 = 1$	$\frac{\dot{\sigma}}{2\sigma}$
Rayleigh	i.n.d. $s_1 = s_2 = 1$	$\frac{\sqrt{\sigma_1^2\sigma_2^2(\dot{\sigma}_2^2+\dot{\sigma}_1^2)}}{(\sigma_2^2+\sigma_1^2)^{3/2}}$
Rayleigh	i.n.d. $s_1(t) = ks_2(t)$	$\frac{\sqrt{k^2\sigma_1^2\sigma_2^2(\dot{\sigma}_2^2+k^2\dot{\sigma}_1^2)}}{(\sigma_2^2+k^2\sigma_1^2)^{3/2}}$
Rayleigh	i.n.d. modulated	$M\frac{\sqrt{d_3}(d_1d_3+d_2^2)}{\sqrt{d_1}(d_1d_3-d_2^2)^2}$

where a, b, and c are constants such that $a \geq 0$, $c > 0$, and $b > -\sqrt{ac}$. Evaluating the condition in (3.28b) requires knowledge of $s_1(t)$ and $s_2(t)$, however, in the special case that the data in the interferer is a replica of the data in the desired signal with different power, i.e., $s_1(t) = ks_2(t)$, d_2 equals zero and therefore the condition in (3.28b) is clearly satisfied. In this case,

$$N = \frac{\sqrt{k^2\sigma_1^2\sigma_2^2(\dot{\sigma}_2^2 + k^2\dot{\sigma}_1^2)}}{(\sigma_2^2 + k^2\sigma_1^2)^{3/2}}. \tag{3.30}$$

Note that the ASR in the unmodulated carrier scenario is a special case of this equation in which $k = 1$. In this case that signals experience i.n.d. Rayleigh fading and $s_1 = s_2 = 1$, the ASR equals $N = \frac{\sqrt{\sigma_1^2\sigma_2^2(\dot{\sigma}_2^2+\dot{\sigma}_1^2)}}{(\sigma_2^2+\sigma_1^2)^{3/2}}$ which is the same as the result previously reported in [7], as expected. Final expressions for the ASR in this scenarios are summarized in Table 3.1 for different cases.

In order to find the MTLL in the Rayleigh/Rayleigh scenario for unmodulated signals, we still need to find F. Using (3.23) and [54, (3.461.3)],

$$\int_0^\infty x^{2n+1}e^{-px^2}dx = \frac{n!}{2p^{n+1}} \tag{3.31}$$

for $p > 0$, one can find

$$F = \int_1^\infty \frac{2y}{s_1^2s_2^2\sigma_1^2\sigma_2^2}\left(\frac{y^2}{s_1^2\sigma_1^2} + \frac{1}{s_2^2\sigma_2^2}\right)^{-2}dy = \frac{s_1^2\sigma_1^2}{s_1^2\sigma_1^2 + s_2^2\sigma_2^2} \tag{3.32}$$

where s_1 and s_2 only represent the power of the transmitted signals and are not functions of time. As a result, $s_1 = ks_2$, and

$$T = 2\sqrt{\frac{\sigma_1^2(\sigma_2^2 + k^2\sigma_1^2)}{\sigma_2^2(\dot{\sigma}_2^2 + k^2\dot{\sigma}_1^2)}}. \tag{3.33}$$

Note that in the special case of Rayleigh fading and unmodulated carriers with same power, the MTLL equals $T = 2\sqrt{\frac{\sigma_1^2(\sigma_2^2+\sigma_1^2)}{\sigma_2^2(\dot{\sigma}_2^2+\dot{\sigma}_1^2)}}$ which agrees with the result reported in [7].

Table 3.2. The average switching rate of an AFC in Rician/Rician fading channels.

Fading	System Model	Average Switching Rate
Rician	i.i.d $s_1 = s_2 = 1$	$\frac{\dot{\sigma}}{2\sigma} \exp\left(-\frac{\mu^2}{\sigma^2}\right) {}_2F_2\left(\frac{1}{2}, \frac{3}{2}; 1, 1; \frac{\mu^2}{\sigma^2}\right)$
Rician	i.n.d. $s_1(t) = ks_2(t)$	$\int_0^\infty t^2 \exp\left[\frac{-t^2}{2s_2^2}\left(\frac{\sigma_1^2k^2+\sigma_2^2}{k^2\sigma_1^2\sigma_2^2}\right) - \frac{\mu_1^2}{2\sigma_1^2} - \frac{\mu_2^2}{2\sigma_2^2}\right]$ $\times \frac{\sqrt{2(\dot{\sigma}_2^2+k^2\dot{\sigma}_1^2)}}{\sqrt{\pi}s_2^3k^2\sigma_1^2\sigma_2^2} I_0\left(\frac{\mu_1 t}{\sigma_1^2 k s_2}\right) I_0\left(\frac{\mu_2 t}{\sigma_2^2 s_2}\right) dt$
Rician	i.n.d. modulated	$\int_0^\infty t^2 \exp\left[-\frac{t^2+2\mu_1^2s_1^2}{2\sigma_1^2s_1^2} - \frac{t^2+\mu_2^2s_2^2}{2\sigma_2^2s_2^2}\right]$ $\times \frac{1}{s_1^4\sigma_1^4\sigma_2^2} I_0\left(\frac{\mu_1 t}{\sigma_1^2 s_1}\right) I_0\left(\frac{\mu_2 t}{\sigma_2^2 s_2}\right) dt$ $\times \int_{-\infty}^\infty \int_0^\infty \exp\left[-\frac{\left(\dot{z}-\alpha_2\left(\frac{\dot{s}_1 s_2}{s_1}-\dot{s}_2\right)\right)^2}{2(s_2^2\dot{\sigma}_2^2+s_1^2\dot{\sigma}_1^2)} - \frac{\alpha_2^2 s_2^2}{2s_1^2\sigma_1^2}\right]$ $\times \frac{\lvert\dot{z}\rvert\alpha_2}{\sqrt{2\pi(s_2^2\dot{\sigma}_2^2+s_1^2\dot{\sigma}_1^2)}} I_0\left(\frac{s_2\alpha_2\mu_1}{s_1\sigma_1^2}\right) d\alpha_2 d\dot{z}$

3.4.2 ASR and MTLL in Rician/Rician scenario

In this case, one can find the ASR using (3.12)-(3.17),

$$N = \frac{s_2^2}{s_1^2\sigma_1^2} \frac{f_Z(0)}{\sqrt{2\pi\Omega}} \int_{-\infty}^{\infty}\int_0^\infty |\dot{z}|\alpha_2 I_0\left(\frac{s_2\alpha_2\mu_1}{s_1\sigma_1^2}\right) \exp\left[-\frac{\left(\dot{z}-\alpha_2\left(\frac{\dot{s}_1 s_2}{s_1}-\dot{s}_2\right)\right)^2}{2(s_2^2\dot{\sigma}_2^2+s_1^2\dot{\sigma}_1^2)} - \frac{\alpha_2^2s_2^2+\mu_1^2s_1^2}{2s_1^2\sigma_1^2}\right] d\alpha_2 d\dot{z} \tag{3.34a}$$

where using (3.17)

$$f_Z(0) = \frac{1}{s_1^2s_2^2\sigma_1^2\sigma_2^2} \int_0^\infty t^2 \exp\left[-\frac{t^2+\mu_1^2s_1^2}{2\sigma_1^2s_1^2} - \frac{t^2+\mu_2^2s_2^2}{2\sigma_2^2s_2^2}\right] I_0\left(\frac{\mu_1 t}{\sigma_1^2 s_1}\right) I_0\left(\frac{\mu_2 t}{\sigma_2^2 s_2}\right) dt. \tag{3.34b}$$

The average switching rate in (3.34) can be evaluated numerically, however, further simplifications can be utilized to find a closed-form expression. If s_1 and s_2 are replicas of each other with different powers, i.e., $s_1(t) = ks_2(t)$, the ASR is equal to $\sqrt{\frac{2\Omega}{\pi}} f_Z(0)$ where $f_Z(0)$ is given in (3.34b). A closed-form expression can be found for $f_Z(0)$ and consequently for N, when the branches experience independent, identically distributed (i.i.d.) Rician fading and $k = 1$, i.e., the transmitted data in the branches are equal. In this case, one can use [54, (6.633.5)] and [54, (9.14.1)] to obtain

$$N = \frac{\dot{\sigma}}{2\sigma} \exp\left(-\frac{\mu^2}{\sigma^2}\right) {}_2F_2\left(\frac{1}{2}, \frac{3}{2}; 1, 1; \frac{\mu^2}{\sigma^2}\right) \tag{3.35}$$

where ${}_pF_q(g_1, g_2, \cdots, g_p; h_1, h_2, \cdots, h_q; \cdot)$ is the hypergeometric function [44], $\sigma^2 = \sigma_1^2 = \sigma_2^2$, $\dot{\sigma}^2 = \dot{\sigma}_1^2 = \dot{\sigma}_2^2$ and $\mu = \mu_1 = \mu_2$. The results are summarized in Table (3.2).

In order to find F and consequently the MTLL, one can employ (3.23),

$$F=\int_{r=1}^{\infty}\int_{t=0}^{\infty}\exp\left[-\frac{t^2}{2}\left(\frac{r^2}{\sigma_1^2 s_1^2}+\frac{1}{\sigma_2^2 s_2^2}\right)-\frac{\mu_1^2}{2\sigma_1^2}-\frac{\mu_2^2}{2\sigma_2^2}\right]\frac{t^3 r}{s_1^2 s_2^2\sigma_1^2\sigma_2^2}I_0\left(\frac{tr\mu_1}{\sigma_1^2 s_1}\right)I_0\left(\frac{t\mu_2}{\sigma_2^2 s_2}\right)dtdr. \tag{3.36}$$

The MTLL can be found using (3.36) and the ASR previously found in this section. In the case of i.n.d. channels and unmodulated carriers with different powers, $s_1 = ks_2$, one has

$$T=\int_{r=1}^{\infty}\int_{x=0}^{\infty}\frac{x^3 r}{s_2}\exp\left[-\frac{x^2}{2s_2^2}\left(\frac{r^2}{\sigma_1^2k^2}+\frac{1}{\sigma_2^2}\right)\right]\frac{\sqrt{2\pi}}{\left(\dot{\sigma}_2^2+k^2\dot{\sigma}_1^2\right)^{1/2}}I_0\left(\frac{xr\mu_1}{\sigma_1^2 ks_2}\right)I_0\left(\frac{x\mu_2}{\sigma_2^2 s_2}\right)dxdr$$
$$\times\left[\int_0^{\infty}t^2\exp\left(-\frac{t^2(k^2\sigma_1^2+\sigma_2^2)}{2s_2^2k^2\sigma_1^2\sigma_2^2}\right)I_0\left(\frac{\mu_1 t}{\sigma_1^2 ks_2}\right)I_0\left(\frac{\mu_2 t}{\sigma_2^2 s_2}\right)dt\right]^{-1}. \tag{3.37}$$

In the special case that the channels are i.i.d. and $s_1 = s_2 = 1$,

$$T=\int_1^{\infty}\int_0^{\infty}\frac{4t^3 r}{\sigma^3\dot{\sigma}}\left[{}_2F_2\left(\frac{1}{2},\frac{3}{2};1,1;\frac{\mu^2}{\sigma^2}\right)\right]^{-1}\exp\left[\frac{-t^2(r^2+1)}{2\sigma^2}\right]I_0\left(\frac{tr\mu}{\sigma^2}\right)I_0\left(\frac{t\mu}{\sigma^2}\right)dtdr. \tag{3.38}$$

3.4.3 ASR and MTLL in Nakagami/Nakagami scenario

In this scenario, using (3.12)-(3.17) one obtains

$$N=f_Z(0)\left(\frac{s_2}{s_1}\right)^{2m_1}\frac{\Gamma(2m_1)m_1^{m_1}}{\Gamma(m_1)(2\sigma_1^2)^{m_1}}\frac{2\gamma^{-m_1}}{\sqrt{2\pi\Omega}}\int_{-\infty}^{\infty}|\dot{z}|\exp\left(-\frac{2\Omega\gamma-\eta^2}{4\Omega^2\gamma}\dot{z}^2\right)D_{-2m_1}\left(-\frac{\eta\dot{z}}{\Omega\sqrt{\gamma}}\right)d\dot{z} \tag{3.39a}$$

where

$$f_Z(0)=\frac{\sqrt{2}\Gamma(m_1+m_2-\frac{1}{2})}{\Gamma(m_1)\Gamma(m_2)}\left(\frac{m_1}{\sigma_1^2 s_1^2}\right)^{m_1}\left(\frac{m_2}{\sigma_2^2 s_2^2}\right)^{m_2}\left(\frac{m_1}{\sigma_1^2 s_1^2}+\frac{m_2}{\sigma_2^2 s_2^2}\right)^{-(m_1+m_2-\frac{1}{2})} \tag{3.39b}$$

$$\gamma=\frac{\eta^2}{\Omega}+\frac{m_1}{\sigma_1^2}\left(\frac{s_2}{s_1}\right)^2 \tag{3.39c}$$

$$\eta=\frac{s_2}{s_1}\dot{s}_1-\dot{s}_2 \tag{3.39d}$$

and where $D_p(\cdot)$ is the parabolic cylinder function [44]. To obtain these results we have used [54, (3.462.1)],

$$\int_0^{\infty}x^{p-1}e^{-ax^2-bx}dx=(2a)^{-p/2}\Gamma(p)\exp\left(\frac{b^2}{8a}\right)D_{-p}\left(\frac{b}{\sqrt{2a}}\right), \tag{3.40}$$

and [54, (3.381.11)],

$$2\int_0^{\infty}x^{2m}e^{-ax^{2n}}dx=\frac{\Gamma(\nu)}{na^{\nu}}, \tag{3.41}$$

where $\nu=\frac{2m+1}{2n}$. In the special case that $s_1(t) = ks_2(t)$, the ASR is equal to $\sqrt{\frac{2\Omega}{\pi}}f_Z(0)$ where $f_Z(0)$ is given in (3.39b). ASR of an AFC in Nakagami/Nakagami fading channels are presented in Table (3.3).

Table 3.3. The average switching rate of an AFC in Nakagami/Nakagami fading channels.

Fading	System Model	Average Switching Rate
Nakagami	i.i.d. $s_1 = s_2 = 1$	$\sqrt{\frac{m}{\pi c_0}} \frac{\dot{\sigma}\Gamma(2m-\frac{1}{2})}{2^{2(m-1)}\Gamma^2(m)}$
Nakagami	i.n.d. $s_1(t) = ks_2(t)$	$\frac{2\Gamma(m_1+m_2-\frac{1}{2})}{\sqrt{\pi}\Gamma(m_1)\Gamma(m_2)} \left(\frac{m_1}{\sigma_1^2 k^2}\right)^{m_1} \left(\frac{m_2}{\sigma_2^2}\right)^{m_2}$ $\times \left(\frac{m_1}{\sigma_1^2 k^2} + \frac{m_2}{\sigma_2^2}\right)^{-m_1-m_2+\frac{1}{2}} \sqrt{\dot{\sigma}_2^2 + k^2\dot{\sigma}_1^2}$
Nakagami	i.n.d. modulated	$\frac{2\Gamma(2m_1)\Gamma(m_1+m_2-\frac{1}{2})}{\Gamma^2(m_1)\Gamma(m_2)\sqrt{\pi\Omega}} \left(\frac{m_2}{\sigma_2^2 s_2^2}\right)^{m_2} \left(\frac{s_2^2 m_1^2}{2s_1^4\sigma_1^4\gamma}\right)^{m_1}$ $\times \left(\frac{m_1}{\sigma_1^2 s_1^2} + \frac{m_2}{\sigma_2^2 s_2^2}\right)^{-(m_1+m_2-\frac{1}{2})}$ $\times \int_{-\infty}^{\infty} \lvert\dot{z}\rvert \exp\left(\frac{\eta^2-2\Omega\gamma}{4\Omega^2\gamma}\dot{z}^2\right) D_{-2m_1}\left(\frac{-\eta\dot{z}}{\Omega\sqrt{\gamma}}\right) d\dot{z}$

By employing (3.23) and after some manipulations, one can use [54, (3.194.2)],

$$\int_u^\infty \frac{x^{\mu-1}dx}{(1+\beta x)^\nu} = \frac{u^{\mu-\nu}}{\beta^\nu(\nu-\mu)} \, {}_2F_1\left(\nu, \nu-\mu; \nu-\mu+1; -\frac{1}{\beta u}\right) \tag{3.42}$$

to obtain

$$F = \frac{\Gamma(m_1+m_2)}{m_2\Gamma(m_1)\Gamma(m_2)} \left(\frac{s_1^2 m_2 \sigma_1^2}{s_2^2 m_1 \sigma_2^2}\right)^{m_2} \times {}_2F_1\left(m_1+m_2, m_2; m_2+1; -\frac{s_1^2 m_2 \sigma_1^2}{s_2^2 m_1 \sigma_2^2}\right). \tag{3.43}$$

Consequently, the MTLL can be found using (3.20). If the channels are i.n.d. and the received signals are unmodulated with different powers, $s_1 = ks_2$,

$$T = \frac{\sqrt{\pi}\,\Gamma(m_1+m_2)}{m_2\Gamma(m_1+m_2-\frac{1}{2})} \left(\frac{\sigma_1^2 k^2}{m_1}\right)^{m_1+m_2} \left(\frac{m_1}{\sigma_1^2 k^2} + \frac{m_2}{\sigma_2^2}\right)^{m_1+m_2-\frac{1}{2}}$$
$$\times (\dot{\sigma}_2^2 + k^2\dot{\sigma}_1^2)^{-1} \, {}_2F_1\left(m_1+m_2, m_2; m_2+1; -\frac{k^2 m_2 \sigma_1^2}{m_1 \sigma_2^2}\right). \tag{3.44}$$

In the special case of i.i.d. channels and unmodulated signals with the same power,

$$T = \frac{\sqrt{\pi}\sigma}{m^{3/2}\dot{\sigma}} \frac{\Gamma(2m)2^{2m-1}}{\Gamma(2m-\frac{1}{2})} \, {}_2F_1\left(2m, m; m+1; -1\right). \tag{3.45}$$

3.5 Numerical Examples and Discussion

In the numerical examples, we focus on the important special case of two-dimensional (2-D) isotropic scattering and an omnidirectional receiving antenna. In this case, $\dot{\sigma}_i^2 = 2\pi^2 f_{m_i}^2 \sigma_i^2$ where f_{m_i} is the maximum Doppler frequency [50]. The signals are assumed to be unmodulated where $s_1 = s_2 = 1$. Moreover, it is assumed that $f_{m_1} = f_{m_2} = f_m$.

Fig. 3.1 shows the ASR of an AFC (normalized to f_m) versus the signal-to-interference ratio (SIR) in a Rician fading channel for different Rice factors, $K_i = \frac{\mu_i^2}{2\sigma_i^2}$. The SIR is the ratio

of the desired signal's average power to the interfering signal's average power given as SIR $= 10\log_{10}\left(\frac{\sigma_1^2}{\sigma_2^2}\left(\frac{1+K_1}{1+K_2}\right)\right)$ for Rician fading. Note that the special case when $K_1 = K_2 = 0$ is equivalent to the Rayleigh fading scenario. As can be seen in this figure, if the desired signal and the interferer have equal Rice factors, the worst case (maximum ASR) happens when the signals have equal powers. The reason is that in this case, the channels will be completely similar and therefore an AFC does not have any tendency to choose either signal. However, if the power in one branch is larger, the AFC locks on that branch for a longer period of time and therefore the ASR decreases. By increasing the Rice factor in both branches (for instance compare $K_1 = K_2 = 0$ to $K_1 = K_2 = 5$), the performance improves in the sense that the ASR decreases. The reason for this behaviour is that for a specific value of SIR, increasing the Rice factor is equivalent to increasing the power in the deterministic part of the fading (LOS component) compared to the random part of the fading (scattering component) which decreases the ASR. Note that in the boundary case that the Rice factors tend to infinity, the amplitudes of both branches are deterministic (constant amplitudes in the case of unmodulated carriers) and the AFC locks on the signal with more power and there will be no switching. In addition, this figure shows that for a constant Rice factor in the interference branch, increasing the Rice factor of the desired branch causes the ASR to decrease (i.e., an improvement in the performance) for larger values of SIR, while it does not have a significant effect on the ASR for small values of SIR. The reason for this behaviour is that for larger values of SIR, the characteristics of the desired branch determine the behaviour of the ASR curve while in the region where the power of the interferer is larger, the Rice factor of the interference branch is the dominant factor.

Fig. 3.2 shows similar results for Nakagami fading and different values of m_1 and m_2. In this case, SIR $= 10\log_{10}\left(\frac{\sigma_1^2}{\sigma_2^2}\right)$. Note that $m_1 = m_2 = 1$ is equivalent to the Rayleigh fading scenario. Comparing the ASR curves for a similar Nakagami fading parameter in the interference branch, $m_2 = 1$, shows that at small values of SIR where the power of the interferer dominates the power of the desired signal, the performance of AFC for different values of m_1 is almost the same. This is because in this region, m_2 has the greatest effect on the behaviour of the ASR curve. However, when the power of the desired signal increases compared to the power of the interferer, AFC has better performance for larger values of m_1.

By considering a specific curve in these figures, for instance $K_1 = K_2 = 0$, it can be seen that decreasing the SIR in the small SIR region, improves the performance of the AFC which might seem surprising. However, one should keep in mind that although the ASR decreases as the SIR decreases in this region, the AFC is locked on the interferer rather than the desired signal for most of the time and therefore the output of the AFC is not very reliable.

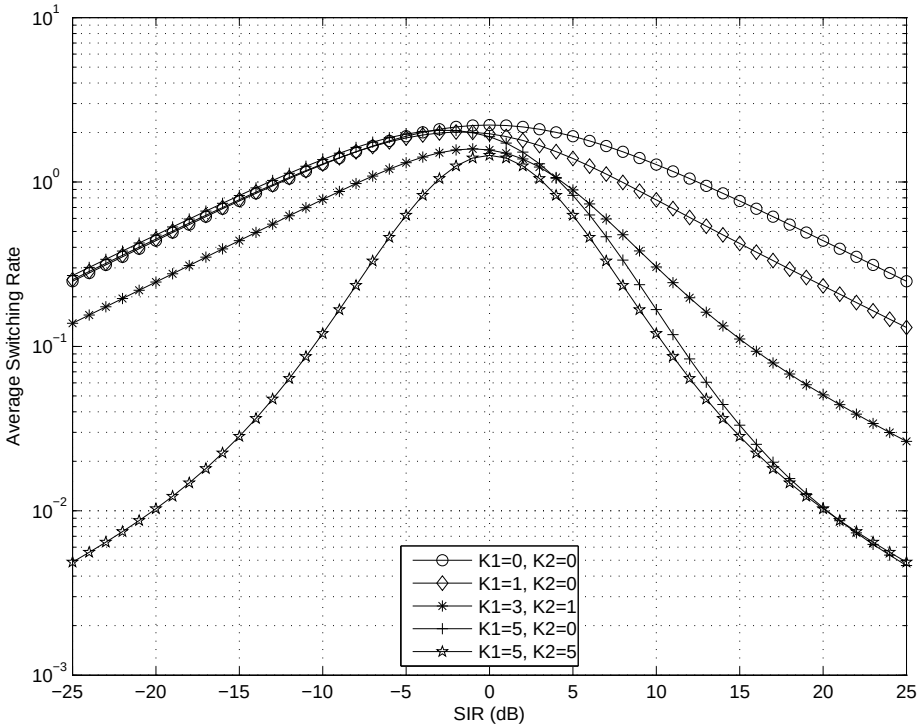

Figure 3.1. The average switching rates of an AFC (normalized to f_m) in a Rician fading scenario for different values of K_1 and K_2.

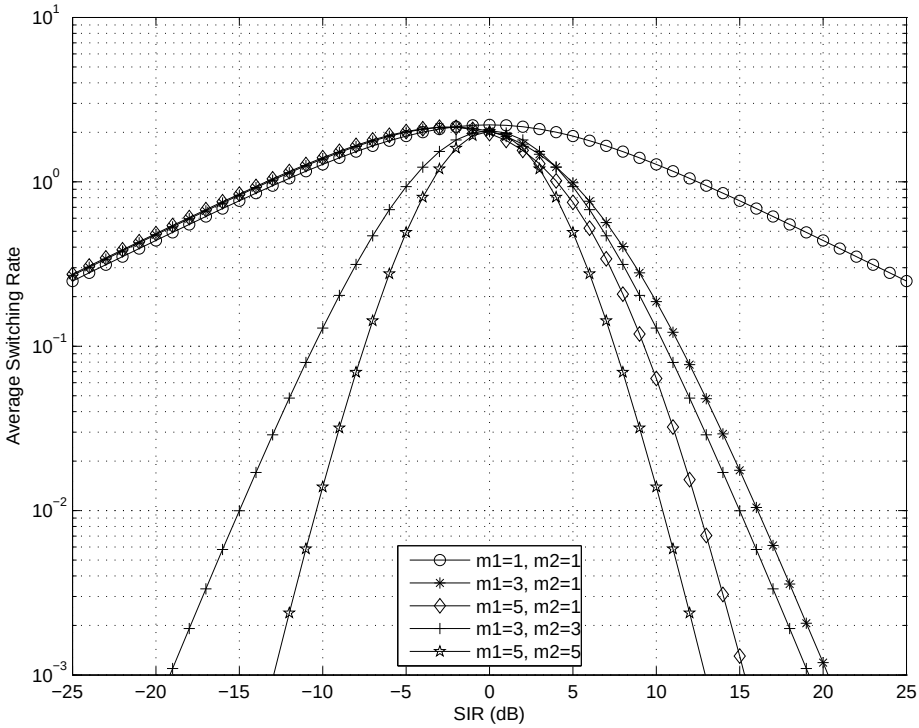

Figure 3.2. The average switching rates of an AFC (normalized to f_m) in a Nakagami fading scenario for different values of m_1 and m_2.

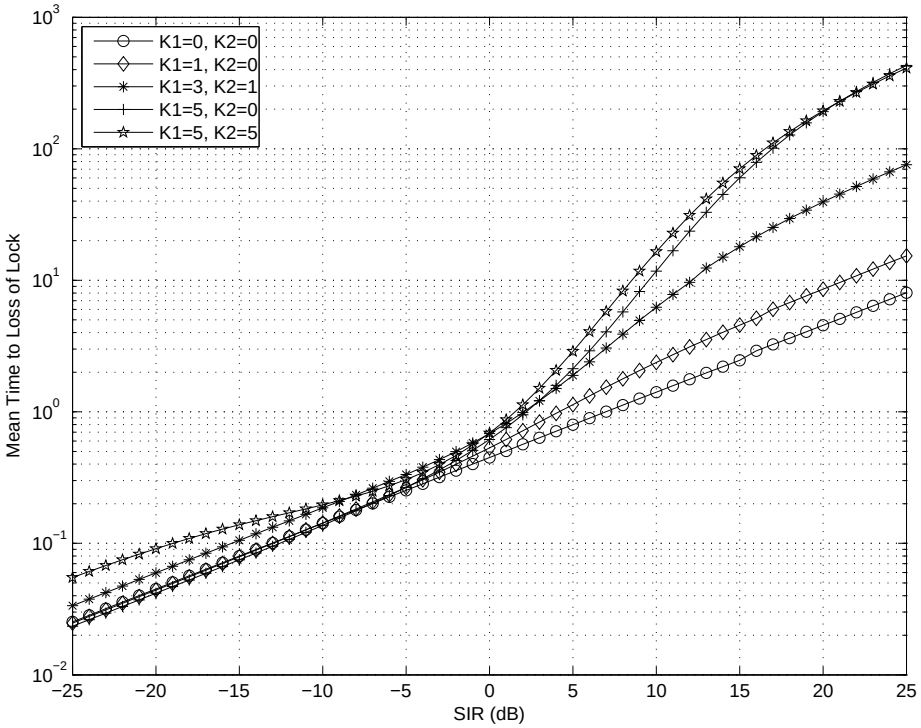

Figure 3.3. The mean time to loss of lock of an AFC, multiplied by the maximum Doppler frequency, in a Rician fading scenario for different values of K_1 and K_2.

Fig. 3.3 shows the MTLL multiplied by f_m of an AFC for Rician fading. It can be seen that if the channel of the desired signal is modeled by larger values of K_1, i.e., stronger LOS component, the performance of the AFC improves in the sense that the MTLL of the AFC increases for the same values of SIR. The same conclusion holds for larger values of m_1 in Fig. 3.4, where the MTLL (multiplied by f_m) in Nakagami fading is shown. Moreover, considering a specific curve in these figures, one can observe that the MTLL does not suffer from the shortcoming of the ASR in the sense that increasing the SIR, increases the MTLL of an AFC. Consequently, we can see that although we need to find the ASR to capture the impact of the transients on the performance of a receiver, we also need to find the MTLL to fully characterize AFC performance.

Note that the results in Figs. 3.1 and 3.2 are normalized to the maximum Doppler frequency and increasing f_m increases the value of the ASR and therefore deteriorates the performance. This is also true for the MTLL which is multiplied by the f_m and therefore an increase in the value of f_m is equivalent to a decrease in MTLL. However if $f_{m_1} \neq f_{m_2}$, the ASR normalized to f_{m_1} increases when f_{m_2} increases compared to f_{m_1}. This can be seen in Fig. 3.5 in which the normalized ASR vs f_{m_2}/f_{m_1} is shown in Rician/Rician scenario and Rayleigh/Rayleigh scenario. This is also true for the MTLL where the AFC has a better performance for smaller values of f_{m_2}, when f_{m_1} is constant.

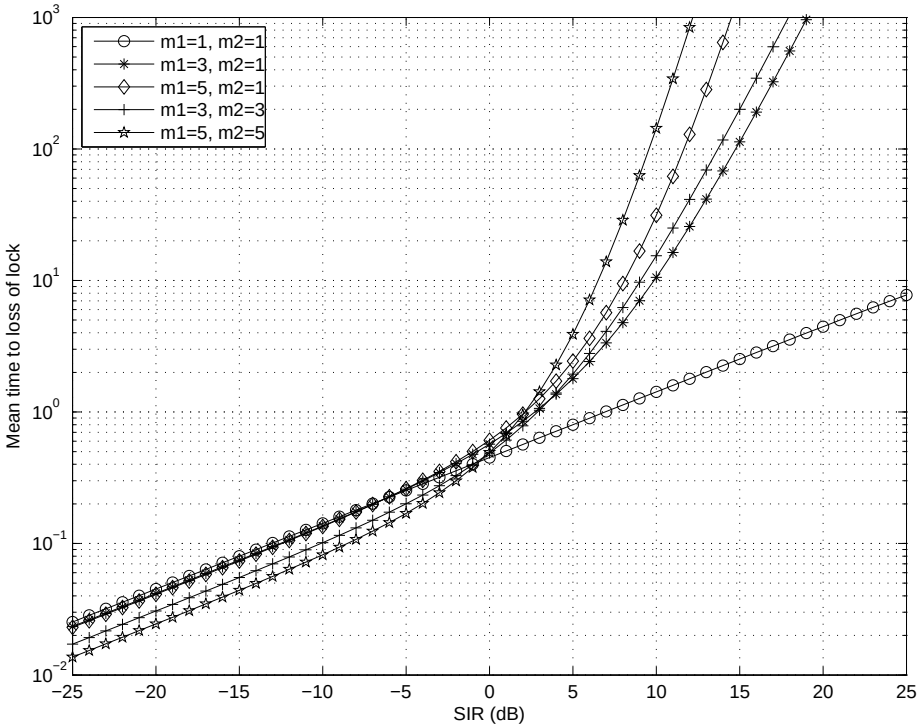

Figure 3.4. The mean time to loss of lock of an AFC, multiplied by the maximum Doppler frequency, in a Nakagami fading scenario for different values of m_1 and m_2.

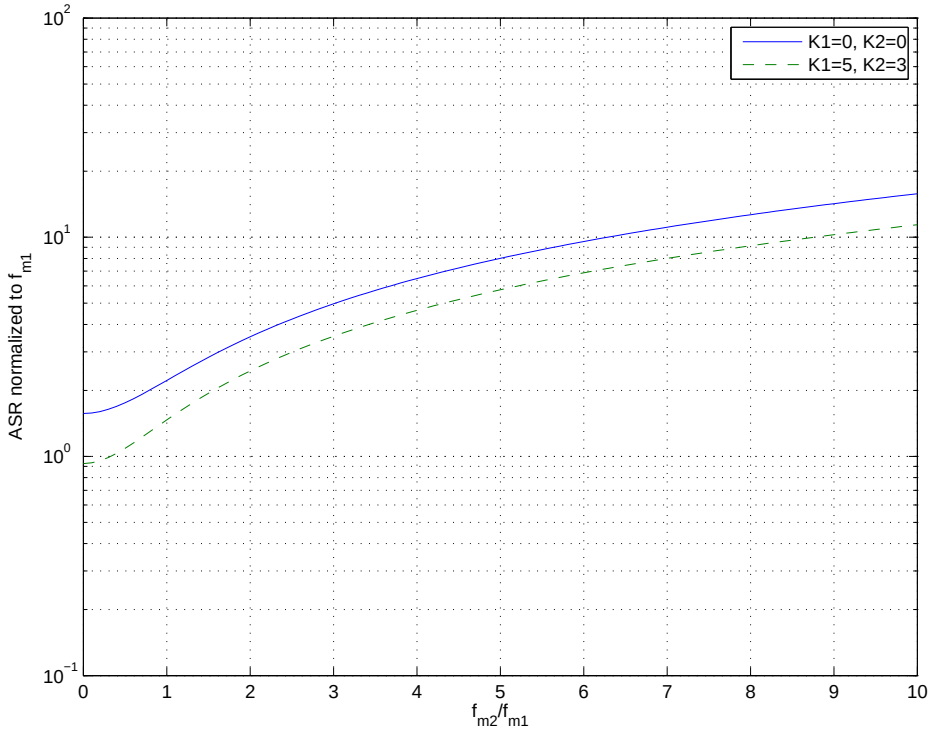

Figure 3.5. The normalized ASR of an AFC in Rician/Rician and Rayleigh/Rayleigh scenario.

3.6 Conclusion

In this chapter, the average switching rate and the mean time to loss of lock of an AFC were derived for fading channels. Both modulated and unmodulated carriers were investigated. In the case of Rayleigh/Rayleigh fading channels, a closed-form expression was derived for the ASR in the general case of modulated carriers and independent non-identically distributed (i.n.d.) channels which depends on the time behaviour of the baseband transmitted signal. Moreover, special cases were investigated for both the ASR and MTLL and compared to previous results in the literature when applicable. A new analytical approach was employed to derive integral form formulas for the ASR and the MTLL of an AFC in Rician/Rician and Nakagami/Nakgami fading channels and closed-form expressions were derived for important special cases. Numerical examples were provided to demonstrate the effect of interference and the channel model on the performances of an AFC in different scenarios.

Chapter 4

Performance of an AFC Loop Corrupted by Interference and Fading in Dual Dissimilar Channels

In many practical scenarios, the desired signal and the interference signal pass through different transmission environments and therefore they can have different fading statistics. For instance, if there is a line-of-sight (LOS) path between the transmitter of the desired signal and the receiver, the channel of the desired signal is better modeled by Rician fading. Meanwhile, there may not be a dominant multipath reflection in the interferer's channel. In this case, the fading affecting the interference signal is better modeled by a Rayleigh (pure scattering) or a Nakagami distribution. Other dissimilar channel scenarios may appear as well when there is not a LOS path between the transmitter of the desired signal and the receiver. In this chapter, we study the performance of an AFC in such fading channels. Rician/Rayleigh, Rayleigh/Rician, Rician/Nakagami, Nakagami/Rician, Nakagami/Rayleigh and Rayleigh/Nakagami scenarios are investigated separately and closed-form expressions and simple single integral form formulas are derived for the ASR and the MTLL of an AFC.

4.1 System and Channel Models

In this chapter, we use the model described in Section 3.1 for the received signals. However, one should note that in the scenarios considered in this chapter, not only the interference channel and the desired channel are independent, but also have dissimilar distributions.

4.2 Average Switching Rate

Considering the same assumptions as previous chapter for the difference between the carrier frequency of the received signals and the modulation, an AFC locks on the signal with larger amplitude [6, Ch. 19].

In order to find the average switching rate, we can use the random process $Z = s_1 A_1 - s_2 A_2$, the difference between the amplitude of the desired signal and the interferer. Consequently, as described in Section 3.2.1, the average switching rate is equal to

$$N = N_Z(0) = \int_{-\infty}^{\infty} |\dot{z}|\, f_{Z,\dot{Z}}(0, \dot{z}) d\dot{z}. \tag{4.1}$$

where $f_{Z,\dot{Z}}(z, \dot{z})$ is the JPDF of Z and its time derivative, $\dot{Z}$.

If the signals are unmodulated, Z and $\dot{Z}$ are independent and consequently (4.1) will be simplified to

$$N = N_Z(0) = f_Z(0) \int_{-\infty}^{\infty} |\dot{z}| f_{\dot{Z}}(\dot{z}) d\dot{z}. \tag{4.2}$$

Moreover, one should note that $\dot{A}_1$ and $\dot{A}_2$ are independent and Gaussian distributed (see (3.3-3.5)). As a result, $\dot{Z} = \dot{A}_1 - \dot{A}_2$ is also Gaussian distributed with a variance equal to $(\dot{\sigma}_1^2 + \dot{\sigma}_2^2)$ where $\dot{\sigma}_1^2$ and $\dot{\sigma}_2^2$ are the variance of the time-derivative of fading in desired branch and interference branch, respectively. Thus,

$$N = f_Z(0) \int_{-\infty}^{\infty} |\dot{z}| \frac{1}{\sqrt{2\pi(\dot{\sigma}_1^2 + \dot{\sigma}_2^2)}} \exp\left(-\frac{\dot{z}^2}{2(\dot{\sigma}_1^2 + \dot{\sigma}_2^2)}\right) d\dot{z} = \sqrt{\frac{2(\dot{\sigma}_1^2 + \dot{\sigma}_2^2)}{\pi}} f_Z(0) \tag{4.3}$$

and $f_Z(0)$ can be found using

$$f_Z(0) = \int_0^{\infty} f_{A_1}(y) f_{A_2}(y) dy. \tag{4.4}$$

However, if the signals are modulated, one can use the definition of the conditional probability density function [42], $f_{Z,\dot{Z}}(z, \dot{z}) = f_{\dot{Z}|Z}(\dot{z}|z) f_Z(z)$, to find

$$N = N_Z(0) = f_Z(0) \int_{-\infty}^{\infty} |\dot{z}| f_{\dot{Z}|Z}(\dot{z}|0) d\dot{z} \tag{4.5a}$$

where

$$f_Z(0) = \int_{y=0}^{\infty} \frac{1}{s_1 s_2} f_{A_1}\left(\frac{y}{s_1}\right) f_{A_2}\left(\frac{y}{s_2}\right) dy. \tag{4.5b}$$

The method used to find $f_{\dot{Z}|Z}(\dot{z}|0)$ depends on the distribution of the fading in channels. To find this conditional PDF, we consider two cases where in the first case the PDF of fading in the desired branch is mathematically simpler than the PDF of fading in the interference branch and in the second case the PDF of fading in the interference branch is mathematically simpler.

4.2.1 Case I: The PDF of fading in the desired branch is mathematically simpler than the PDF of fading in the interference branch.

In this case, after differentiating Z with respect to time and using the definition of Z to find A_1 as a function of Z and A_2, one has

$$\dot{Z} = s_1\dot{A}_1 - s_2\dot{A}_2 + \left(\frac{\dot{s}_1 s_2}{s_1} - \dot{s}_2\right) A_2 + \frac{\dot{s}_1}{s_1} Z. \tag{4.6}$$

We know that $\dot{A}_1$ and $\dot{A}_2$ are both zero-mean normally distributed random processes. Also, recall that $\dot{A}_1$ and $\dot{A}_2$ are assumed to be independent. As a result, if Z and A_2 are given, $\dot{Z}$ is equal to the summation of two scaled zero-mean independent random processes and a constant. Consequently,

$$f_{\dot{Z}|A_2,Z}(\dot{z}|\alpha_2, 0) = \frac{1}{\sqrt{2\pi\Omega}} \exp\left[-\frac{\left(\dot{z} - \alpha_2\left(\frac{\dot{s}_1 s_2}{s_1} - \dot{s}_2\right)\right)^2}{2\Omega}\right] \tag{4.7a}$$

where

$$\Omega = s_1^2\dot{\sigma}_1^2 + s_2^2\dot{\sigma}_2^2. \tag{4.7b}$$

Moreover, using the fundamental transformation theorem [42], it can be shown that

$$f_{A_2|Z}(\alpha_2|0) = \frac{s_2}{s_1} f_{A_1}\left(\frac{s_2}{s_1}\alpha_2\right). \tag{4.8}$$

Consequently, one can use the theorem of total probability [42] to show

$$f_{\dot{Z}|Z}(\dot{z}|z=0) = \int_0^\infty f_{\dot{Z}|A_2,Z}(\dot{z}|\alpha_2, 0) f_{A_2|Z}(\alpha_2|0) d\alpha_2 \tag{4.9}$$

and then, the ASR can be found using Eqs. (4.5)-(4.9).

4.2.2 Case II: The PDF of fading in the interference branch is mathematically simpler than the PDF of fading in the desired branch.

Similar to the previous case, we can use the time-derivative of Z. One has,

$$\dot{Z} = s_1\dot{A}_1 - s_2\dot{A}_2 + \dot{s}_1 A_1 - \dot{s}_2 A_2. \tag{4.10}$$

If we substitute $A_2 = \frac{s_1}{s_2}A_1 - \frac{1}{s_2}Z$ into (4.10),

$$\dot{Z} = s_1\dot{A}_1 - s_2\dot{A}_2 + \left(\dot{s}_1 - \frac{\dot{s}_2 s_1}{s_2}\right) A_1 + \frac{\dot{s}_2}{s_2} Z. \tag{4.11}$$

Since $\dot{A}_1$ and $\dot{A}_2$ are both zero-mean Gaussian distributed random processes and $\dot{A}_1$ and $\dot{A}_2$ are independent, if Z and A_2 are given, $\dot{Z}$ is equal to the summation of two scaled zero-mean random processes and a constant. Consequently,

$$f_{\dot{Z}|A_1,Z}(\dot{z}|\alpha_1, z=0) = \frac{1}{\sqrt{2\pi\Omega}} \exp\left[-\frac{(\dot{z} - \alpha_1(\dot{s}_1 - \frac{\dot{s}_2 s_1}{s_2}))^2}{2\Omega}\right] \tag{4.12a}$$

where

$$\Omega = s_1^2\dot{\sigma}_1^2 + s_2^2\dot{\sigma}_2^2. \tag{4.12b}$$

We can also find $f_{A_1|Z}(\alpha_1|z=0)$ using $A_1 = \frac{s_2}{s_1}A_2 + \frac{1}{s_1}Z$. By employing the fundamental transformation theorem [42], one has

$$f_{A_1|Z}(\alpha_1|z=0) = \frac{s_1}{s_2} f_{A_2}\left(\frac{s_1}{s_2}\alpha_1\right). \tag{4.13}$$

One can use (4.12) and (4.13) to find $f_{\dot{Z}|Z}(\dot{z}|z=0)$ by employing the theorem of total probability [42],

$$f_{\dot{Z}|Z}(\dot{z}|z=0) = \int_0^\infty f_{\dot{Z}|A_1,Z}(\dot{z}|\alpha_1, z=0) f_{A_1|Z}(\alpha_1|z=0) d\alpha_1. \tag{4.14}$$

It is worth mentioning that both of these methods can be used in either cases, however, in order to obtain simpler expressions, we considered two cases and used different methods in each case to find the average switching rate.

One should note that in the special case that the transmitted signal in the desired branch is a replica of the transmitted signal in the interference branch, i.e., $s_1(t) = ks_2(t)$ where k is a constant, $\dot{s}_1(t)s_2(t) = \dot{s}_2(t)s_1(t)$ and therefore

$$f_{\dot{Z}|Z}(\dot{z}|0) = \frac{1}{\sqrt{2\pi\Omega}} \exp\left(-\frac{\dot{z}^2}{2\Omega}\right). \tag{4.15}$$

Consequently, the average switching rate in both cases is equal to

$$N = f_Z(0)\int_{-\infty}^{\infty} |\dot{z}| \frac{1}{\sqrt{2\pi\Omega}} \exp\left(-\frac{\dot{z}^2}{2\Omega}\right) d\dot{z} = \sqrt{\frac{2\Omega}{\pi}} f_Z(0) \tag{4.16}$$

where $f_Z(0)$ can be found using (4.5b) and Ω is defined in (4.12b).

4.3 Mean Time to Loss of Lock

In order to find the MTLL of unmodulated signals using (3.20), we need to find the probability that the amplitude of the desired signal is larger than the amplitude of the interference signal, F. To find this probability we consider the two cases described in the previous section based on the simplicity of the distribution of fading in channels.

4.3.1 Case I: The PDF of fading in the desired branch is mathematically simpler than the PDF of fading in the interference branch.

In this case, we can use the method described in Section 3.3 to find F. As a result,

$$F = \int_{y=1}^{\infty}\int_{t=0}^{\infty} \frac{t}{s_1 s_2} f_{A_1}\left(\frac{ty}{s_1}\right) f_{A_2}\left(\frac{t}{s_2}\right) dtdy. \tag{4.17}$$

4.3.2 Case II: The PDF of fading in the interference branch is mathematically simpler than the PDF of fading in the desired branch.

Since we want to find $F = Pr[s_1 A_1 > s_2 A_2]$ and this probability is equal to $1 - Pr[s_1 A_1 \leq s_2 A_2]$, we can first find $Pr[s_1 A_1 \leq s_2 A_2]$. One can easily show that

$$Pr[s_1 A_1 \leq s_2 A_2] = \int_{v=1}^{\infty} \int_{t=0}^{\infty} \frac{t}{s_1 s_2} f_{A_1}\left(\frac{t}{s_1}\right) f_{A_2}\left(\frac{tv}{s_2}\right) dt dv. \tag{4.18}$$

Consequently,

$$F = 1 - \int_{v=1}^{\infty} \int_{t=0}^{\infty} \frac{t}{s_1 s_2} f_{A_1}\left(\frac{t}{s_1}\right) f_{A_2}\left(\frac{tv}{s_2}\right) dt dv. \tag{4.19}$$

4.4 Application to Dissimilar Fading Channels

In this section, the ASR and MTLL are derived for different dissimilar fading channels.

4.4.1 Rician/Rayleigh

In this scenario, there is an LOS path between the desired signal's transmitter and receiver while the interferer's channel is modeled by pure scattering. Using the method described in Subsection 4.2.2, the ASR of an AFC for modulated carriers is

$$N = \int_{-\infty}^{\infty} \left[1 + d_2 \sqrt{\frac{\pi}{d_1}} \dot{z} \exp\left(\frac{\dot{z}^2 d_2^2}{d_1}\right) \operatorname{erfc}\left(-\frac{\dot{z} d_2}{\sqrt{d_1}}\right)\right] M_1 f_Z(0) |\dot{z}| \exp\left(-\frac{\dot{z}^2}{2\Omega}\right) d\dot{z}$$

where

$$f_Z(0) = \sqrt{\frac{\pi}{2}} \frac{{d_3}^{-3/2}}{s_1^2 s_2^2 \sigma_1^2 \sigma_2^2} \exp(-K_1)\, {}_1F_1\left(\frac{3}{2}; 1; \frac{K_1}{s_1^2 \sigma_1^2 d_3}\right) \tag{4.20a}$$

$$M_1 = \frac{1}{2 d_1 \sigma_2^2 \sqrt{2\pi\Omega}} \left(\frac{s_1}{s_2}\right)^2 \tag{4.20b}$$

$$d_1 = \frac{s_1^2}{2 s_2^2 \sigma_2^2} + 2\Omega d_2^2 \tag{4.20c}$$

$$d_2 = \frac{\dot{s}_1 s_2 - \dot{s}_2 s_1}{2 s_2 \Omega} \tag{4.20d}$$

$$d_3 = \left(\frac{s_1^2 \sigma_1^2 + s_2^2 \sigma_2^2}{s_1^2 s_2^2 \sigma_1^2 \sigma_2^2}\right) \tag{4.20e}$$

and where ${}_1F_1(p; q; \cdot)$ is the confluent hypergeometric function [44]. In order to find the MTLL, one can use the method in subsection 4.3.2. Consequently using [54, (6.631.4)],

$$\int_0^{\infty} x^{\nu+1} e^{-a x^2} J_\nu(\beta x) dx = \frac{\beta^\nu}{(2a^{\nu+1})} \exp\left(-\frac{\beta^2}{4a}\right), \tag{4.21}$$

one can find F,

$$F = 1 - \frac{1}{s_1^2 \sigma_1^2 d_3} \exp\left(-\frac{K_1}{s_2^2 \sigma_2^2 d_3}\right). \tag{4.22}$$

The ASR of an AFC in this scenario are summarized in Table 4.1 for several cases.

Table 4.1. The average switching rate of an AFC in Rician/Rayleigh fading channels.

System Model	Average Switching Rate
i.i.d. $s_1 = s_2 = 1$	$\frac{\dot{\sigma}}{2\sigma}\exp(-K_1){}_1F_1\left(\frac{3}{2};1;\frac{K_1}{2}\right)$
i.n.d. $s_1(t) = ks_2(t)$	$\frac{{d_3}^{-3/2}\sqrt{\Omega}}{s_1^2 s_2^2\sigma_1^2\sigma_2^2}\exp(-K_1)\,{}_1F_1\left(\frac{3}{2};1;\frac{K_1}{s_1^2\sigma_1^2 d_3}\right)$
i.n.d. modulated	$\sqrt{\frac{\pi}{2}}\frac{{d_3}^{-3/2}}{s_1^2 s_2^2\sigma_1^2\sigma_2^2}\exp(-K_1)\,{}_1F_1\left(\frac{3}{2};1;\frac{K_1}{s_1^2\sigma_1^2 d_3}\right)M_1$ $\int_{-\infty}^{\infty}\left[1+d_2\sqrt{\frac{\pi}{d_1}}\dot{z}\exp\left(\frac{\dot{z}^2 d_2^2}{d_1}\right)\operatorname{erfc}\left(-\frac{\dot{z}d_2}{\sqrt{d_1}}\right)\right]\lvert\dot{z}\rvert\exp\left(-\frac{\dot{z}^2}{2\Omega}\right)d\dot{z}$

4.4.2 Rayleigh/Rician

In this scenario, the desired signal is subject to Rayleigh fading while the interferer is subject to Rician fading. Using the method described in Subsection 4.2.1,

$$N=\int_{-\infty}^{\infty}\left[1+d_5\sqrt{\frac{\pi}{d_4}}\dot{z}\exp\left(\frac{\dot{z}^2 d_5^2}{d_4}\right)\operatorname{erfc}\left(-\frac{\dot{z}d_5}{\sqrt{d_4}}\right)\right]\times M_2 f_Z(0)|\dot{z}|\exp\left(-\frac{\dot{z}^2}{2\Omega}\right)d\dot{z}$$

where

$$f_Z(0)=\sqrt{\frac{\pi}{2}}\frac{{d_3}^{-3/2}}{s_1^2 s_2^2\sigma_1^2\sigma_2^2}\exp(-K_2)\,{}_1F_1\left(\frac{3}{2};1;\frac{K_2}{s_2^2\sigma_2^2 d_3}\right) \tag{4.23a}$$

$$M_2=\frac{1}{2d_4\sigma_1^2\sqrt{2\pi\Omega}}\left(\frac{s_2}{s_1}\right)^2 \tag{4.23b}$$

$$d_4=\frac{s_2^2}{2s_1^2\sigma_1^2}+2\Omega d_5^2 \tag{4.23c}$$

$$d_5=\frac{(\dot{s}_2 s_1-\dot{s}_1 s_2)}{2\Omega s_1} \tag{4.23d}$$

where in these equations, the signals are modulated and therefore s_1 and s_2 are both functions of time. Table 4.2 shows the ASR of an AFC in Rayleigh/Rician fading channels. In this scenario and for unmodulated signals, F is equal to

$$F=\frac{1}{s_2^2\sigma_2^2 d_3}\exp\left(-\frac{K_2}{s_1^2\sigma_1^2 d_3}\right). \tag{4.24}$$

This equation can be used to find the MTLL of an AFC in this scenario.

4.4.3 Rician/Nakagami

In the case that $x_1(t)$ and $x_2(t)$ have Rician and Nakagami fading, respectively, the ASR can be found using the method in Subsection 4.2.2

$$\begin{aligned}N=&\frac{2\Gamma\left(m_2+\frac{1}{2}\right)\Gamma(2m_2){m_2}^{2m_2}s_1^{2m_2-2}}{\Gamma^2(m_2)(s_2^2\sigma_2^2)^{2m_2}\sigma_1^2(2d_6)^{m_2}d_7^{m_2+\frac{1}{2}}\sqrt{\pi\Omega}}{}_1F_1\left(m_2+\frac{1}{2};1;\frac{K_1}{s_1^2\sigma_1^2 d_7}\right) \\ &\times\int_{-\infty}^{\infty}|\dot{z}|\exp\left[\left(\frac{d_2^2}{d_6}-\frac{1}{2\Omega}\right)\dot{z}^2-K_1\right]D_{-2m_2}\left(-\frac{2d_2\dot{z}}{\sqrt{d_6}}\right)d\dot{z}\end{aligned} \tag{4.25a}$$

Table 4.2. The average switching rate of an AFC in Rayleigh/Rician fading channels.

System Model	Average Switching Rate
i.i.d. $s_1 = s_2 = 1$	$\frac{\dot{\sigma}}{2\sigma}\exp(-K_2){}_1F_1\left(\frac{3}{2};1;\frac{K_2}{2}\right)$
i.n.d. $s_1 = ks_2$	$\frac{{d_3}^{-3/2}\sqrt{\Omega}}{s_1^2 s_2^2 \sigma_1^2 \sigma_2^2}\exp(-K_2)\,{}_1F_1\left(\frac{3}{2};1;\frac{K_2}{s_2^2\sigma_2^2 d_3}\right)$
i.n.d.	$\sqrt{\frac{\pi}{2}}\frac{{d_3}^{-3/2}}{s_1^2 s_2^2 \sigma_1^2 \sigma_2^2}\exp(-K_2)\,{}_1F_1\left(\frac{3}{2};1;\frac{K_2}{s_2^2\sigma_2^2 d_3}\right) M_2$ $\int_{-\infty}^{\infty}\left[1+d_5\sqrt{\frac{\pi}{d_4}}\dot{z}\exp\left(\frac{\dot{z}^2 d_5^2}{d_4}\right)\operatorname{erfc}\left(-\frac{\dot{z}d_5}{\sqrt{d_4}}\right)\right]\lvert\dot{z}\rvert\exp\left(-\frac{\dot{z}^2}{2\Omega}\right)d\dot{z}$

Table 4.3. The average switching rate of an AFC in Rician/Nakagami fading channels.

System Model	Average Switching Rate
i.i.d. $s_1 = s_2 = 1$	$\frac{2\sqrt{2}\Gamma(m_2+\frac{1}{2}){m_2}^{m_2}\exp(-K_1)\dot{\sigma}}{\sqrt{\pi}\Gamma(m_2)(m_2+1)^{m_2+\frac{1}{2}}\sigma}$
i.n.d. $s_1 = ks_2$	$\frac{2{m_2}^{m_2}\Gamma(m_2+\frac{1}{2})\exp(-K_1)}{\Gamma(m_2)(s_2^2\sigma_2^2)^{m_2}s_1^2\sigma_1^2 d_7^{m_2+\frac{1}{2}}}\sqrt{\frac{\Omega}{\pi}}{}_1F_1\left(m_2+\frac{1}{2};1;\frac{K_1}{s_1^2\sigma_1^2 d_7}\right)$
i.n.d.	$\frac{2\Gamma\left(m_2+\frac{1}{2}\right)\Gamma(2m_2){m_2}^{2m_2}{s_1}^{2m_2-2}}{\Gamma^2(m_2)(s_2^2\sigma_2^2)^{2m_2}\sigma_1^2(2d_6)^{m_2}d_7^{m_2+\frac{1}{2}}\sqrt{\pi\Omega}}{}_1F_1\left(m_2+\frac{1}{2};1;\frac{K_1}{s_1^2\sigma_1^2 d_7}\right)$ $\times\int_{-\infty}^{\infty}\lvert\dot{z}\rvert\exp\left[\left(\frac{d_2^2}{d_6}-\frac{1}{2\Omega}\right)\dot{z}^2-K_1\right]D_{-2m_2}\left(-\frac{2d_2\dot{z}}{\sqrt{d_6}}\right)d\dot{z}$

where

$$d_6 = 4\Omega d_2^2 + \frac{m_2}{\sigma_2^2}\left(\frac{s_1}{s_2}\right)^2 \tag{4.25b}$$

$$d_7 = \frac{1}{s_1^2\sigma_1^2} + \frac{m_2}{s_2^2\sigma_2^2} \tag{4.25c}$$

and where $D_p(\cdot)$ is the parabolic cylinder function [44]. In this scenario, F can be found using (4.19),

$$F = 1 - \int_0^{\infty}\frac{t\,\Gamma\left(m_2,\frac{m_2 t^2}{2s_2^2\sigma_2^2}\right)}{s_1^2\sigma_1^2\,\Gamma(m_2)}\exp\left(\frac{-t^2}{2s_1^2\sigma_1^2}-K_1\right)I_0\left(\frac{\sqrt{2K_1}}{s_1\sigma_1}t\right)dt, \tag{4.26}$$

where $\Gamma(q,x)$ is the incomplete gamma function defined in [54, (6.5.3)]. In table 4.3, different expressions for the ASR of an AFC in Rician/Nakagami fading are shown.

Table 4.4. The average switching rate of an AFC in Nakagami/Rician fading channels.

System Model	Average Switching Rate
i.i.d. $s_1 = s_2 = 1$	$\frac{2\sqrt{2}\Gamma(m_1+\frac{1}{2}){m_1}^{m_1}\exp(-K_2)\dot{\sigma}}{\sqrt{\pi}\Gamma(m_1)(m_1+1)^{m_1+\frac{1}{2}}\sigma}$
i.n.d. $s_1 = ks_2$	$\frac{2{m_1}^{m_1}\Gamma(m_1+\frac{1}{2})\exp(-K_2)}{\Gamma(m_1)(s_1^2\sigma_1^2)^{m_1}s_2^2\sigma_2^2 d_9^{m_1+\frac{1}{2}}}\sqrt{\frac{\Omega}{\pi}}{}_1F_1\left(m_1+\frac{1}{2};1;\frac{K_2}{s_2^2\sigma_2^2 d_9}\right)$
i.n.d.	$\frac{2\Gamma\left(m_1+\frac{1}{2}\right)\Gamma(2m_1){m_1}^{2m_1}{s_2}^{2m_1-2}}{\Gamma^2(m_1)(s_1^2\sigma_1^2)^{2m_1}\sigma_2^2(2d_8)^{m_1}d_9^{m_1+\frac{1}{2}}\sqrt{\pi\Omega}}{}_1F_1\left(m_1+\frac{1}{2};1;\frac{K_2}{s_2^2\sigma_2^2 d_9}\right)$ $\times\int_{-\infty}^{\infty}\lvert\dot{z}\rvert\exp\left[\left(\frac{d_5^2}{d_8}-\frac{1}{2\Omega}\right)\dot{z}^2-K_2\right]D_{-2m_1}\left(-\frac{2d_5\dot{z}}{\sqrt{d_8}}\right)d\dot{z}$

4.4.4 Nakagami/Rician

In this scenario, the desired signal experiences Nakagami fading while the interference signal experiences Rician fading. Using Eqs. (4.5)-(4.9) one has

$$N=\frac{2\Gamma\left(m_1+\frac{1}{2}\right)\Gamma(2m_1){m_1}^{2m_1}s_2^{2m_1-2}}{\Gamma^2(m_1)(s_1^2\sigma_1^2)^{2m_1}\sigma_2^2(2d_8)^{m_1}d_9^{m_1+\frac{1}{2}}\sqrt{\pi\Omega}}{}_1F_1\left(m_1+\frac{1}{2};1;\frac{K_2}{s_2^2\sigma_2^2 d_9}\right)$$
$$\times\int_{-\infty}^{\infty}\lvert\dot{z}\rvert\exp\left[\left(\frac{d_5^2}{d_8}-\frac{1}{2\Omega}\right)\dot{z}^2-K_2\right]D_{-2m_1}\left(-\frac{2d_5\dot{z}}{\sqrt{d_8}}\right)d\dot{z}$$

where

$$d_8=4\Omega d_5^2+\frac{m_1}{\sigma_1^2}\left(\frac{s_2}{s_1}\right)^2 \tag{4.27a}$$

$$d_9=\frac{1}{s_2^2\sigma_2^2}+\frac{m_1}{s_1^2\sigma_1^2} \tag{4.27b}$$

and

$$F=\int_0^{\infty}\frac{t\Gamma\left(m_1,\frac{m_1t^2}{2s_1^2\sigma_1^2}\right)}{s_2^2\sigma_2^2\,\Gamma(m_1)}\exp\left(\frac{-t^2}{2s_2^2\sigma_2^2}-K_2\right)I_0\left(\frac{\sqrt{2K_2}t}{s_2\sigma_2}\right)dt. \tag{4.28}$$

Table 4.4 shows expressions for the ASR of an AFC in this scenario for different cases.

4.4.5 Nakagami/Rayleigh

In this scenario, the desired signal experiences Nakagami fading and the interference signal experiences Rayleigh fading. One, using the method in Subsection 4.2.2, has

$$N=\int_{-\infty}^{\infty}\left[1+d_2\sqrt{\frac{\pi}{d_1}}\dot{z}\exp\left(\frac{\dot{z}^2d_2^2}{d_1}\right)\operatorname{erfc}\left(-\frac{\dot{z}d_2}{\sqrt{d_1}}\right)\right]$$
$$\times\frac{\sqrt{2}{m_1}^{m_1}\Gamma(m_1+\frac{1}{2})M_1}{\Gamma(m_1)(s_1^2\sigma_1^2)^{m_1}s_2^2\sigma_2^2{d_9}^{m_1+\frac{1}{2}}}\lvert\dot{z}\rvert\exp\left(-\frac{\dot{z}^2}{2\Omega}\right)d\dot{z} \tag{4.29}$$

Table 4.5. The average switching rate of an AFC in Nakagami/Rayleigh fading channels.

System Model	Average Switching Rate
i.i.d. $s_1 = s_2 = 1$	$\sqrt{\frac{2}{\pi}}\frac{\dot{\sigma}}{\sigma}\frac{\Gamma(m_1+\frac{1}{2})}{\Gamma(m_1)}\frac{2m_1^{m_1}}{(m_1+1)^{m_1+\frac{1}{2}}}$
i.n.d. $s_1 = ks_2$	$\sqrt{\frac{\Omega}{\pi}}\frac{\Gamma(m_1+\frac{1}{2})}{\Gamma(m_1)}\frac{2m_1^{m_1}}{(s_1^2\sigma_1^2)^{m_1}s_2^2\sigma_2^2}\left(\frac{m_1}{s_1^2\sigma_1^2}+\frac{1}{s_2^2\sigma_2^2}\right)^{-m_1-\frac{1}{2}}$
i.n.d.	$\int_{-\infty}^{\infty}\left[1+d_2\sqrt{\frac{\pi}{d_1}}\dot{z}\exp\left(\frac{\dot{z}^2d_2^2}{d_1}\right)\operatorname{erfc}\left(-\frac{\dot{z}d_2}{\sqrt{d_1}}\right)\right]$ $\times\frac{\sqrt{2}m_1^{m_1}\Gamma(m_1+\frac{1}{2})M_1}{\Gamma(m_1)(s_1^2\sigma_1^2)^{m_1}s_2^2\sigma_2^2{d_9}^{m_1+\frac{1}{2}}}\lvert\dot{z}\rvert\exp\left(-\frac{\dot{z}^2}{2\Omega}\right)d\dot{z}$

where M_1, d_1 and d_2 are defined in (4.20). In this case,

$$F = 1 - \left(\frac{m_1}{m_1 + \frac{s_1^2\sigma_1^2}{s_2^2\sigma_2^2}}\right)^{m_1}. \tag{4.30}$$

The results are provided in table 4.5 for several cases.

4.4.6 Rayleigh/Nakagami

In this scenario, one has

$$N = \int_{-\infty}^{\infty}\left[1+d_5\sqrt{\frac{\pi}{d_4}}\dot{z}\exp\left(\frac{\dot{z}^2d_5^2}{d_4}\right)\operatorname{erfc}\left(-\frac{\dot{z}d_5}{\sqrt{d_4}}\right)\right] \times\frac{\sqrt{2}m_2^{m_2}\Gamma(m_2+\frac{1}{2})M_2}{\Gamma(m_2)(s_2^2\sigma_2^2)^{m_2}s_1^2\sigma_1^2{d_7}^{m_2+\frac{1}{2}}}\lvert\dot{z}\rvert\exp\left(-\frac{\dot{z}^2}{2\Omega}\right)d\dot{z} \tag{4.31}$$

where M_2, d_4 and d_5 are defined in (4.23). Moreover, it can be shown using (4.17) that

$$F = \frac{m_2^{m_2}}{\left(\frac{s_2^2\sigma_2^2}{s_1^2\sigma_1^2}+m_2\right)^{m_2}}. \tag{4.32}$$

In table 4.6, different expressions for ASR of an AFC cab be found for this scenario.

4.5 Numerical Examples and Discussion

In the numerical examples, the special case of two dimensional isotropic scattering and an omnidirectional receiving antenna is considered. In this case, $c_{i2} = 2\pi^2 f_{m_i}^2 c_{i0}$ for $i = 1, 2$ where f_{m_i} is the maximum Doppler frequency [50]. Moreover, we assume that $f_m = f_{m_1} = f_{m_2}$ and $s_1 = s_2 = 1$.

In Fig. 4.1, the ASR of an AFC (normalized to f_m) versus SIR is shown in a Rician/Nakagami scenario where SIR $= 10\log_{10}\left(\frac{c_{10}(1+K_1)}{c_{20}}\right)$. Note that $K_i = 0$ and $m_i = 1$ are equivalent to Rayleigh fading. It can be seen that for small values of SIR, m_2 is the parameter that determines

Table 4.6. The average switching rate of an AFC in Rayleigh/Nakagami fading channels.

System Model	Average Switching Rate
i.i.d. $s_1 = s_2 = 1$	$\sqrt{\frac{2}{\pi}}\frac{\dot{\sigma}}{\sigma}\frac{\Gamma(m_2+\frac{1}{2})}{\Gamma(m_2)}\frac{2m_2^{m_2}}{(m_2+1)^{m_2+\frac{1}{2}}}$
i.n.d. $s_1 = ks_2$	$\sqrt{\frac{\Omega}{\pi}}\frac{\Gamma\left(m_2+\frac{1}{2}\right)}{\Gamma(m_2)}\frac{2m_2^{m_2}}{(s_2^2\sigma_2^2)^{m_2}s_1^2\sigma_1^2}\left(\frac{m_2}{s_2^2\sigma_2^2}+\frac{1}{s_1^2\sigma_1^2}\right)^{-m_2-\frac{1}{2}}$
i.n.d.	$\int_{-\infty}^{\infty}\left[1+d_5\sqrt{\frac{\pi}{d_4}}\dot{z}\exp\left(\frac{\dot{z}^2d_5^2}{d_4}\right)\operatorname{erfc}\left(-\frac{\dot{z}d_5}{\sqrt{d_4}}\right)\right]$ $\times\frac{\sqrt{2}m_2^{m_2}\Gamma(m_2+\frac{1}{2})M_2}{\Gamma(m_2)(s_2^2\sigma_2^2)^{m_2}s_1^2\sigma_1^2{d_7}^{m_2+\frac{1}{2}}}\lvert\dot{z}\rvert\exp\left(-\frac{\dot{z}^2}{2\Omega}\right)d\dot{z}$

the shape of the ASR curve, while for large values of SIR, this shape is determined by K_1. This behavior can be better observed by considering the cases where m_2 is constant while K_1 increases. It can be seen that the ASR curve is almost the same when the interferer is stronger than the desired signal; however, when the desired signal is stronger than the interferer, the ASR decreases more significantly for larger values of K_1.

A similar behavior can be seen in Fig. 4.2 where the ASR of an AFC is shown in a Nakagami/Rician scenario. In this case, the SIR is defined as SIR $= 10\log_{10}\left(\frac{c_{10}}{c_{20}(1+K_2)}\right)$.

Figs. 4.3 and 4.4 show the MTLL of an AFC (multiplied by f_m) in Rician/Nakagami and Nakagami/Rician scenarios, respectively, for different fading parameters. Comparing these figures, one can see that for large values of SIR (more than 10 dB), the slope of the MTLL curve in a Rician/Nakagami scenario decreases as the SIR increases, while in a Nakagami/Rician scenario, the MTLL increases with an approximately constant slope in a log/log plot.

4.6 Conclusion

In this chapter, closed-form expressions and simple single integral form formulas were derived for the average switching rate and the mean time to loss of lock of an AFC in dissimilar fading channels. Rayleigh, Rician and Nakagami-*m* fading channels were considered. Numerical examples were provided to investigate the effect of a single interference and multipath fading on the performance of an AFC.

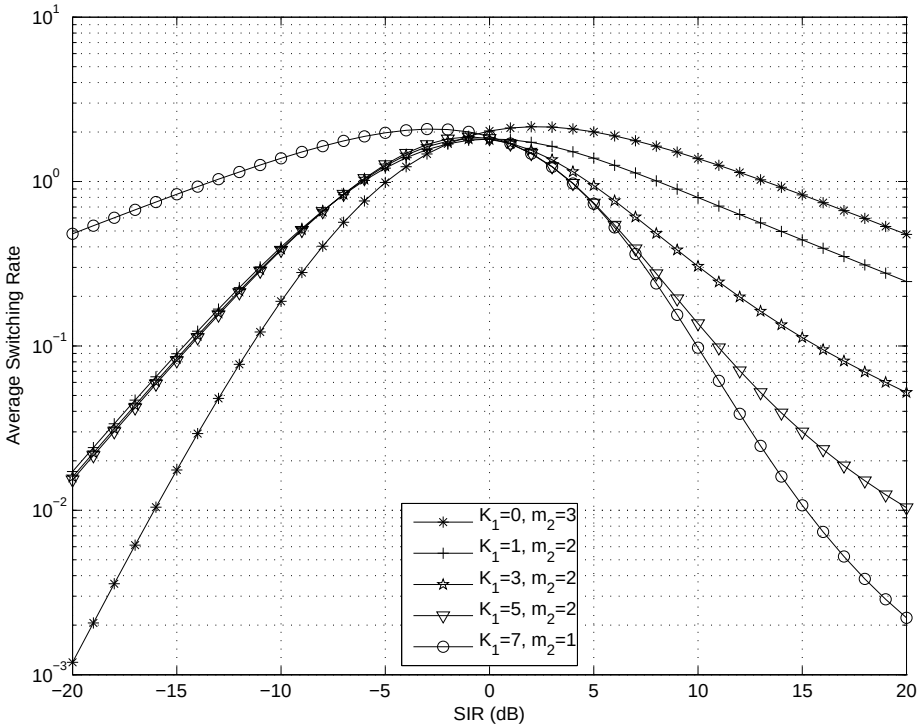

Figure 4.1. The ASR of an AFC (normalized to f_m) in Rician/Nakagami fading.

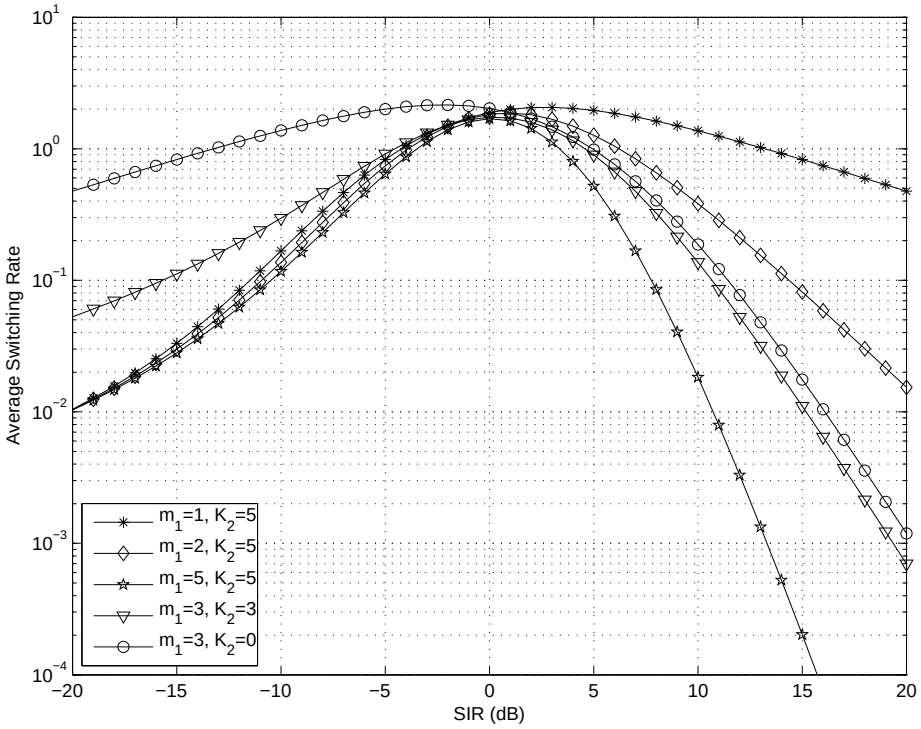

Figure 4.2. The ASR of an AFC (normalized to f_m) in Nakagami/Rician fading scenario.

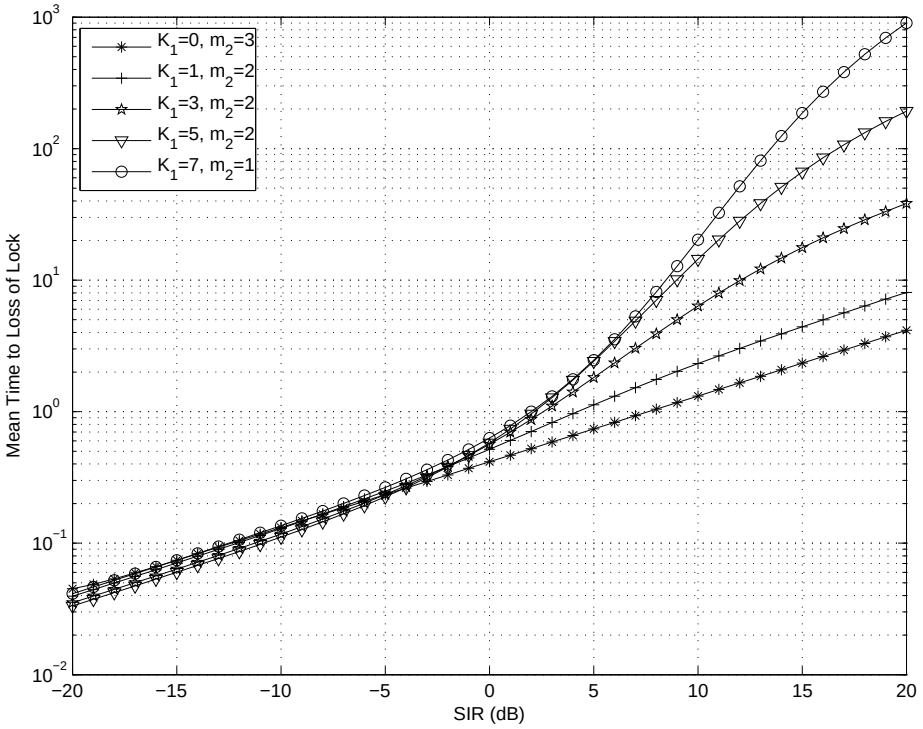

Figure 4.3. The MTLL of an AFC (multiplied by f_m) in Rician/Nakagami fading scenario.

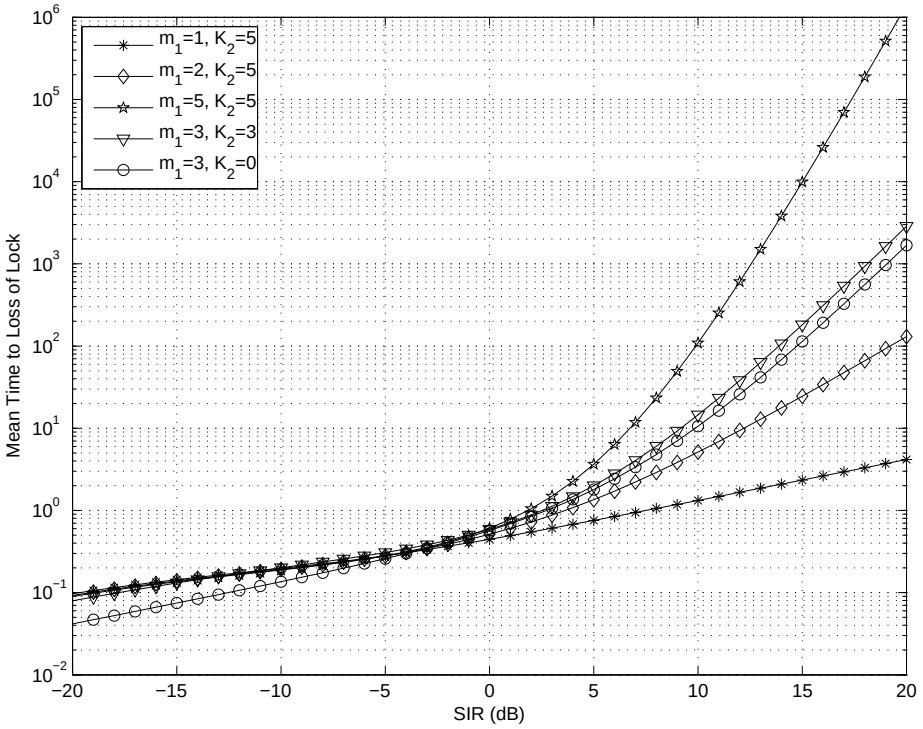

Figure 4.4. The MTLL of an AFC (multiplied by f_m) in Nakagami/Rician fading scenario.

Chapter 5

Performance of an AFC Loop in the Presence of a Single Interferer in Noisy Fading Channels

In this chapter, we investigate the performance of an AFC in Rician and Rayleigh fading channels in the presence of an interference signal where both of the signals are subject to additive Gaussian noise.

5.1 System and Channel Models

The modulated received signals considered in this chapter can be modeled as

$$x_i(t) = s_i(t)A_i(t)\cos(\omega_i t + \zeta_i(t) + \Phi_i(t)) + N_i(t) \qquad i = 1, 2 \tag{5.1}$$

where $s_i(t)$ is the amplitude of the transmitted data, $\zeta_i(t)$ is its phase, ω_i is the carrier angular frequency, $A_i(t)$ is a random process representing the effect of multipath fading and $\Phi_i(t)$ is a random process uniformly distributed in $[0, 2\pi)$; $N_i(t)$ denotes the Gaussian noise in the system. Note that the noise is not white, since it has passed through a bandpass filter in the intermediate-frequency (IF) portion of the receiver. As a result, it can be modeled as

$$N_i(t) = N_{c_i}(t)\cos(\omega_i t) - N_{s_i}(t)\sin(\omega_i t) \qquad i = 1, 2 \tag{5.2}$$

where N_{c_i} and N_{s_i} are the in-phase and quadrature components of the process N_i. The joint probability density function (JPDF) of N_{c_i} and N_{s_i} and their time derivatives, $\dot{N}_{c_i}$ and $\dot{N}_{s_i}$, depend on the power spectral density (PSD) of the noise, $W_{N_i}(f)$. If this PSD is symmetric around the carrier frequency of the received signal, one has [55]

$$f_{N_{c_i},N_{s_i},\dot{N}_{c_i},\dot{N}_{s_i}}(n_{c_i}, n_{s_i}, \dot{n}_{c_i}, \dot{n}_{s_i}) = \frac{1}{4\pi^2 b_{i0} b_{i2}} \exp\left(-\frac{n_{c_i}^2 + n_{s_i}^2}{2b_{i0}}\right) \exp\left(-\frac{\dot{n}_{c_i}^2 + \dot{n}_{s_i}^2}{2b_{i2}}\right) \tag{5.3a}$$

where

$$b_{in} = (2\pi)^n \int_0^\infty (f - f_i)^n W_{N_i}(f) df \tag{5.3b}$$

and f_i is the carrier frequency. One case satisfying these conditions is when the bandpass filter is symmetric around its center frequency and the IF mixer is biased such that the carrier frequency and the center frequency of the filter coincide.

In this study, we consider independent Rician channels, with PDF

$$f_{A_i}(a_i) = \frac{a_i}{c_{i0}} \exp\left(-\frac{a_i^2 + \mu_i^2}{2c_{i0}}\right) I_0\left(\frac{a_i \mu_i}{c_{i0}}\right) \tag{5.4}$$

where $2c_{i0}$ is the power in the scatter component and μ_i^2 is the power in the LOS component. Note that Rayleigh fading is a special case of Rician when $\mu_i = 0$. In (5.1), since $\Psi_i = \zeta_i + \Phi_i$ has a uniform distribution in $[0, 2\pi)$, $A_i \cos(\Psi_i)$ and $A_i \sin(\Psi_i)$ are normally distributed with expected values equal to μ_{c_i} and μ_{s_i} respectively [42]. These expected values are related to μ_i by

$$\mu_i = \sqrt{\mu_{c_i}^2 + \mu_{s_i}^2}. \tag{5.5}$$

Consequently, (5.1) can be rewritten as

$$x_i(t) = [N_{c_i}(t) + s_i(t)(A_{c_i}(t) + \mu_{c_i})] \cos(\omega_i t) - [N_{s_i}(t) + s_i(t)(A_{s_i}(t) + \mu_{s_i})] \sin(\omega_i t) \tag{5.6}$$

where A_{c_i} and A_{s_i} are i.i.d and have normal distributions with expected values equal to zero. If the PSD of the received signals are symmetric around their carrier frequencies, then [55]

$$f_{A_{c_i}, A_{s_i}, \dot{A}_{c_i}, \dot{A}_{s_i}}(a_{c_i}, a_{s_i}, \dot{a}_{c_i}, \dot{a}_{s_i}) = \frac{1}{4\pi^2 c_{i0} c_{i2}} \exp\left(-\frac{a_{c_i}^2 + a_{s_i}^2}{2c_{i0}}\right) \exp\left(-\frac{\dot{a}_{c_i}^2 + \dot{a}_{s_i}^2}{2c_{i2}}\right) \tag{5.7a}$$

where

$$c_{in} = (2\pi)^n \int_{f_i - f_{m_i}}^{f_i + f_{m_i}} (f - f_i)^n W_i(f) df \qquad n = 0, 2, \tag{5.7b}$$

and where f_{m_i} is the maximum Doppler frequency and $W_i(f)$ is the PSD of the unmodulated received signal.

5.2 Average Switching Rate and Mean Time to Loss of Lock

Similar to the previous chapters, one can find the average switching rate and the mean time to loss of lock by studying the relative statistics of the received signals' amplitudes.

5.2.1 ASR and MTLL in Rician fading channels

Assigning R_1 and R_2 to the amplitudes of the noisy desired signal and the noisy interference signal respectively, one can define $Z = R_1 - R_2$ to be the difference between the received signals' amplitudes. Since $R_1 > R_2$ is equivalent to $Z > 0$ and $R_2 > R_1$ is equivalent to $Z < 0$, the ASR

of an AFC, N, is equivalent to the zero-crossing rate (both positive going and negative going) of Z, $N_Z(0)$. One has [43]

$$N = N_Z(0) = \int_{-\infty}^{\infty} |\dot{z}|\, f_{Z,\dot{Z}}(0,\dot{z}) d\dot{z} \tag{5.8}$$

where $f_{Z,\dot{Z}}(z,\dot{z})$ is the JPDF of Z and its time derivative, $\dot{Z}$. This equation can be used to find the ASR of an AFC in the case of modulated and unmodulated received signals.

The MTLL of an AFC for unmodulated signals, T, can be found using [53]

$$T = \frac{2F}{N} \tag{5.9a}$$

where

$$F = \int_{x=1}^{\infty} \int_{t=0}^{\infty} t f_{R_1}(tx) f_{R_2}(t) dt dx \tag{5.9b}$$

is the probability that $R_1 > R_2$ and $f_{R_1}(r_1)$ and $f_{R_2}(r_2)$ are the PDF of R_1 and R_2, respectively.

Since the received signals and noise are narrowband, one can rewrite (5.6) as

$$x_i(t) = R_i(t)\cos(\omega_i t + \Theta_i(t)) \qquad i = 1,2 \tag{5.10a}$$

where

$$R_i = \sqrt{U_i^2 + V_i^2} \tag{5.10b}$$

$$\tan(\Theta_i) = \frac{V_i}{U_i} \tag{5.10c}$$

$$U_i = N_{c_i} + s_i(A_{c_i} + \mu_{c_i}) \tag{5.10d}$$

$$V_i = N_{s_i} + s_i(A_{s_i} + \mu_{s_i}). \tag{5.10e}$$

By differentiating (5.10d) and (5.10e) with respect to time,

$$\dot{U}_i = \dot{N}_{c_i} + s_i\dot{A}_{c_i} + \dot{s}_i(A_{c_i} + \mu_{c_i}) \tag{5.11}$$

$$\dot{V}_i = \dot{N}_{s_i} + s_i\dot{A}_{s_i} + \dot{s}_i(A_{s_i} + \mu_{s_i}) \tag{5.12}$$

It can be shown that

$$f_{U_i,\dot{U}_i}(u_i,\dot{u}_i) = k_i \exp\left[-\frac{1}{2(1-\delta_i^2)}\left(\frac{(u_i - s_i\mu_{c_i})^2}{\sigma_{i0}^2} - \frac{2\delta_i(u_i - s_i\mu_{c_i})(\dot{u}_i - \dot{s}_i\mu_{c_i})}{\sigma_{i0}\sigma_{i2}} + \frac{(\dot{u}_i - \dot{s}_i\mu_{c_i})^2}{\sigma_{i2}^2}\right)\right] \tag{5.13a}$$

and

$$f_{V_i,\dot{V}_i}(v_i,\dot{v}_i) = k_i \exp\left[-\frac{1}{2(1-\delta_i^2)}\left(\frac{(v_i + s_i\mu_{s_i})^2}{\sigma_{i0}^2} - \frac{2\delta_i(v_i + s_i\mu_{s_i})(\dot{v}_i + \dot{s}_i\mu_{s_i})}{\sigma_{i0}\sigma_{i2}} + \frac{(\dot{v}_i + \dot{s}_i\mu_{s_i})^2}{\sigma_{i2}^2}\right)\right] \tag{5.13b}$$

where

$$k_i = \frac{1}{2\pi\sigma_{i0}\sigma_{i2}\sqrt{1-\delta_i^2}}, \tag{5.13c}$$

$$\sigma_{i0}^2 = s_i^2 c_{i0} + b_{i0}, \tag{5.13d}$$

$$\sigma_{i2}^2 = \dot{s}_i^2 c_{i0} + s_i^2 c_{i2} + b_{i2}, \tag{5.13e}$$

$$\delta_i = \frac{c_{i0} s_i \dot{s}_i}{\sqrt{(s_i^2 c_{i0} + b_{i0})(\dot{s}_i^2 c_{i0} + s_i^2 c_{i2} + b_{i2})}}. \tag{5.13f}$$

Considering the definition of U_i, $\dot{U}_i$, V_i, and $\dot{V}_i$, one can see that U_i and $\dot{U}_i$ are independent of V_i and $\dot{V}_i$. Thus,

$$f_{U_i,\dot{U}_i,V_i,\dot{V}_i}(u_i,\dot{u}_i,v_i,\dot{v}_i) = f_{U_i,\dot{U}_i}(u_i,\dot{u}_i) f_{V_i,\dot{V}_i}(v_i,\dot{v}_i).$$

The Jacobian of the transformation from the $(U_i, \dot{U}_i, V_i, \dot{V}_i)$-space to the $(R_i, \dot{R}_i, \Theta_i, \dot{\Theta}_i)$-space is equal to R_i^{-2}. Therefore,

$$f_{R_i,\dot{R}_i,\Theta_i,\dot{\Theta}_i}(r_i,\dot{r}_i,\theta_i,\dot{\theta}_i) = r_i^2 k_i^2 \exp\left[-\frac{1}{2(1-\delta_i^2)}\left(\frac{g_{i1}}{\sigma_{i0}^2} - \frac{2\delta_i g_{i2}}{\sigma_{i0}\sigma_{i2}} + \frac{g_{i3}}{\sigma_{i2}^2}\right)\right] \tag{5.14a}$$

where

$$g_{i1} = r_i^2 - 2r_i\mu_i s_i \cos(\theta_i + \xi_i) + \mu_i^2 s_i^2 \tag{5.14b}$$

$$g_{i2} = r_i\dot{r}_i + \mu_i^2 s_i\dot{s}_i - \mu_i(r_i\dot{s}_i + \dot{r}_i s_i)\cos(\theta_i + \xi_i) + r_i\dot{\theta}_i\mu_i s_i \sin(\theta_i + \xi_i) \tag{5.14c}$$

$$g_{i3} = \dot{r}_i^2 + r_i^2\dot{\theta}_i^2 + \mu_i^2\dot{s}_i^2 + 2\mu_i\dot{s}_i[r_i\dot{\theta}_i\sin(\theta_i + \xi_i) - \dot{r}_i\cos(\theta_i + \xi_i)] \tag{5.14d}$$

$$\cos(\xi_i) = \frac{\mu_{c_i}}{\mu_i} \tag{5.14e}$$

$$\sin(\xi_i) = \frac{\mu_{s_i}}{\mu_i}. \tag{5.14f}$$

Then, integrating $f_{R_i,\dot{R}_i,\Theta_i,\dot{\Theta}_i}(r_i,\dot{r}_i,\theta_i,\dot{\theta}_i)$ over θ_i and $\dot{\theta}_i$ yields

$$f_{R_i,\dot{R}_i}(r_i,\dot{r}_i) = \frac{r_i}{(2\pi)^{3/2}\sqrt{1-\delta_i^2}\sigma_{i2}\sigma_{i0}^2}\int_{\upsilon=0}^{2\pi}\exp[\kappa_{i1} + 2\kappa_{i2}\cos(\upsilon) + \kappa_{i3}\cos(2\upsilon)]d\upsilon \tag{5.15a}$$

where

$$\kappa_{i1} = -\frac{1}{2(1-\delta_i^2)}\left(\frac{r_i^2}{\sigma_{i0}^2} - \frac{2\delta_i r_i\dot{r}_i}{\sigma_{i0}\sigma_{i2}} + \frac{\dot{r}_i^2}{\sigma_{i2}^2}\right) + \gamma_{i1} \tag{5.15b}$$

$$\kappa_{i2} = r_i\gamma_{i2} + \dot{r}_i\gamma_{i3} \tag{5.15c}$$

$$\kappa_{i3} = -\frac{\mu_i^2}{4(1-\delta_i^2)}\left(\frac{\dot{s}_i}{\sigma_{i2}} - \frac{\delta_i s_i}{\sigma_{i0}}\right)^2 \tag{5.15d}$$

$$\gamma_{i1} = -\frac{\mu_i^2}{4(1-\delta_i^2)}\left(\frac{s_i^2}{\sigma_{i0}^2}(2-\delta_i^2) - \frac{2\delta_i s_i\dot{s}_i}{\sigma_{i0}\sigma_{i2}} + \frac{\dot{s}_i^2}{\sigma_{i2}^2}\right) \tag{5.15e}$$

$$\gamma_{i2} = \frac{\mu_i}{2(1-\delta_i^2)}\left(\frac{s_i}{\sigma_{i0}^2} - \frac{\delta_i\dot{s}_i}{\sigma_{i0}\sigma_{i2}}\right) \tag{5.15f}$$

$$\gamma_{i3} = \frac{\mu_i}{2(1-\delta_i^2)}\left(\frac{\dot{s}_i}{\sigma_{i2}^2} - \frac{\delta_i s_i}{\sigma_{i0}\sigma_{i2}}\right). \tag{5.15g}$$

Since the desired channel and the interference channel are independent, R_1 and $\dot{R}_1$ are independent of R_2 and $\dot{R}_2$. Thus,

$$f_{R_1,\dot{R}_1,R_2,\dot{R}_2}(r_1,\dot{r}_1,r_2,\dot{r}_2) = f_{R_1,\dot{R}_1}(r_1,\dot{r}_1) f_{R_2,\dot{R}_2}(r_2,\dot{r}_2).$$

The Jacobian of the transformation from $(R_1, \dot{R}_1, R_2, \dot{R}_2)$-space to $(Z, \dot{Z}, R_2, \dot{R}_2)$-space is $J = 1$. One has

$$f_{Z,\dot{Z},R_2,\dot{R}_2}(z,\dot{z},r_2,\dot{r}_2) = f_{R_1,\dot{R}_1}(z+r_2,\dot{z}+\dot{r}_2) f_{R_2,\dot{R}_2}(r_2,\dot{r}_2). \tag{5.16}$$

Then integrating (5.16) over r_2 and $\dot{r}_2$ using [54, (3.462.7)],

$$\int_0^\infty x^2 e^{-\mu x^2 - 2\nu x} dx = -\frac{\nu}{2\mu^2} + \sqrt{\frac{\pi}{\mu^5}} \frac{2\nu^2+\mu}{4} e^{\frac{\nu^2}{\mu}} \left[1 - \operatorname{erf}\left(\frac{\nu}{\sqrt{\mu}}\right)\right] \tag{5.17}$$

for $\mu > 0$, yields

$$f_{Z,\dot{Z}}(0,\dot{z}) = \int_0^{2\pi}\int_0^{2\pi} \left[\frac{q_2}{q_1^2} + \frac{\sqrt{\pi}}{\sqrt{2}} \frac{q_2^2+q_1}{q_1^{5/2}} \exp\left(\frac{q_2^2}{2q_1}\right) \operatorname{erfc}\left(\frac{-q_2}{\sqrt{2q_1}}\right)\right] \Upsilon \exp(\Delta) d\upsilon_1 d\upsilon_2 \tag{5.18a}$$

where

$$\Upsilon = \frac{1}{(2\pi)^{5/2}\sqrt{(1-\delta_1^2)(1-\delta_2^2)}\sigma_{12}\sigma_{10}^2\sigma_{22}\sigma_{20}^2 p_1} \tag{5.18b}$$

$$\Delta = 2\dot{z}\gamma_{13}\cos(\upsilon_1) + \kappa_{13}\cos(2\upsilon_1) + \kappa_{23}\cos(2\upsilon_2) + \gamma_{11} + \gamma_{21} - \frac{\dot{z}^2}{2\sigma_{12}^2(1-\delta_1^2)} + \frac{\Xi^2}{2p_1^2} \tag{5.18c}$$

$$q_1 = \frac{1}{\sigma_{10}^2(1-\delta_1^2)} + \frac{1}{\sigma_{20}^2(1-\delta_2^2)} - \frac{p_2^2}{p_1^2} \tag{5.18d}$$

$$q_2 = 2\gamma_{12}\cos(\upsilon_1) + 2\gamma_{22}\cos(\upsilon_2) + \frac{\Xi p_2}{p_1^2} + \frac{\dot{z}\delta_1}{\sigma_{12}\sigma_{10}(1-\delta_1^2)} \tag{5.18e}$$

$$p_1 = \sqrt{\frac{1}{\sigma_{12}^2(1-\delta_1^2)} + \frac{1}{\sigma_{22}^2(1-\delta_2^2)}} \tag{5.18f}$$

$$p_2 = \frac{\delta_1}{\sigma_{12}\sigma_{10}(1-\delta_1^2)} + \frac{\delta_2}{\sigma_{22}\sigma_{20}(1-\delta_2^2)} \tag{5.18g}$$

$$\Xi = -\frac{\dot{z}}{\sigma_{12}^2(1-\delta_1^2)} + 2\gamma_{13}\cos(\upsilon_1) + 2\gamma_{23}\cos(\upsilon_2). \tag{5.18h}$$

Using (5.8) and (5.18), one can evaluate the ASR of AFC numerically. However, if the carriers are unmodulated, i.e., $\dot{s}_i = 0$ for $i = 1, 2$, (5.15) simplifies to

$$f_{R_i,\dot{R}_i}(r_i,\dot{r}_i) = \frac{1}{\sqrt{2\pi}\sigma_{i2}} \exp\left(-\frac{\dot{r}_i^2}{2\sigma_{i2}^2}\right) \times \frac{r_i}{\sigma_{i0}^2} \exp\left(-\frac{r_i^2+\mu_i^2 s_i^2}{2\sigma_{i0}^2}\right) I_0\left(\frac{\mu_i s_i r_i}{\sigma_{i0}^2}\right). \tag{5.19}$$

It can be seen that R_i and $\dot{R}_i$ are independent. Therefore, Z and $\dot{Z}$ are independent as well and $f_{Z,\dot{Z}}(0,\dot{z}) = f_Z(0) f_{\dot{Z}}(\dot{z})$. Moreover, $\dot{R}_1$ and $\dot{R}_2$ are independent Gaussian random processes and

therefore $\dot{Z} = \dot{R}_1 - \dot{R}_2$ is also Gaussian. Consequently, it can be shown that

$$N_Z(0) = \frac{\sqrt{2(\sigma_{12}^2+\sigma_{22}^2)}}{\sqrt{\pi}\sigma_{10}^2\sigma_{20}^2}\int_0^\infty t^2 I_0\left(\frac{\mu_1 s_1 t}{\sigma_{10}^2}\right) I_0\left(\frac{\mu_2 s_2 t}{\sigma_{20}^2}\right)\exp\left[-\frac{t^2}{2}\left(\frac{\sigma_{10}^2+\sigma_{20}^2}{\sigma_{10}^2\sigma_{20}^2}\right) - \frac{\mu_1^2 s_1^2}{2\sigma_{10}^2} - \frac{\mu_2^2 s_2^2}{2\sigma_{20}^2}\right] dt. \tag{5.20}$$

The final results for the ASR of an AFC are shown in Table 5.1.

In order to find F in (5.9b), we should find the PDF of R_i. Considering (5.10d) and (5.10e), one can see that U_i and V_i are independent Gaussian random processes with common variances and nonzero means equal to $s_i\mu_{c_i}$ and $s_i\mu_{s_i}$, respectively. After some manipulations, one has

$$f_{R_i}(r_i) = \frac{r_i}{b_{i0}+s_i^2 c_{i0}}\exp\left(-\frac{r_i^2+s_i^2\mu_i^2}{2(b_{i0}+s_i^2 c_{i0})}\right) I_0\left(\frac{r_i s_i \mu_i}{b_{i0}+s_i^2 c_{i0}}\right) \tag{5.21}$$

Then F can be found using (5.9b),

$$F = \int_{x=1}^\infty\int_{t=0}^\infty \frac{t^3 x}{\sigma_{10}^2\sigma_{20}^2}\exp\left(-\frac{t^2x^2+s_1^2\mu_1^2}{2\sigma_{10}^2} - \frac{t^2+s_2^2\mu_2^2}{2\sigma_{20}^2}\right) I_0\left(\frac{txs_1\mu_1}{\sigma_{10}^2}\right) I_0\left(\frac{ts_2\mu_2}{\sigma_{20}^2}\right) dtdx. \tag{5.22}$$

Then the mean time to loss of lock can be evaluated numerically using (5.9a). In the case of i.n.d. channels and unmodulated signals,

$$\begin{aligned} T = &\int_{x=1}^\infty\int_{y=0}^\infty y^3 x\exp\left(-\frac{y^2x^2}{2\sigma_{10}^2} - \frac{y^2}{2\sigma_{20}^2}\right) I_0\left(\frac{yxs_1\mu_1}{\sigma_{10}^2}\right) I_0\left(\frac{ys_2\mu_2}{\sigma_{20}^2}\right) dydx \\ &\times\sqrt{\frac{2\pi}{\sigma_{12}^2+\sigma_{22}^2}}\left[\int_0^\infty t^2\exp\left(-\frac{t^2}{2\sigma_{10}^2} - \frac{t^2}{2\sigma_{20}^2}\right) I_0\left(\frac{\mu_1 s_1 t}{\sigma_{10}^2}\right) I_0\left(\frac{\mu_2 s_2 t}{\sigma_{20}^2}\right) dt\right]^{-1}. \end{aligned} \tag{5.23}$$

If the signals have equal power and the channels are i.i.d.,

$$T = \left[{}_2F_2\left(\frac{1}{2},\frac{3}{2};1,1;\frac{\mu^2}{\sigma_0^2}\right)\right]^{-1}\int_{x=1}^\infty\int_{t=0}^\infty \frac{4t^3x}{\sigma_0^3\sigma_2}\exp\left[-\frac{t^2(x^2+1)}{2\sigma_0^2}\right] I_0\left(\frac{tx\mu}{\sigma_0^2}\right) I_0\left(\frac{t\mu}{\sigma_0^2}\right) dtdx. \tag{5.24}$$

It is worth mentioning that if the power of noise is negligible compared to the power of signal in both branches, i.e., large SNR approximation, the ASR and MTLL of the AFC in the case of i.n.d. Rayleigh fading and unmodulated carriers is $N = \frac{\sqrt{c_{10}c_{20}(c_{12}+c_{22})}}{(c_{10}+c_{20})^{3/2}}$ and $T = 2\sqrt{\frac{c_{10}(c_{10}+c_{20})}{c_{20}(c_{12}+c_{22})}}$, respectively, which agrees with the results previously reported in [7].

5.2.2 ASR and MTLL in Rayleigh fading channels

In this case, one can use the random process $Y = \frac{R_1}{R_2}$ to find the ASR and MTLL. Since $R_1 > R_2$ is equivalent to $Y > 1$ and $R_2 > R_1$ is equivalent to $Y < 1$, the ASR of an AFC, N, is equivalent to the level crossing rate (both positive going and negative going) of Y through 1, $N_Y(1)$. One has [43]

$$N = N_Y(1) = \int_{-\infty}^\infty |\dot{y}|\, f_{Y,\dot{Y}}(1,\dot{y})d\dot{y} \tag{5.25}$$

Table 5.1. The average switching rate of an AFC in Rician/Rician fading noisy channels.

System Model	Average Switching Rate
i.i.d. $s_1 = s_2 = 1$	$\frac{\sigma_2}{2\sigma_0} \exp\left(-\frac{\mu^2}{\sigma_0^2}\right) {}_2F_2\left(\frac{1}{2}, \frac{3}{2}; 1, 1, \frac{\mu^2}{\sigma_0^2}\right)$
i.n.d. $\dot{s}_1 = \dot{s}_2 = 0$	$\int_0^\infty t^2 \exp\left[-\frac{t^2+\mu_1^2 s_1^2}{2\sigma_{10}^2} - \frac{t^2+\mu_2^2 s_2^2}{2\sigma_{20}^2}\right]$ $\times \frac{\sqrt{2(\sigma_{12}^2+\sigma_{22}^2)}}{\sqrt{\pi}\sigma_{10}^2\sigma_{20}^2} I_0\left(\frac{\mu_1 s_1 t}{\sigma_{10}^2}\right) I_0\left(\frac{\mu_2 s_2 t}{\sigma_{20}^2}\right) dt$
i.n.d. modulated	$\Upsilon \int_{-\infty}^{\infty} \lvert\dot{z}\rvert \int_0^{2\pi} \int_0^{2\pi} \exp(\Delta) d\upsilon_1 d\upsilon_2 d\dot{z}$ $\times \left[\frac{q_2}{q_1^2} + \frac{\sqrt{\pi}}{\sqrt{2q_1}} \frac{q_2^2+q_1}{q_1^2} \exp\left(\frac{q_2^2}{2q_1}\right) \operatorname{erfc}\left(\frac{-q_2}{\sqrt{2q_1}}\right)\right]$

where $f_{Y,\dot{Y}}(y,\dot{y})$ is the JPDF of Y and its time derivative $\dot{Y}$. In order to find the ASR, one should first find $f_{Y,\dot{Y}}(y,\dot{y})$. Since Rayleigh distribution is a special case of Rician distribution in which $\mu_i = \mu_{c_i} = \mu_{s_i} = 0$, (5.15) simplifies to

$$f_{R_i,\dot{R}_i}(r_i,\dot{r}_i) = \frac{r_i}{\sigma_{i0}^2\sigma_{i2}\sqrt{2\pi(1-\delta_i^2)}} \exp\left[-\frac{1}{2(1-\delta_i^2)}\left(\frac{r_i^2}{\sigma_{i0}^2} - \frac{2\delta_i r_i \dot{r}_i}{\sigma_{i0}\sigma_{i2}} + \frac{\dot{r}_i^2}{\sigma_{i2}^2}\right)\right]. \tag{5.26}$$

Since the channels are independent and also the received signals are independent, the envelopes of the signals are also independent. As a result,

$$f_{R_1,\dot{R}_1,R_2,\dot{R}_2}(r_1,\dot{r}_1,r_2,\dot{r}_2) = f_{R_1,\dot{R}_1}(r_1,\dot{r}_1) f_{R_2,\dot{R}_2}(r_2,\dot{r}_2).$$

One can use the fundamental transformation theorem to obtain $f_{Y,\dot{Y},R_2,\dot{R}_2}(y,\dot{y},r_2,\dot{r}_2)$ with respect to $f_{R_1,\dot{R}_1,R_2,\dot{R}_2}(r_1,\dot{r}_1,r_2,\dot{r}_2)$. After some manipulations,

$$f_{Y,\dot{Y},R_2,\dot{R}_2}(y,\dot{y},r_2,\dot{r}_2) = M r_2^4 y \exp\left[-(D_1 r_2^2 + 2D_2 r_2 \dot{r}_2 + D_3 \dot{r}_2^2)\right] \tag{5.27a}$$

where

$$M = \frac{1}{2\pi\sigma_{10}^2\sigma_{20}^2\sigma_{12}\sigma_{22}\sqrt{(1-\delta_1^2)(1-\delta_2^2)}}, \tag{5.27b}$$

$$D_1 = \frac{1}{2}\left[\frac{y^2}{(1-\delta_1^2)\sigma_{10}^2} + \frac{1}{(1-\delta_2^2)\sigma_{20}^2} - \frac{2\delta_1 y\dot{y}}{(1-\delta_1^2)\sigma_{10}\sigma_{12}} + \frac{\dot{y}^2}{(1-\delta_1^2)\sigma_{12}^2}\right], \tag{5.27c}$$

$$D_2 = \frac{1}{2}\left[-\frac{\delta_1 y^2}{(1-\delta_1^2)\sigma_{10}\sigma_{12}} - \frac{\delta_2}{(1-\delta_2^2)\sigma_{20}\sigma_{22}} + \frac{y\dot{y}}{(1-\delta_1^2)\sigma_{12}^2}\right], \tag{5.27d}$$

$$D_3 = \frac{1}{2}\left[\frac{y^2}{(1-\delta_1^2)\sigma_{12}^2} + \frac{1}{(1-\delta_2^2)\sigma_{22}^2}\right]. \tag{5.27e}$$

The JPDF of Y and $\dot{Y}$ can be determined by integrating (5.27a) over r_2 and $\dot{r}_2$, i.e.,

$$f_{Y,\dot{Y}}(y,\dot{y}) = \int_{r_2=0}^{\infty} \int_{\dot{r}_2=-\infty}^{\infty} f_{Y,\dot{Y},R_2,\dot{R}_2}(y,\dot{y},r_2,\dot{r}_2) dr_2 d\dot{r}_2. \tag{5.28}$$

Note that we only need $f_{\Lambda,\dot{\Lambda}}(1,\dot{\lambda})$ to find the average switching rate. Using [54, (3.461.2)],

$$\int_0^\infty x^{2n} e^{-px^2} dx = \frac{(2n-1)!!}{2(2p)^n}\sqrt{\frac{\pi}{p}} \tag{5.29}$$

for n being an integer and $p > 0$, one has

$$f_{Y,\dot{Y}}(1,\dot{y}) = \frac{m}{(\dot{y}^2 + 2d_2\dot{y} + d_1)^{5/2}} \tag{5.30a}$$

where

$$m = \frac{3[(1-\delta_1^2)\sigma_{12}^2 + (1-\delta_2^2)\sigma_{22}^2]^2}{2\sigma_{10}^2\sigma_{20}^2} \tag{5.30b}$$

$$d_1 = \frac{\sigma_{12}^2}{\sigma_{10}^2} + \frac{\sigma_{22}^2}{\sigma_{20}^2} - 2\delta_1\delta_2\frac{\sigma_{12}\sigma_{22}}{\sigma_{10}\sigma_{20}} + (1-\delta_2^2)\frac{\sigma_{22}^2}{\sigma_{10}^2} + (1-\delta_1^2)\frac{\sigma_{12}^2}{\sigma_{20}^2} \tag{5.30c}$$

$$d_2 = \frac{\delta_2\sigma_{22}}{\sigma_{20}} - \frac{\delta_1\sigma_{12}}{\sigma_{10}}. \tag{5.30d}$$

As a result, the average switching rate of an AFC can be obtained using 3.29 as

$$N = N_Y(1) = \frac{2m(d_1 + d_2^2)}{3\sqrt{d_1}(d_1 - d_2^2)^2} \tag{5.31}$$

if $|d_2| < \sqrt{d_1}$. The final results for the ASR of an AFC in Rayleigh fading noisy channels are shown in Table 5.2.

In order to find the MTLL, we also need to find F. Since U_i is equal to the summation of two independent Gaussian random processes (see (5.10d)), it is Gaussian as well. The same discussion holds for V_i and it can be easily seen that U_i and V_i are i.i.d. and have zero means. By some manipulations, the distribution of R_i can be found to be Rayleigh where

$$f_{R_i}(r_i) = \frac{r_i}{b_{i0} + s_i^2 c_{i0}} \exp\left(-\frac{r_i^2}{2(b_{i0} + s_i^2 c_{i0})}\right). \tag{5.32}$$

Using (5.9b) and after some manipulations, it can be shown that F is equal to

$$F = \frac{b_{10} + s_1^2 c_{10}}{b_{10} + b_{20} + s_1^2 c_{10} + s_2^2 c_{20}}. \tag{5.33}$$

The MTLL in the case of unmodulated received signals in i.n.d. channels will be equal to

$$T = 2\left(\frac{\sigma_{10}}{\sigma_{20}}\right)\sqrt{\frac{\sigma_{10}^2 + \sigma_{20}^2}{\sigma_{12}^2 + \sigma_{22}^2}}. \tag{5.34}$$

If the signals have equal power,

$$T = 2\sqrt{\frac{(c_{10} + b_{10})(c_{10} + c_{20} + b_{10} + b_{20})}{(c_{20} + b_{20})(c_{12} + c_{22} + b_{12} + b_{22})}}. \tag{5.35}$$

In the special case of i.i.d. channels and $s_1 = s_2 = 1$,

$$T = 2\sqrt{\frac{c_0 + b_0}{c_2 + b_2}}. \tag{5.36}$$

Table 5.2. The average switching rate of an AFC in Rayleigh/Rayleigh fading noisy channels.

System Model	Average Switching Rate
i.i.d. $s_1 = s_2 = 1$ $\dot{s}_1 = \dot{s}_2 = 0$	$\frac{1}{2}\sqrt{\frac{c_2+b_2}{c_0+b_0}}$
i.n.d. $s_1 = s_2 = 1$ $\dot{s}_1 = \dot{s}_2 = 0$	$\frac{\sqrt{(c_{10}+b_{10})(c_{20}+b_{20})(c_{12}+c_{22}+b_{12}+b_{22})}}{(c_{10}+c_{20}+b_{10}+b_{20})3/2}$
i.n.d. $\dot{s}_1 = \dot{s}_2 = 0$	$\frac{\sigma_{10}\sigma_{20}}{(\sigma_{10}^2+\sigma_{20}^2)}\sqrt{\frac{\sigma_{12}^2+\sigma_{22}^2}{\sigma_{10}^2+\sigma_{20}^2}}$
i.n.d. modulated	$\frac{2m(d_1+d_2^2)}{3\sqrt{d_1}(d_1-d_2^2)^2}$

5.3 Numerical Examples

In the numerical examples, we consider the special case of two-dimensional (2-D) isotropic scattering and an omnidirectional receiving antenna. It is assumed that the bandpass filter of the IF portion of the receiver is an ideal flat filter such that it does not affect the shape of the PSD of the received signals. In this scenario, $c_{i2} = 2\pi^2 f_{m_i}^2 c_{i0}$ for $i = 1, 2$ where f_{m_i} is the maximum Doppler frequency [50]. The carriers are assumed to be unmodulated such that $s_1 = s_2 = 1$ and the maximum Doppler frequencies of the received signals are assumed to be equal, $f_{m_1} = f_{m_2} = f_m$. Moreover, the bandpass filter is assumed to have a bandwidth equal to $2f_m$ and therefore $b_{i2} = \frac{4}{3}\pi^2 f_m^2 b_{i0}$. In Fig. 5.1, the ASR of an AFC (normalized to f_m) versus the signal-to-noise ratio (SNR) of the desired signal is shown for different signal-to-interference ratios (SIRs) for Rayleigh fading channels. The SNR and SIR are defined as $\text{SNR}_i = 10\log_{10}\left(\frac{c_{i0}}{b_{i0}}\right)$ and $\text{SIR} = 10\log_{10}\left(\frac{c_{10}}{c_{20}}\right)$ for Rayleigh fading. The SNR of the interference is assumed to be equal to 10 dB. It can be seen that for large values of SIR, increasing the SNR of the desired signal increases the ASR which means the performance of the AFC deteriorates. For smaller values of SIR (for instance, -20 dB), the AFC is locked on the desired signal for small values of SNR_1 and increasing SNR_1 causes the AFC to lock on the interferer which is also equivalent to loss of performance. This behavior can be observed more clearly in Fig. 5.2 where the MTLL of an AFC (multiplied by f_m) is shown versus SNR_1. The reason for this behaviour is that when the SIR and SNR_2 are constant, decreasing SNR_1 is equivalent to increasing the amplitude of the noisy desired signal compared to the amplitude of the noisy interferer. Observing these results, one can conclude that there is a trade-off for the SNR of the desired signal; while

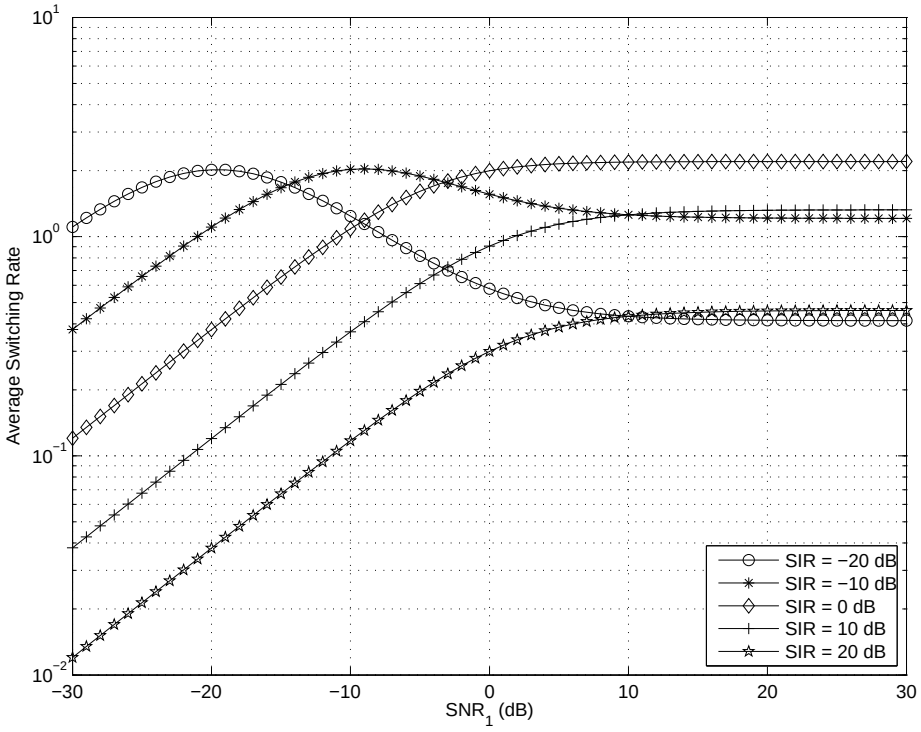

Figure 5.1. The ASR of an AFC (normalized to f_m) in Rayleigh fading for $\text{SNR}_2 = 10$ dB.

having a large SNR makes the AFC more robust to the loss of lock due to the effect of noise, it also makes the AFC more vulnerable to the loss of lock due to an interference signal.

Fig. 5.3 shows the ASR of an AFC (normalized to f_m) in a Rician fading scenario for different Rice factors defined as $K_i = \frac{\mu_i^2}{2c_{i0}}$. In a Rician scenario, the SIR and SNR are defined as $\text{SNR}_i = 10\log_{10}\left(\frac{c_{i0}(1+K_i)}{b_{i0}}\right)$ and $\text{SIR} = 10\log_{10}\left(\frac{c_{10}(1+K_1)}{c_{20}(1+K_2)}\right)$, respectively. The SIR and SNR_2 are assumed to be equal to 10 dB.

In Figs. 5.4 and 5.5, the ASR and MTLL of an AFC versus SIR are shown for different values of Rice factor. Two cases of noise-free desired signal and $\text{SNR}_1 = 0$ dB are considered when $\text{SNR}_2 = 10$ dB. It can be seen that at small values of SIR, the MTLL is increased when the signal is noisier. This is because the desired signal is weak compared to the interference and noise is the dominant part which determines the MTLL in branch 1. However at large values of SIR, the performance of the AFC is better for larger values of SNR_1 when the desired signal has a large LOS component (for example $K_1 = 3$). This behavior can be explained by considering (5.19). One can see that the JPDF of R_i and $\dot{R}_i$ is equivalent to the JPDF of a Rician random process and its time derivative. Since decreasing the SNR in this case is equivalent to decreasing the Rice factor of this new random process, $\acute{K}_i = \frac{\mu_i^2}{2(c_{i0}+b_{i0})}$, and since the level crossing rate of a Rician random process

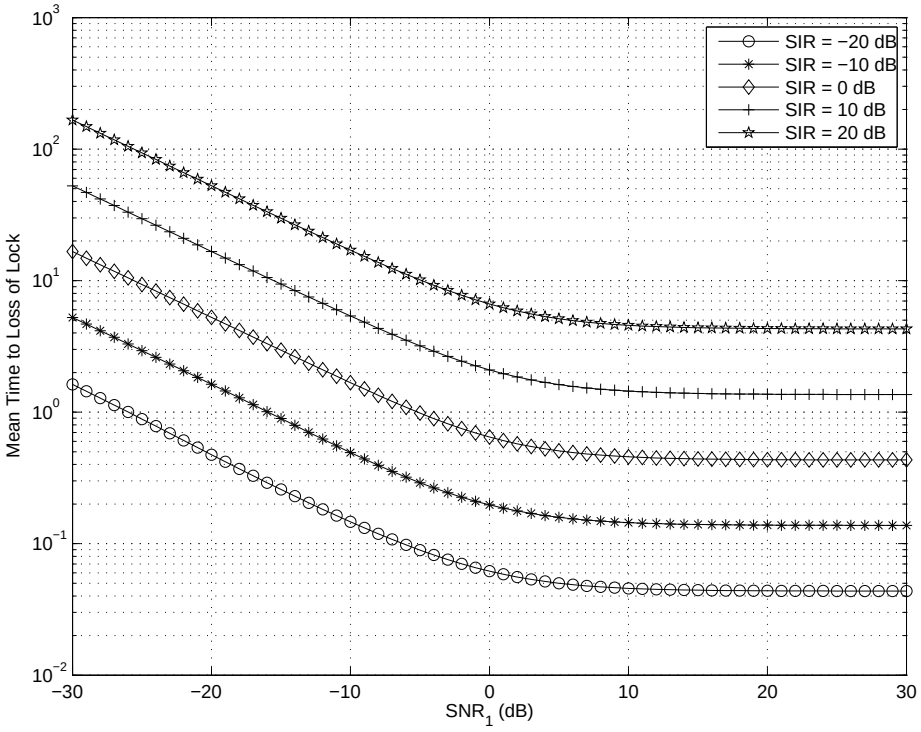

Figure 5.2. The MTLL of an AFC (multiplied by f_m) in Rayleigh fading for $\text{SNR}_2 = 10$ dB.

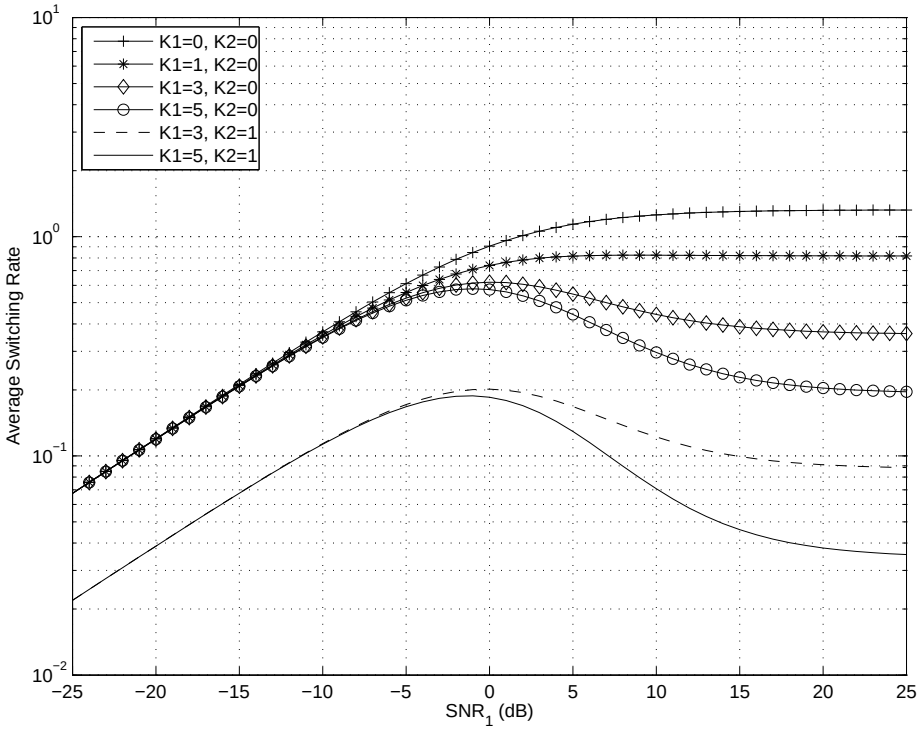

Figure 5.3. The ASR of an AFC (normalized to f_m) in Rician fading for $\text{SNR}_2 = 10$ dB and $\text{SIR} = 10$ dB.

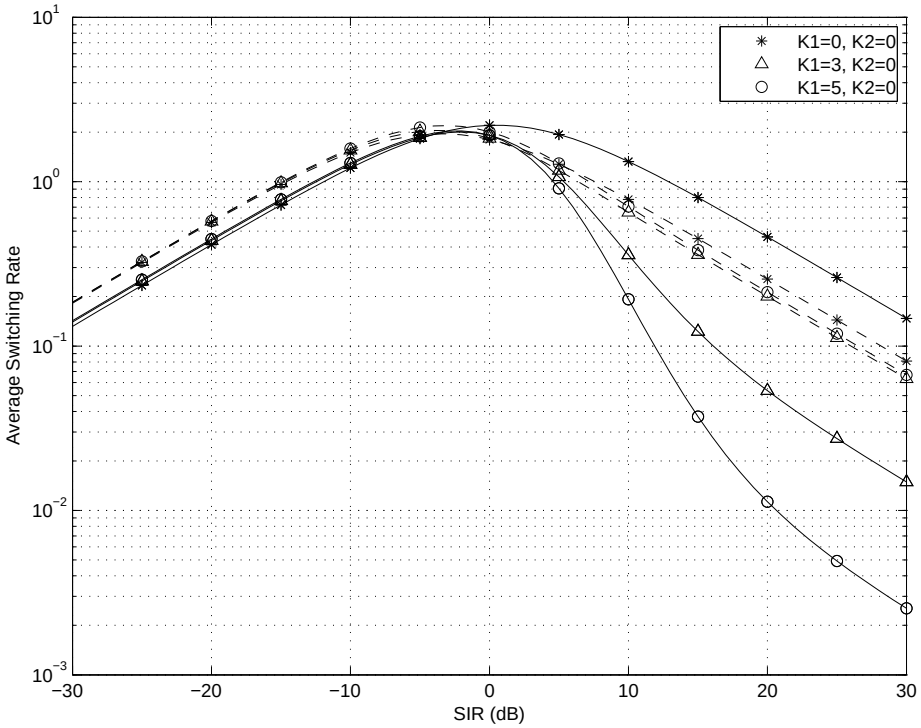

Figure 5.4. The ASR of an AFC (normalized to f_m) in Rician fading for $\text{SNR}_2 = 10$ dB. The solid lines represent the case of a noise-free desired signal and the dashed lines represent the case of $\text{SNR}_1 = 0$ dB.

is very sensitive to its Rice factor [50], the AFC has a better performance at large values of SNR.

5.4 Conclusion

In this chapter, we have investigated the effect of a single interferer on the performance of an AFC in noisy fading channels. Closed-from expressions and integral form formulas were derived for the ASR and the MTLL of an AFC when the channels are subject to Rayleigh and Rician fading and Gaussian noise. Numerical examples were presented to demonstrate the effect of noise on the performance of an AFC in such scenarios. It was shown that in some scenarios the performance of an AFC improves when the tracked signal becomes noisier.

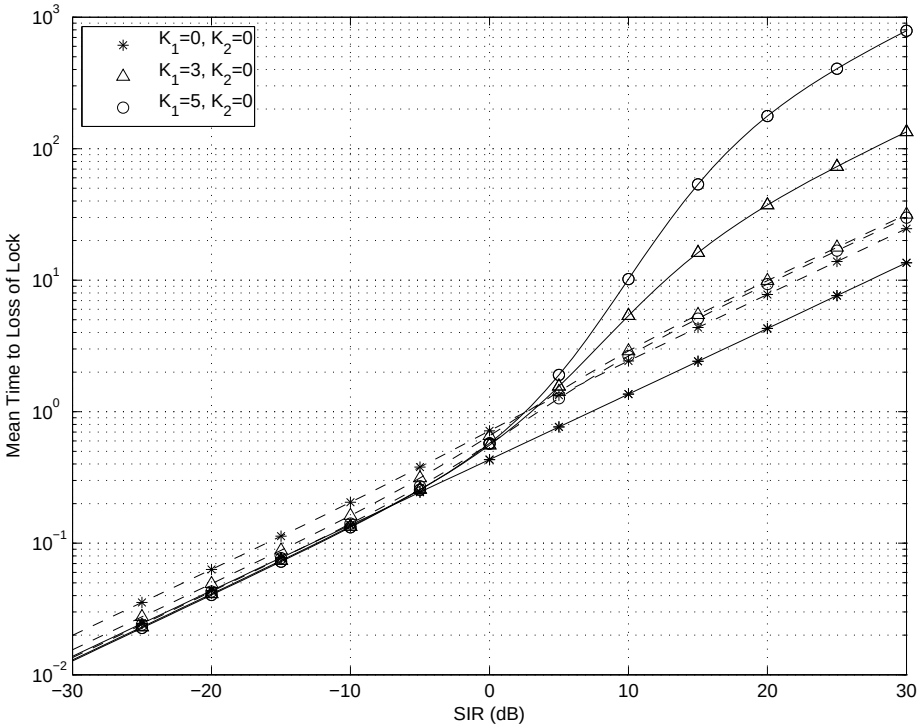

Figure 5.5. The MTLL of an AFC (multiplied by f_m) in Rician fading for $\mathrm{SNR}_2 = 10$ dB. The solid lines represent the case of a noise-free desired signal and the dashed lines represent the case of $\mathrm{SNR}_1 = 0$ dB.

Chapter 6

Lower Bounds to the Performance of Bit Synchronizers in ISI Channels

Although many synchronizers have been introduced and investigated for ISI-free systems in the literature, practical cases in which ISI plays an important role are not well investigated. In this chapter, this problem is investigated and true NDA ML synchronizer is derived in ISI channels. Moreover, some bounds are introduced and applied to the performance of synchronizers in ISI channels.

6.1 Maximum Likelihood Estimator for ISI Channels

In [14]–[16] the ML estimator of the timing offset for one symbol interval observation has been derived for binary pulse amplitude modulation (PAM) in the case that the symbol duration is equal to the inverse of sampling rate. The results have been also extended to the case of several bit intervals observation in an ISI-free channel. The non-data-aided (NDA) ML criterion is

$$\hat{\tau} = \arg\max_{\tilde{\tau}} \sum_{i} \log\left[\cosh\left(\frac{2q_i(\tilde{\tau})}{N_0}\right)\right] \tag{6.1}$$

where $q_i(\tilde{\tau}) = r(t) * p(-t)|_{t=iT+\tilde{\tau}}$, $\hat{\tau}$ is the estimated timing offset, $N_0/2$ is the two-sided spectral density of the additive white Gaussian noise, $r(t)$ is the received signal, T is the inverse of the sampling rate, $p(t)$ is the pulse shape with a duration equal to T, and $*$ denotes the convolution operation. Note that the summation in (6.1) is over the symbols that are received during the observation period, LT.

The purpose of this section is to derive the NDA ML criterion for symbol timing recovery in an ISI channel. In this study, we consider a binary PAM signal. The baseband model of the received signal, $r(t)$, can be expressed as

$$r(t) = x(t,\tau) + n(t) \tag{6.2a}$$

$$x(t,\tau) = \sum_{i} c_i g(t - iT - \tau) \tag{6.2b}$$

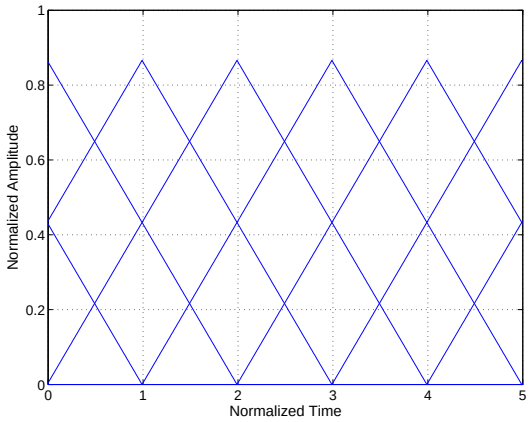

Figure 6.1. A sequence of 1s sent using triangular pulses with $M = 2$ and $L = 5$.

where $n(t)$ is the additive white Gaussian noise (AWGN) with two-sided spectral density equal to $N_0/2$, $g(t)$ is the received pulse shape (a truncated pulse with a duration equal to $2MT$), T is the inverse of the sampling rate and τ is the timing offset which can be modeled as an uniformly distributed random variable in $[0, T)$; in this equation, c_i is the ith transmitted data symbol and is a zero-mean random variable such that for any two transmitted data symbols, $E[c_i c_j] = C\delta(i - j)$, where $E[\cdot]$ denotes the expectation operation, $\delta(\cdot)$ is the Kronecker delta function and C is the energy of each bit.

Conditioned on τ, there are 2^{2M+L-1} equally probable signal waveforms for $x(t, \tau)$ during an observation time equal to LT. In Fig. 6.1, this is shown for a sequence of 1s sent using a triangular pulse with duration equal to $4T$ and an observation time equal to $5T$. As can be seen in this figure, 8 symbols are involved during this observation time. Since the probability of sending 1 or -1 is assumed to be 0.5 and the symbols are sent independently, there are 2^8 equally probable signal waveforms.

Conditioned on τ, these signal waveforms, $s_k(t, \tau)$, can be represented using the Karhunen-Loéve (KL) expansion [13]. Considering a complete orthonormal basis $\{\psi_i(t)\}$, one has

$$s_k(t, \tau) = \sum_{i=1}^{\infty} s_{ki}(\tau)\psi_i(t) \tag{6.3a}$$

$$s_{ki}(\tau) = \int_{\tau+jT}^{\tau+(j+L)T} s_k(t, \tau)\psi_i(t)dt. \tag{6.3b}$$

Similarly, $r(t)$ and $n(t)$ can be represented using the KL expansion during the interval $[\tau + jT, \tau + (j + L)T)$, conditioned on τ. If the kth signal waveform is received during the observation period,

by denoting the truncated vector representation of these signals by a prime, one has

$$\mathbf{r}' = \mathbf{s}'_k + \mathbf{n}'. \tag{6.4}$$

Since the elements of $\mathbf{n}'$ are independent Gaussian random variables, one has

$$P(\mathbf{r}'|\tau, \mathbf{s}'_k) = \prod_{i=1}^{N} \frac{1}{\sqrt{\pi N_0}} \exp\left(-\frac{|r_i - s_{ki}|^2}{N_0}\right) = \frac{1}{(\pi N_0)^{N/2}} \exp\left(-\frac{1}{N_0}\sum_{i=1}^{N}|r_i - s_{ki}|^2\right)$$

where N is the length of the truncated vectors. Having this conditional probability density function (PDF) and considering the fact that all the 2^{2M+L-1} possible signal waveforms are equiprobable, one can find

$$P(\mathbf{r}'|\tau) = A \sum_{k=1}^{2^{2M+L-1}} \exp\left(-\frac{1}{N_0}\sum_{i=1}^{N}|r_i - s_{ki}|^2\right) \tag{6.5}$$

where A is a constant and therefore has no impact on the location of the maximum of $P(\mathbf{r}'|\tau)$. Moreover, one has

$$\sum_{i=1}^{N}|r_i - s_{ki}|^2 = \sum_{i=1}^{N}|r_i|^2 + \sum_{i=1}^{N}|s_{ki}|^2 - 2\sum_{i=1}^{N} r_i s_{ki} \tag{6.6}$$

and since $\exp\left(-\frac{1}{N_0}\sum_{i=1}^{N}|r_i|^2\right)$ is a constant, instead of finding the maximum of $P(\mathbf{r}'|\tau)$, one can equivalently find the maximum of $\Lambda(\mathbf{r}'|\tau)$ where

$$\Lambda(\mathbf{r}'|\tau) = \sum_{k=1}^{2^{2M+L-1}} \exp\left(-\frac{1}{N_0}\sum_{i=1}^{N}|s_{ki}|^2 + \frac{2}{N_0}\sum_{i=1}^{N} r_i s_{ki}\right). \tag{6.7}$$

Note that the timing offset found using the truncated vector representation of signals is an approximation to the real timing offset. In order to find the true value of this timing offset, N should tend to infinity. Since [13]

$$\lim_{N\to\infty}\sum_{i=1}^{N}|s_{ki}|^2 = \int_{\tau+jT}^{\tau+(j+L)T}|s_k(t,\tau)|^2 dt$$

$$\lim_{N\to\infty}\sum_{i=1}^{N} r_i s_{ki} = \int_{\tau+jT}^{\tau+(j+L)T} r(t)s_k(t,\tau)dt$$

one has

$$\hat{\tau} = \arg\max_{\tau} \sum_{k=1}^{2^{2M+L-1}} \exp\left(-\frac{1}{N_0}\int_{\tau+jT}^{\tau+(j+L)T}|s_k(t,\tau)|^2 dt + \frac{2}{N_0}\int_{\tau+jT}^{\tau+(j+L)T} r(t)s_k(t,\tau)dt\right). \tag{6.8}$$

Note that since for every signal waveform, there is a signal waveform with an opposite sign, (6.8) can be simplified by considering only the signal waveforms for which $c_1 = 1$. After some manipulations, one obtains

$$\hat{\tau} = \arg\max_{\tau} \sum_{k=1}^{2^{2M+L-2}} \left[\exp\left(-\frac{1}{N_0}\int_{\tau+jT}^{\tau+(j+L)T}|s_k(t,\tau)|^2 dt\right)\cosh\left(\frac{2}{N_0}\int_{\tau+jT}^{\tau+(j+L)T} r(t)s_k(t,\tau)dt\right)\right]. \tag{6.9}$$

6.2 A Lower Bound on the Detection Theory Bound (DTB)

The DTB (also known as the Ziv-Zakai bound) is a lower bound on the mean square estimation error of the timing offset, *i.e.*

$$\mathrm{MSE} = E\left[\left(\frac{\tau-\hat{\tau}}{T}\right)^2\right] \geq \mathrm{DTB} \tag{6.10a}$$

where

$$\mathrm{DTB} = E_{\underline{c}}\left[\int_{\theta=0}^{1} G_w\left(\int_{\upsilon=0}^{1-\theta} P_e(\upsilon,\upsilon+\theta|\underline{c})d\upsilon\right)\theta d\theta\right] \tag{6.10b}$$

and where $\underline{c}$ is a vector denoting the sequence of the transmitted bits, $G_w(f(\theta))$ is a transform that fills the valleys of $f(\theta)$ with respect to θ (see Fig. 6.2 as an example) and $P_e(\upsilon,\upsilon+\theta|\underline{c})$ is the minimum probability of error in deciding between signals

$$x_1(t) = \sum_n c_i g(t-nT-\upsilon T) \tag{6.11}$$

$$x_2(t) = \sum_n c_n g(t-nT-(\upsilon+\theta)T) \tag{6.12}$$

when transmitted with equal probability. One has [16, Ch.4]

$$P_e(\upsilon,\upsilon+\theta|\underline{c}) = Q\left(\sqrt{\frac{d_{12}^2}{2N_0}}\right) \tag{6.13a}$$

where

$$\begin{aligned} d_{12}^2 &= \int_0^{LT}(x_1(t)-x_2(t))^2dt = \int_0^{LT}x_1^2(t)dt + \int_0^{LT}x_2^2(t)dt - 2\int_0^{LT}x_1(t)x_2(t)dt \\ &= E_1 + E_2 - 2\rho_{12} \end{aligned} \tag{6.13b}$$

and where $Q(\cdot)$ is the Q-function defined at [44], LT is the observation time, E_1 and E_2 are the energies of $x_1(t)$ and $x_2(t)$ during LT, and ρ_{12} is the correlation of $x_1(t)$ and $x_2(t)$.

For the sake of simplicity, $G_w(f(\theta))$ in (6.10) can be replaced by $f(\theta)$. Note that if $f(\theta)$ is a non-increasing function of θ in $[0,1)$, $G_w(f(\theta)) = f(\theta)$; otherwise, this replacement weakens the bound. Consequently, one has

$$\mathrm{DTB} \geq E_{\underline{c}}\left[\int_{\theta=0}^{1}\theta\int_{\upsilon=0}^{1-\theta}Q\left(\sqrt{\frac{d_{12}^2}{2N_0}}\right)d\upsilon d\theta\right] = \int_{\theta=0}^{1}\theta\int_{\upsilon=0}^{1-\theta}E_{\underline{c}}\left[Q\left(\sqrt{\frac{d_{12}^2}{2N_0}}\right)\right]d\upsilon d\theta \tag{6.14}$$

where the equality is a result of the linearity of the integration operation. Since $Q(y)$ is a convex function for $y \geq 0$, using Jensen's inequality [56] one has $E_{\underline{c}}[Q(y)] \geq Q\left(E_{\underline{c}}[y]\right)$. Moreover, $\sqrt{y}$ is a concave function for $y \geq 0$. By employing Jensen's inequality, one has $E_{\underline{c}}\left[\sqrt{y}\right] \leq \sqrt{E_{\underline{c}}[y]}$.

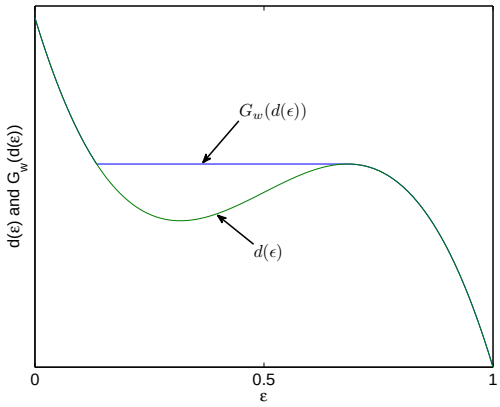

Figure 6.2. An example function $d(\epsilon)$ and its transform $G_w(d(\epsilon))$.

Considering these inequalities and since $Q(\cdot)$ is monotonically decreasing,

$$E_{\underline{c}}\left[Q\left(\sqrt{\frac{d_{12}^2}{2N_0}}\right)\right] \geq Q\left(E_{\underline{c}}\left[\sqrt{\frac{d_{12}^2}{2N_0}}\right]\right) \geq Q\left(\sqrt{\frac{E_{\underline{c}}[d_{12}^2]}{2N_0}}\right). \tag{6.15}$$

In order to find $E_{\underline{c}}\left[d_{12}^2\right]$, one can use (6.13b) to obtain

$$E_{\underline{c}}\left[d_{12}^2\right] = E_{\underline{c}}\left[E_1\right] + E_{\underline{c}}\left[E_2\right] - 2E_{\underline{c}}\left[\rho_{12}\right]. \tag{6.16}$$

Using the definition of $x_1(t)$ in (6.11) the first term in the right side is equal to

$$\begin{aligned} E_{\underline{c}}\left[E_1\right] &= \int_0^{LT} \sum_n \sum_m E_{\underline{c}}[c_n c_m] g(t-nT-\upsilon T) g(t-mT-\upsilon T) dt \\ &= \int_0^{LT} \sum_n C g^2(t-nT-\upsilon T) dt = \int_0^{LT} \sum_m \frac{C}{T} F(\frac{m}{T}) \exp\left(j2\pi m\left(\frac{t-\upsilon T}{T}\right)\right) dt \end{aligned} \tag{6.17}$$

where in the last equality, the Poisson summation formula [57] is used; in this equation, $F(f) = \mathcal{F}\left[g^2(t)\right]$, where $\mathcal{F}[\cdot]$ is the Fourier transform operator. By changing the order of integration and summation in (6.17), one has

$$E_{\underline{c}}\left[E_1\right] = \sum_m CLF(\frac{m}{T}) \exp(-j2\pi m\upsilon)\delta(m) = CLF(0) \tag{6.18}$$

where $F(0)$ is equal to the energy of a single pulse, E_g,

$$F(0) = E_g = \int_{-\infty}^{\infty} g^2(t)dt = \int_{-MT}^{MT} g^2(t)dt. \tag{6.19}$$

Similarly, one obtains

$$E_{\underline{c}}\left[E_2\right] = E_{\underline{c}}\left[E_1\right] = CLF(0). \tag{6.20}$$

The third term in the right side of (6.16) can be found in a similar way,

$$\begin{aligned} E_{\underline{c}}\left[\rho_{12}\right] &= \int_0^{LT} \sum_n \sum_m E_{\underline{c}}[c_n c_m] g(t-nT-\upsilon T) g(t-mT-(\upsilon+\theta)T) dt \\ &= \int_0^{LT} \sum_n C g(t-nT-\upsilon T) g(t-nT-(\upsilon+\theta)T) dt \\ &= \int_0^{LT} \sum_m \frac{C}{T} H(\frac{m}{T}) \exp\left(j2\pi m \left(\frac{t-\upsilon T}{T}\right)\right) dt \end{aligned} \tag{6.21}$$

where in the last equality, the Poisson summation formula is used again; in this equation, $H(f) = \mathcal{F}\left[g(t)g(t-\theta T)\right]$. By changing the order of integration and summation in (6.21), one has

$$E_{\underline{c}}\left[\rho_{12}\right] = \sum_m CLH(\frac{m}{T}) \exp(-j2\pi m\upsilon)\delta(m) = CLH(0) \tag{6.22}$$

where $H(0) = \int_{-\infty}^{\infty} g(t)g(t-\theta T)dt$. One can use (6.22), (6.20) and (6.16) to obtain

$$E_{\underline{c}}[d_{12}^2] = 2CL[F(0) - H(0)] = 2CLE_g[\rho(0) - \rho(\theta)] = 2E_bL(1-\rho(\theta)) \tag{6.23}$$

where E_b is the energy of one bit and $\rho(\theta) = \frac{1}{E_g}\int_{-\infty}^{\infty} g(t-\theta T)g(t)dt$ is the normalized autocorrelation function of $g(t)$. Substituting (6.23) and (6.15) into (6.14), yields

$$\text{DTB} \geq \text{LDTB} \tag{6.24a}$$

where

$$\text{LDTB} = \int_0^1 \left[Q\left(\sqrt{\frac{E_b}{N_0}L(1-\rho(\theta))}\right)\right] \theta(1-\theta)d\theta. \tag{6.24b}$$

Note that when the SNR tends to zero, $Q\left(\sqrt{\frac{E_b}{N_0}L(1-\rho(\theta))}\right)$ tends to $1/2$. As a result,

$$\lim_{E_b/N_0 \to 0} \text{LDTB} = \frac{1}{2}\int_0^1 \theta(1-\theta)d\theta = \frac{1}{12} \tag{6.25}$$

which is equal to the variance of a uniform random variable, as desired.

6.3 Simulation and Discussion

The pulse used in this study is the well known square-root raised cosine pulse [2] with a roll-off factor $\beta = 0.35$. Fig. 6.3 shows the normalized square-root raised cosine pulse with a duration equal to $12T$ ($M = 6$). The MSE is used to measure the performance of the synchronizers, where $\text{MSE} = E\left[\left(\frac{\tau-\hat{\tau}}{T}\right)^2\right]$. In Fig. 6.4, the performance of the ML synchronizer in an ISI channel is shown and is compared to the performances of the ISI-free ML synchronizer and the zero-crossing-

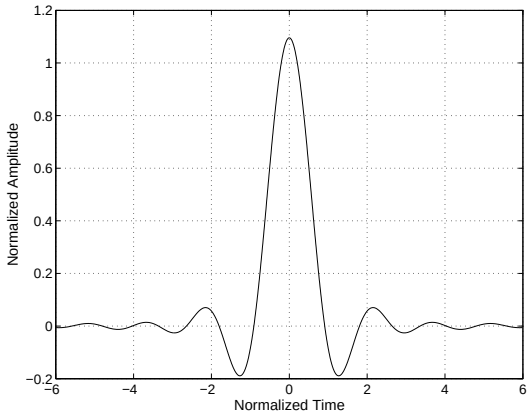

Figure 6.3. Normalized square-root raised cosine pulse with $\beta = 0.35$ and $M = 6$.

based synchronizer (ZCBS) [17], defined as[1]

$$\hat{\tau} = \frac{T}{2\pi} \arg \left\{ \sum_i \exp\left[j2\pi t(i)/T \right] \right\} + \frac{T}{2} \tag{6.26}$$

where $t(i)$ is the sequence of zero-crossings of the received signal after passing through the matched filter. In addition, the DTB, LDTB, and MCRB are shown in this figure. Note that the MCRB for the MSE of a PAM modulated signal is equal to [1]

$$\text{MCRB} = \frac{1}{8\pi^2 \xi L} \frac{1}{E_b/N_0} \tag{6.27}$$

where $\xi = T^2 \frac{\int_{-\infty}^{\infty} f^2 |G(f)|^2 df}{\int_{-\infty}^{\infty} |G(f)|^2 df}$ and $G(f)$ is the Fourier transform of $g(t)$.

The square-root raised cosine pulse used in this figure has a duration equal to $6T$ ($M = 3$) and the observation time is equal to $5T$. As can be seen in this figure, the performance of the ZCBS in an ISI channel is better than the performance of the ISI-free ML synchronizer, as was reported in [17]. However, the performance of the optimum synchronizer (true ML) expressed in (6.9) is much better than both of these methods. Moreover, it can be seen that the DTB provides a very tight lower bound for the MSE of the true ML synchronizer while the MCRB does not provide a tight lower bound. Adding this shortcoming of the MCRB to its behaviour at small values of SNR, one can conclude that the MCRB is not a very appropriate candidate as a lower bound in ISI channels. However, as mentioned before, the complexity of the DTB which requires the Monte Carlo method to find an expectation over all the possible waveforms, is a serious disadvantage for this lower bound.

In Fig. 6.5, the DTB, LDTB, and MCRB are shown for the square-root raised cosine pulse with $\beta = 0.35$ and $M = 3$ and where $L = 5$. It can be seen that the MSE of both the DTB and LDTB

[1] Since the timing offset in [17] is modeled as a uniform random variable in $[-T/2, T/2)$ and in this letter it is modeled as a uniform random variable in $[0, T)$, $T/2$ is addedfrustrated to the ZCBS equation to make (6.26) consistent with the ZCBS equation in [17].

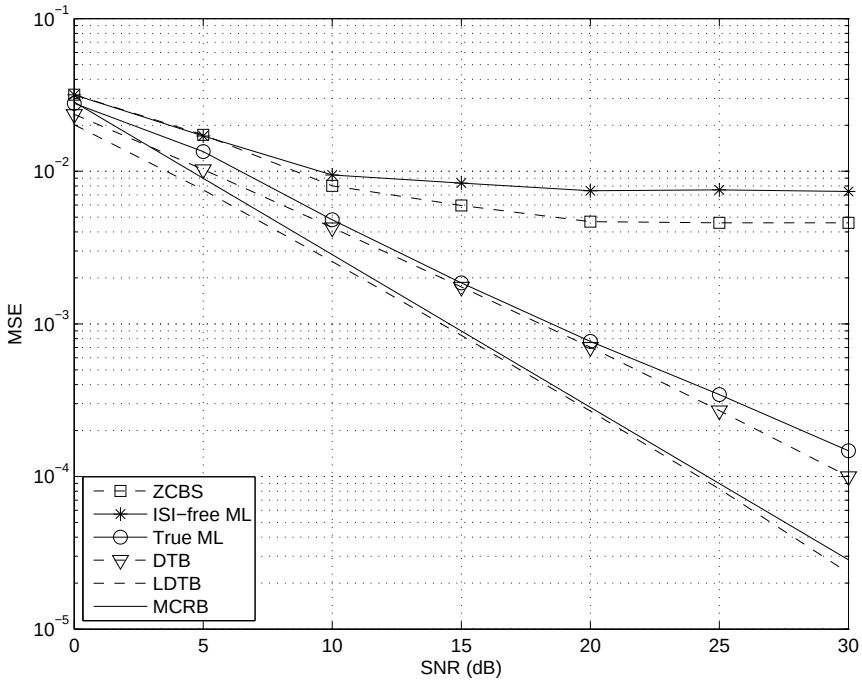

Figure 6.4. The performance of the ZCBS, ISI-free ML synchronizer, true ML synchronizer, DTB, LDTB, and MCRB in an ISI channel. The truncated square-root raised cosine pulses have $\beta = 0.35$, $M = 3$, and the observation time is equal to $5T$.

tend to the variance of a uniform distribution at small values of SNR, while the MSE of the MCRB increases without limit at small values of SNR and therefore the MCRB is not a lower bound in this region. Although the LDTB is a lower bound on the DTB, it does not suffer from the complexity problem of the DTB and since its computation only requires evaluating a single definite integral on the interval $[0, 1]$, it can be computed very fast.

Fig. 6.6 shows the MCRB and LDTB for two different values of observation time. It can be seen that the LDTB is a good match for the MCRB for moderate values of SNR for both of these observation times. Also, considering its appropriate behaviour at small values of SNR and its simplicity in computation, it is a good alternative for the MCRB in ISI channels for small to moderate values of SNR. At large values of SNR (e.g. larger than 30 dB), the gap between the LDTB and the MCRB increases. However, since in practical applications values of SNR more than 30 dB are uncommon, the LDTB is a good alternative for MCRB in practice.

6.4 Conclusions

In this chapter, the ML criterion for timing recovery of a sequence of PAM signals in the presence of ISI and noise was derived. It was shown that the ML criterion derived for an ISI-free channel

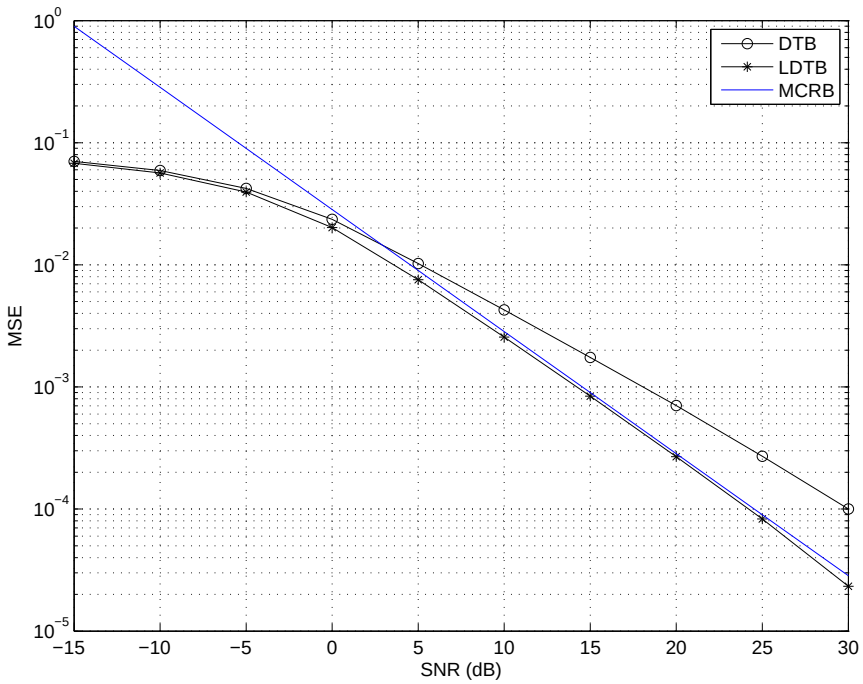

Figure 6.5. The DTB, LDTB, and MCRB for a sequence of truncated square-root raised cosine pulses with $\beta = 0.35$, $M = 3$, and $L = 5$.

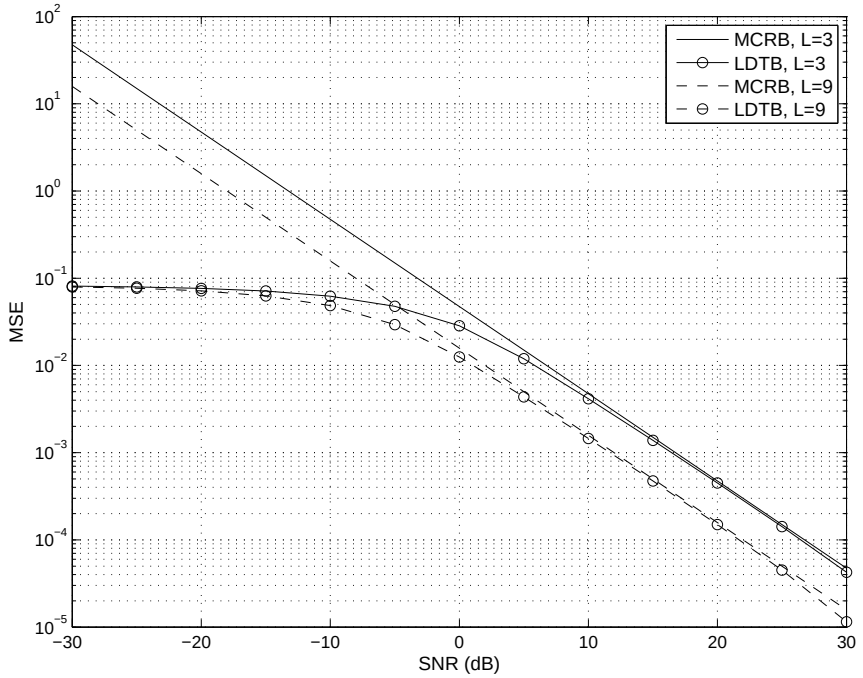

Figure 6.6. The LDTB and MCRB for a sequence of truncated square-root raised cosine pulses with $\beta = 0.35$, $M = 6$, and two different observation times.

underestimates the optimal performance significantly and cannot be used as a proper lower bound on the MSE of synchronizers operating in ISI. The detection theory bound was used as a lower bound on the MSE of the timing offset and it was shown that this lower bound is a tight lower bound on the MSE of the ML synchronizer. A lower bound was derived for the DTB which is much simpler to compute than the DTB. This lower bound was compared to the MCRB and DTB and it was shown that at small values of SNR, the LDTB exhibits the correct behaviour of the DTB while at moderate values of SNR, it is almost as tight as the MCRB.

Bibliography

[1] U. Mengali and A. N. D'Andrea, *Synchronization Techniques for Digital Receivers*. NY: Plenum, 1997.

[2] J. G. Proakis and M. Salehi, *Digital Communications*, 5th ed. NY: McGraw-Hill, 2008.

[3] H. Meyr and G. Ascheid, *Synchronization in Digital Communications*. NY: Wiley, 1990, vol. I.

[4] F. Natali, "AFC tracking algorithms," *IEEE Transactions on Communications*, vol. 32, no. 8, pp. 935–947, Aug. 1984.

[5] A. Goldsmith, *Wireless Communications*. NY: Cambridge University Press, 2005.

[6] E. J. Baghdady, *Lectures on Communication System Theory*. NY: McGraw-Hill, 1961.

[7] G. Lank and I. Reed, "Average time to loss of lock for an automatic frequency control loop with two fading signals, and a related probability distribution (corresp.)," *IEEE Trans. Inf. Theory*, vol. 12, no. 1, pp. 73–75, Jan. 1966.

[8] Y. D. Yao and A. U. H. Sheikh, "Outage probability analysis for microcell mobile radio systems with cochannel interferers in rician/rayleigh fading environment," *Electronics Letters*, vol. 26, pp. 864–866, Jun. 1990.

[9] ——, "Investigations into cochannel interference in microcellular mobile radio systems," *IEEE Transactions on Vehicular Technology*, vol. 41, no. 2, pp. 114–123, May 1992.

[10] J. R. Haug and D. R. Ucci, "Outage probability of microcellular radio systems in a rayleigh/rician fading environment," in *Communications, 1992. ICC 92, Conference record, SUPERCOMM/ICC '92, Discovering a New World of Communications. IEEE International Conference on*, Chicago, IL, Jun. 1992, pp. 306–310.

[11] J.-C. Lin, W.-C. Kao, Y. T. Su, and T.-H. Lee, "Outage and coverage considerations for microcellular mobile radio systems in a shadowed-rician/shadowed-nakagami environment," *IEEE Transactions on Vehicular Technology*, vol. 48, no. 1, pp. 66–75, Jan. 1999.

[12] L. Franks, "Carrier and bit synchronization in data communication–a tutorial review," *IEEE Transactions on Communications*, vol. 28, pp. 1107–1121, Aug. 1980.

[13] H. L. Van Trees, *Detection, Estimation, and Modulation: Part I*. NY:Wiley, 1968.

[14] A. L. McBride and A. P. Sage, "Optimum estimation of bit synchronization," *IEEE Transactions on Aerospace and Electronic Systems*, vol. 5, no. 3, pp. 525–536, May 1969.

[15] P. Wintz and E. Luecke, "Performance of optimum and suboptimum synchronizers," *IEEE Transactions on Communication Technology*, vol. 17, no. 3, pp. 380–389, Jun. 1969.

[16] R. D. Gitlin and J. Salz, "Timing recovery in pam systems," *Bell Syst. Tech. J.*, vol. 50, no. 3, pp. 1645–1669, May–Jun 1969.

[17] E. Fogel and M. Gavish, "Performance evaluation of zero-crossing-based bit synchronizers," *IEEE Transactions on Communications*, vol. 37, no. 6, pp. 663–665, Jun. 1989.

[18] H. Cramer, *Mathematical Methods of Statistics*. NJ: Princeton Univ. Press, 1946.

[19] A. N. D'Andrea, U. Mengali, and R. Reggiannini, "The modified Cramer-Rao bound and its application to synchronization problems," *IEEE Transactions on Communications*, vol. 42, pp. 1391–1399, Feb./Apr. 1994.

[20] A. Weiss and E. Weinstein, "Composite bound on the attainable mean square error in passive time-delay estimation from ambiguity prone signals (corresp.)," *IEEE Transactions on Information Theory*, vol. 28, no. 6, pp. 977–979, Nov. 1982.

[21] S. C. White and N. C. Beaulieu, "On the application of the Cramer-Rao and detection theory bounds to mean square error of symbol timing recovery," *IEEE Transactions on Communications*, vol. 40, no. 10, pp. 1635–1643, Oct. 1992.

[22] S. Bellini and G. Tartara, "Bounds on error in signal parameter estimation," *IEEE Transactions on Communications*, vol. 22, no. 3, pp. 340–342, Mar. 1974.

[23] ——, "Correction to "bounds on error in signal parameter estimation"," *IEEE Transactions on Communications*, vol. 23, no. 4, pp. 486–486, Apr. 1975.

[24] D. Chazan, M. Zakai, and J. Ziv, "Improved lower bounds on signal parameter estimation," *IEEE Transactions on Information Theory*, vol. 21, no. 1, pp. 90–93, Jan. 1975.

[25] N. C. Beaulieu and S. C. White, "A lower bound on the mean square error of symbol timing recovery for NRZ rectangular signals," *IEEE Transactions on Communications*, vol. 43, no. 7, Jul. 1995.

[26] A. N. D'Andrea and U. Mengali, "Noise performance of two frequency-error detectors derived from maximum likelihood estimation methods," *IEEE Transactions on Communications*, vol. 42, pp. 793–802, 1994.

[27] D. Messerschmitt, "Frequency detectors for PLL acquisition in timing and carrier recovery," *IEEE Transactions on Communications*, vol. 27, no. 9, pp. 1288–1295, Sep. 1979.

[28] H. Sari and S. Moridi, "New phase and frequency detectors for carrier recovery in PSK and QAM systems," *IEEE Transactions on Communications*, vol. 36, no. 9, pp. 1035–1043, Sep. 1988.

[29] C. Cahn, "Improving frequency acquisition of a costas loop," *IEEE Transactions on Communications*, vol. 25, no. 12, pp. 1453–1459, Dec. 1977.

[30] F. Gardner, "Properties of frequency difference detectors," *IEEE Transactions on Communications*, vol. 33, no. 2, pp. 131–138, Feb. 1985.

[31] A. N. D'Andrea and U. Mengali, "Performance of a quadricorrelator driven by modulated signals," *IEEE Transactions on Communications*, vol. 38, no. 11, pp. 1952–1957, Nov. 1990.

[32] ——, "Design of quadricorrelators for automatic frequency control systems," *IEEE Transactions on Communications*, vol. 41, no. 6, pp. 988–997, Jun. 1993.

[33] C. G. Yoon, S. Y. Lee, and C. W. Lee, "Digital logic implementation of the quadricorrelators for frequency detector," in *Circuits and Systems, 1994., Proceedings of the 37th Midwest Symposium on*, vol. 2, Lafayette, LA, Aug. 1994, pp. 757–760.

[34] T. Alberty and V. Hespelt, "A new pattern jitter free frequency error detector," *IEEE Transactions on Communications*, vol. 37, no. 2, pp. 159–163, Feb. 1989.

[35] F. Natali, "Noise performance of a cross-product AFC with decision feedback for DPSK signals," *IEEE Transactions on Communications*, vol. 34, no. 3, pp. 303–307, Mar. 1986.

[36] A. N. D'Andrea, A. Ginesi, and U. Mengali, "Frequency detectors for CPM signals," *IEEE Transactions on Communications*, vol. 43, no. 234, pp. 1828–1837, 1995.

[37] M. Ferguson and P. Mantey, "Automatic frequency control via digital filtering," *IEEE Transactions on Audio and Electroacoustics*, vol. 16, no. 3, pp. 392–397, Sep. 1968.

[38] S. Anguirre and S. Hinedi, "Two novel automatic frequency tracking loops," *IEEE Transactions on Aerospace and Electronic Systems*, vol. 25, no. 5, pp. 749–760, Sep. 1989.

[39] T. Chiou, "On the probability density function and stability properties for a cross-product frequency-locked loop," in *Proc. ION GNSS*, 2007.

[40] M. K. Simon and M. S. Alouini, *Digital Communications over Fading Channels*, 2nd ed. NJ: Wiley, 2004.

[41] W. C. Jakes, Ed., *Microwave Mobile Communications*. NY: Wiley, 1974.

[42] A. Papoulis, *Probability, Random Variables, and Stochastic Processes*, 2nd ed. NY: McGraw-Hill, 1984.

[43] S. O. Rice, "Mathematical analysis of random noise," *Bell Sys. Tech. J.*, vol. 24, pp. 46–156, Jan. 1945.

[44] M. Abramowitz and I. A. Stegun, *Handbook of Mathematical Functions with Formulas, Graphs, and Mathematical Tables*, 9th ed. NY: Dover, 1970.

[45] W. C. Lindsey and M. K. Simon, *Telecommunication Systems Engineering*. NJ: Prentice Hall, 1972.

[46] K. Mueller and M. Muller, "Timing recovery in digital synchronous data receivers," *IEEE Transactions on Communications*, vol. 24, no. 5, pp. 516–531, May 1976.

[47] F. Gardner, "A BPSK/QPSK timing-error detector for sampled receivers," *IEEE Transactions on Communications*, vol. 34, no. 5, pp. 423–429, May 1986.

[48] M. Moeneclaey, "A fundamental lower bound on the performance of practical joint carrier and bit synchronizers," *IEEE Transactions on Communications*, vol. 32, no. 9, pp. 1007–1012, Sep. 1984.

[49] R. E. Ziemer and W. H. Tranter, *Principles of Communications: Systems, Modulation, and Noise.* MA: Houghton Mifflin, 1985.

[50] G. L. Stüber, *Principles of Mobile Communications*, 2nd ed. MA: Kluwer, 2000.

[51] S. O. Rice, "Statistical properties of a sine wave plus noise," *Bell Sys. Tech. J.*, vol. 27, pp. 109–157, Jan. 1948.

[52] M. D. Yacoub, J. E. V. Bautista, and L. Guerra de Rezende Guedes, "On higher order statistics of the nakagami-m distribution," *IEEE Trans. Veh. Technol.*, vol. 48, no. 3, pp. 790–794, May 1999.

[53] S. O. Rice, "Distribution of the duration of fades in radio transmission," *Bell Sys. Tech. J.*, vol. 37, pp. 581–635, May 1958.

[54] I. S. Gradshteyn and I. M. Rizhik, *Table of Integrals, Series, and Products*, 7th ed. SD: Academic Press, 2007.

[55] D. Middleton, “Spurious signals caused by noise in triggered circuits,” *J. Appl. Phys.*, vol. 19, pp. 817–830, 1948.

[56] T. M. Cover and J. A. Thomas, *Elements of Information Theory*, 2nd ed. NY: Wiley, 2006.

[57] A. Zygmund, *Trigonometric series*, 3rd ed. Cambridge: Cambridge University Press, 2002.